Friedrich Schiller University Jena

Faculty of Biological Sciences

Institute of Nutritional Sciences

Characterization of two *Caenorhabditis elegans* Orthologs of Selenium-binding Protein 1, Associated with Aging

Dissertation

To fulfill the requirements for the degree of

„doctor rerum naturalium“ (Dr. rer. nat.).

Submitted to the Council of the Faculty of Biological Sciences

of Friedrich Schiller University Jena

by Karl Köhnlein, M.Sc.

born on 20.05.1989, in Albstadt

Reviewers

Prof. Dr. Lars-Oliver Klotz, Friedrich Schiller University, Institute for Nutrition, Nutrigenomik, Jena, Germany.

Dr. Christoph Kaether, Leibniz Institute on Aging – Fritz Lipmann Institute (FLI), Jena, Germany

Prof. Dr. Wim Wätjen, Martin Luther University Halle-Wittenberg, Institute for Agricultural and Food Sciences, Halle(Saale), Germany.

Date of public defense: 16.10.2020

Table of contents

Abbreviations

2DGE	Two-dimensional gel electrophoreses
3-MP	3-Mercaptopyruvate
AGE	Advanced glycation end product
Arg	Arginine
ARP	Argpyrimidine
C. elegans	Caenorhabditis elegans
CBS	Cystathionine-β-synthase
CEL	Carboxyethyl lysine
CGC	Caenorhabditis genetics center
CGL; CTH	Cystathionine-γ-lyase
CML	Carboxymethyl lysine
Cys	Cysteine
Cysxx	Cysteine at position xx
DIO	Iodothyronine deiodase
DKK1	Dickkopf-related protein 1
E. coli	Eschericia coli
EFSEC	Selenocysteine-specific elongation factor
FTC	Fluorescein-5-thiosemicarbazide
GCS	Glutamylcysteine synthetase
GPX	Glutathione peroxidase
GSH	Glutathione
GST	Glutathione S-transferase
H_2S	Hydrogen sulfide
HbA1c	Glycated hemoglobin
HDL	High density lipoprotein
JNK	c-Jun N-terminal kinase
LDL	Low density lipoprotein
Lys	Lysine
MD	Mean difference
MeSeCys	Methylselenocysteine
MG-H1	Methylglyoxal-derived hydroimidazolone
MPST	Mercaptopyruvate sulfurtransferase
MTO	Methanethiol oxidase
NF-κB	Nuclear factor 'kappa-light-chain-enhancer' of activated B-cells
NGM	Nematode growth medium
PEN	Pentosidine
PPAR-γ	Peroxisomal proliferator-activated receptor gamma
PRDX	Peroxiredoxin
RCT	Randomized control trial
ROS	Reactive oxygen species

Sec	Selenocysteine
SECIS	Selenocysteine insertion sequence
SELENBP1	Selenium-binding protein 1
SeMet	Selenomethionine
Ser	Serine
SOD	Superoxide dismutase
SPB2	Secis binding protein 2
SPS2	Selenophosphate synthetase
T2D	Type 2 diabetes
TNF-α	Tumor necrosis factor-α
TRXR	Thioredoxin reductase

Tables

Figures

1 Introduction

1.1 The trace element selenium

Selenium is a trace element and is regarded as essential for the expression of selenoproteins in all kingdoms of life (Jiang et al. 2013). It is part of the group of chalcogens and is located below sulfur in the periodic table of elements. Its configuration of valence electrons is similar to sulfur and it therefore has similar chemical properties to some degree. Both elements are good nucleophiles making them important for biological redox processes. Due to the bigger atomic radius of selenium compared to sulfur, selenium is a better nucleophile than sulfur, enabling it to react even faster with reactive oxygen species (ROS) in living cells. Moreover, certain oxygen-selenium compounds are reduced much faster than the sulfur analogs, which allows it to take part in redox reactions more often without being permanently oxidized (Reich and Hondal 2016; Steinmann et al. 2010).

1.2 Association of selenium intake with the risk for cancer.

Although selenium is regarded as an essential trace element, the impact of selenium on the risk of different medical conditions like cancer or diabetes have been discussed controversially. Regarding its contribution to cancer, *Vinceti et al.* published a systematic review including eleven randomized control trials (RCT) with forty-four thousand participants and 70 observational longitudinal studies including another 2.3 million participants. In the RCTs, no effect of selenium supplementation could be found regarding cancer risk (1.01-fold). Depending on the inclusion criteria, they reported a mild (0.81-fold) to no observable effect (1.02-fold) for cancer mortality upon selenium supplementation. Moreover, no change in risk for colorectal cancer, non-melanoma skin cancer, lung cancer, breast cancer, bladder cancer or prostate cancer was observed after selenium supplementation. These studies were ranked with 'high' or 'moderate' quality of the evidence according to the GRADE guidelines but consisted of 88 % male participants, which might have skewed the results. On the contrary, evaluating the observational longitudinal studies, they found that lower cancer mortality (0.76-fold) and lower cancer incidence (0.72-fold) were associated with the highest category of selenium exposure. They also found a decreased risk for lung cancer,

breast cancer, stomach cancer, colorectal and prostate cancer when participants with the highest selenium exposure were compared to participants with lowest selenium exposure (Vinceti et al. 2018a). However, all observational longitudinal studies exhibited a 'very low' certainty of the evidence according to the GRADE guidelines. These studies were either inconsistent, had a risk of bias, publication bias or precision issues. Overall, the authors conclude that there is no evidence of selenium supplementation or increased selenium intake through the diet, of having an impact on cancer in human.

1.3 Increased selenium status is associated with increased risk for type-2 diabetes

High selenium intake has been associated with the risk of type 2 diabetes (T2D). However, this association is being discussed controversially until today. A systematic review of Vinceti et al. aimed to evaluate the evidence on the association between selenium and T2D. They performed a meta-analysis on several epidemiological studies and RCTs, including a total of around 70,000 participants in the epidemiological studies and a total of around 10,000 participants in the RCTs. Analyzing epidemiological studies revealed that, regarding 45 μg/l for plasma/serum selenium levels or 23 μg/day for dietary intake as reference, plasma/serum selenium levels as well as dietary intake correlated positively with the risk ratio for T2D. A similar positive association was found analyzing the effect of the RCTs, in which 200 μg selenium/day were administered as selenized yeast or selenomethionine (Vinceti et al. 2018b).

Steinbrenner et al. suggested that excess selenium might interfere with insulin signaling and glucose uptake. One proposed possibility was by selenium influencing proteins involved in insulin signal transduction directly or by elevating the expression of redox-active selenoproteins such as *glutathione peroxidase 1* (GPX1), which might scavenge reactive oxygen species that are important for the insulin signaling cascade (Steinbrenner et al. 2010).

Recently, *Stróżyk et al.* published a small systematic review aiming to get a more detailed understanding on the functions of selenium in glucose metabolism, more specifically T2D. They evaluated fasting insulin levels, fasting plasma glucose, glycated hemoglobin (HbA1c), insulin resistance (HOMA-IR), beta cell function (HOMA-R) and different lipid parameters in adults with T2D. Due to the specificity of these parameters they were only able to include 4 RCTs with a total of 241 participants, which fit all inclusion criteria. They reported that no

consistent changes were found regarding the lipid profile (total cholesterol, LDL, HDL or triglycerides). Moreover, glycated hemoglobin (HbA1c) and fasting plasma glucose didn't show any significant difference following selenium supplementation. However, they found that selenium supplementation reduced fasting insulin levels (8 weeks: MD -5.8 μIU/mL; 12 weeks: MD -3.6 μIU/mL) and resulted a small decrease in insulin resistance (8 weeks: HOMA-IR: MD -1.0; 12 weeks: HOMA-IR: MD -1.6) and beta cell function (8 weeks: HOMA-B: MD -13.6; 12 weeks: HOMA-B: MD -22.6) (Stróżyk et al. 2019).

Despite the significant findings in this study its clinical value is limited due to the small sample size, risk of population bias (three out of four RCTs included were performed in the same country) and heterogeneity of the population. Although selenium supplementation slightly improved some parameters of T2D it reduced beta-cell function, which can be regarded as a negative outcome. Future analyses need to be performed to get a better understanding on the role of selenium in diabetes. Taken together, there is substantial evidence that selenium might be associated with the risk of T2D by mechanisms which have to be clarified in more detail.

1.4 Selenium-containing proteins

The selenoproteome – the entirety of all selenium-containing proteins – consists of proteins that fall into three classes. The best studied class are the selenoproteins, which carry the 21st proteinogenic amino acid, selenocysteine (Sec), as part of their primary structure. In eukaryotes, the integration of Sec into the amino acid chain follows a non-canonical process involving a *selenocysteine insertion sequence* (SECIS) element in the respective mRNA 3'-untranslated region (UTR), at a suitable distance from an UGA stop codon that is then recoded to a Sec codon as follows. Upon translation of a selenoprotein, the SECIS element recruits the *SECIS binding protein 2* (SPB2), which binds to the stem-loop-stem-loop structure of the SECIS element. SBP2 also binds the *selenocysteine-specific elongation factor* (EFSEC) which, in turn, binds the Sec-tRNA$^{[Ser]Sec}$. This tRNA contains the UGA anticodon UCA (5'→3') and is first charged with serine (Ser), whose hydroxl group (OH) is then converted into a selenol group (SeH), creating selenocysteine. The RNA containing the SECIS elements is then folded backwards to the ribosome at the UGA codon. There, the *eukaryotic ribosomal protein L30* (eL30) anchors SBP2 and EFSEC, binding the Sec-tRNA$^{[Ser]Sec}$, to the large ribosomal subunit, after which Sec can be inserted into the amino acid sequence (Martin et al. 1996; Mix et al. 2007;

Vindry et al. 2018). This process is very energy demanding because of its complex nature and the highly regulated processes involved in the incorporation of this single amino acid (Mix et al. 2007). Therefore, the incorporation of selenocysteine instead of cysteine (Cys) or serine needs to yield certain biological advantages for the organism.

Selenocysteine differs from Cys only by containing a selenol group instead of a thiol group at the β-carbon. The most important difference for biological systems might be their biochemical properties. The pKa value of the selenohydryl group of Sec was reported to be considerably lower than that of the sulfhydryl group of Cys (5.24 vs. 8.25) in a standard acid-base titration (Figure 1), which makes Sec a stronger nucleophile under physiological conditions. Additionally, the redox potential of Sec (-488 mV) was also reported to be much lower compared to Cys (-233 mV), measured via cyclic voltammetry. For comparison, the standard reduction potential of glutathione, the most abundant antioxidant in a cell is reportedly around -240 mV (Huber and Criddle 1967; Jacob et al. 2003; Rost and Rapoport 1964). This seems to be an important property for selenoproteins being able to catalyze the turnover of their substrates. For instance, mammalian thioredoxin reductase, in which Sec was replaced by Cys in the active site, was shown to have a 100-fold reduced catalytic activity to reduce oxidized thioredoxin compared to regular Sec containing thioredoxin (Zhong et al. 2000).

The human selenoproteome consists of 25 selenoproteins, many catalyzing important reactions for cellular or organismal health. These reactions include maintenance of cellular redox status (*thioredoxin reductases*; TRXR), detoxification of intra- and extracellular peroxides (GPX), production of thyroid hormones (*iodothyronine deiodases*; DIO), homeostasis and transport of selenium (*selenoprotein P*; SELENOP), amino acid recovery (*methionine sulfoxide reductase*; MSR) and production of the precursor substance for Sec synthesis, selenophosphate (*selenophosphate synthetase 2*; SPS2) (Kasaikina et al. 2012; Papp et al. 2007).

The incorporation of selenomethionine (SeMet) instead of methionine (Met) into the primary structure of proteins yields the second class of selenium containing proteins and can affect all Met containing proteins, since this process appears to be random (Bierla et al. 2013). The substitution of methionine with SeMet does not alter the amino acid structure. It can, however, alter the stability of proteins, and the activity of enzymes when methionine is replaced near the active site (Bernard et al. 1995; Boles et al. 1991; Schrauzer 2000). In yeast and plants SeMet is the major organoselenium compound and also one of the major selenium stores. It is produced from selenocysteine as an intermediate for other methylated or volatile selenium compounds (Papp et al. 2007; White 2017).

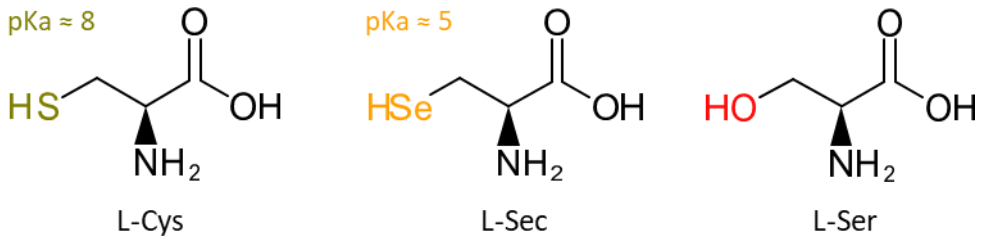

Figure 1 Comparison of L-cysteine, L-selenocysteine and L-serine.
L-cysteine (L-Cys), L-selenocysteine (L-Sec) and L-serine (L-Ser) are shown from left to right. All share the same amino acid backbone but have different functional groups at the β-carbon. Changes of pKa values for the sulfhydryl group (green) and the selenohydryl (yellow) are depicted according to (Huber and Criddle, 1967).

Hints of a third class of selenium containing proteins were first discovered in rodents in the 1970s and 1980s. After injection of Se^{75}-labled selenite into rats or mice, researchers detected selenium containing proteins in tissue extracts of kidney, liver and blood which were distinct from GPX – the only well-known selenoprotein at that time (Burk 1973; Millar 1972; Raymond F.Burk and Paula E.Gregory 1982). In 1989, *Bansal et al.* detected a 56 and 14 kDa mouse protein, binding Se^{75} and being distinct from GPX, which were termed "selenium-binding proteins" (Bansal et al. 1989). The cDNA sequence of the 56 kDa protein was discovered one year later by the same researchers and termed SLP56 (Bansal et al. 1990). The term *selenium-binding protein* was retained, when later a homolog of SLP56 was identified in humans. This protein became later known as the *selenium-binding protein 1* (SELENBP1). Evidence of a SLP56 homolog was discovered shortly before in mouse, binding a cytochrome P450 metabolite of acetaminophen (Pumford et al. 1992). This protein later was termed *AP56* or *selenium-binding protein 2* (SELENBP2). However, a human homolog binding a similar metabolite, has not been identified until now.

1.5 Selenium-binding protein 1

Until today, the biological function of SELENBP1 remains unclear. In humans, it seems to be ubiquitously expressed. Gene transcription was identified throughout the gastro-intestinal tract, in the peripheral and central nervous system, in different hematopoietic cells, in reproductive organs of males and females, as well as in skin, muscle, kidney, lung, heart and some glandular organs (Stelzer et al. 2016). Abundance of SELENBP1 protein levels were detected in similar organs. Antibody staining showed SELENBP1 in thyroid gland, liver, kidney, male and female reproductive organs, adipose tissue, bone marrow (Uhlen et al. 2015), red blood cells (Goodman et al. 2007; Pallotta et al. 2013; Roux-Dalvai et al. 2008), skeletal muscle (Gueugneau et al. 2014) and brain (Glatt et al. 2005). Arguably, this ubiquitous expression might indicate a general importance for normal cellular function throughout the human body.

1.5.1 SELENBP1 is a methanethiol/ethanethiol oxidase

Recently, the enzymatic activity of SELENBP1 was discovered. Studying sulfur metabolism in a marine environment, *Eyice et al.* discovered a bacterial enzyme exhibiting *methanethiol oxidase* (MTO) activity. Methanethiol is a volatile sulfur compound originating from the degradation of sulfur-containing amino acids amongst other sources. They demonstrated that MTO was able to oxidize methanethiol into formaldehyde, hydrogen sulfide and supposedly hydrogen peroxide in a copper-dependent manner. Ethanethiol, but not dimethylsulfide, was also found to be a substrate for MTO. They were able to map the 46 kDa protein to the selenium-binding protein superfamily with an amino acid sequence identity of 26 % to human SELENBP1. However, no selenium was found in the MTO isolate from bacteria, using ICP-MS. MTO sequence identity was shown to be high in all branches of life (archaea: 26-29 %, bacteria: 50-79 %, eukarya: 26 %; SELENBP1). At pH 8.2, the enzyme was found in a tetrameric state. However at nearly physiological pH of 7.2, MTO was detected in a monomeric and tetrameric state (Eyice et al. 2018).

Inspired by these findings, *Pol et al.* conducted a study investigating patients with extraoral halitosis, who accumulated methanethiol and precursor substances, such as dimethylsulfide, dimethylsulfoxide, and dimethylsulfone. The authors finally confirmed that the human but also mouse SELENBP1 exhibited MTO activity. The halitosis patients showed mutations in

different genetic loci of SELENBP1, had lower SELENBP1 protein levels and lower MTO activity in tissue lysates compared to healthy subjects. *Pol et al.* demonstrated that Km-values of human and mouse tissue, expressing SELENBP1, was 4-6 nM and hypothesized that this might enable fast clearance of methanethiol to keep intracellular concentrations of methanethiol below a certain threshold, so it can be detected nasally. Until now, MTO activity of SELENBP1 has not been demonstrated to be important in a biochemical context. It can be speculated whether the interaction of SELENBP1 with different redox active proteins (see below) is dependent on its hydrogen peroxide production by conversion of methanethiol (Pol et al. 2018).

1.5.2 Is SELENBP1 a selenium-binding protein?

Up to now, it remains unclear whether SELENBP1 is able to bind selenium under physiological conditions. As mentioned before, mammalian SELENBP was discovered in mouse liver, binding ^{75}Se (Bansal et al. 1989). Later, it was demonstrated that also the bacterium Methanococcus vannielii (*M. vannielii*) expresses a selenium-binding protein which was able to incorporate ^{75}Se but only effectively under reducing conditions (Patteson et al. 2005). However, analysis of human SELENBP1 revealed opposing characteristics. Incubation of recombinant SELENBP1 with ^{75}Se showed an incorporation of selenium at low nanomolar concentrations (≈1 nM), visible via autoradiography, in a non-reducing SDS-PAGE. However, under reducing conditions, ^{75}Se bands strongly faded and were only visible with supplementation of around 10 nM selenium and above (Jeong et al. 2009).

In vitro and *in silico* analysis of *M. vannielii* SELENBP revealed that Cys59, which is located in a semi-flexible loop between two beta-sheets, seemed to be the motif most likely to bind selenium, due to its high accessibility compared to other cysteines and its local environment of charged and hydrophobic amino acids (Suzuki et al. 2008). After modelling human SELENBP1 to the homolog of Sulfolobus tokodaii (*S. tokodaii;* PDB: 2ECE), *Raucci et al.* predicted, that, like Cys59 in the *M. vannielii* protein, Cys57 was located in a loop between two beta sheets, suggesting that it was the most accessible cysteine residue. Furthermore, they reported that Cys57 was more prone to be exposed under neutral pH than under acidic conditions. Together with the findings of *Jeong et al.*, this leaves room for the hypothesis, that the binding of selenium to SELENBP1 might be more likely under non-reducing conditions (Raucci et al. 2011).

First evidence on the importance of Cys57 was provided by *Ying et al.*. By mutating Cys57 to glycine (SELENBP1^{Gly}) they showed that selenium-induced toxicity to cells expressing the mutated protein was elevated compared to cells transfected with a plasmid encoding the native protein. Protein half-life of SELENBP1^{Gly} was reduced compared to normal SELENBP1 and also failed to activate one of the SELENBP1 effector targets, p53. Unfortunately, the binding of selenium to SELENBP1 was not assessed during that study (Ying et al. 2015b). Taken together, there is still not enough evidence to conclude that SELENBP1 is able to bind selenium. However, there is evidence on the biological importance of the proposed selenium-binding site Cys57 for the activation of SELENBP1 targets. Although predicted to bind selenium, the actual binding of selenium by Cys57 remains to be demonstrated under physiological conditions (Kelley et al. 2015). Judging from the 3D-model of SELENBP1 generated by *Protein Homology/analogY Recognition Engine V 2.0* (Phyre^2), Cys57 does not seem to be the only cysteine residue exposed to the surface (Results: Figure 12). Therefore, also other motifs might be involved in the binding of selenium.

SELENBP1 carries two putative thioredoxin motifs (CxxC) at amino acid position five to eight and at 80 to 83. This motif was shown to be a crucial part for disulfide bond reduction of thioredoxin or isomerization of protein-disulfide isomerase (Schultz et al. 1999). Investigating the functional consequences of replacing ”xx” with different amino acids in CxxC of *human protein-disulfide isomerase*, *Horibe et al.* showed that the substitution of proline-histidine or glycine-histidine as "xx" with serine-methionine, significantly diminished its enzymatic activity (Horibe et al. 2004). Thioredoxin carrying proline-serine, proline-lysine, proline-arginine or proline-histidine as "xx", protected cells best against cadmium toxicity, while cells with arginine-tyrosine as "xx" in thioredoxin, showed the best protection against noxious copper concentrations, followed by proline-serine and prolin-histidin (Quan et al. 2007). Thus, it seems as if a either a combination of a positively charged and an uncharged amino acid or the presence of a heterocyclic or aromatic amino acid within CxxC, confers a high redox activity. It is therefore questionable, whether the combination of two uncharged residues as "xx" i.e. asparagine-glycine (aa6, aa7) and serine-serine (aa81, aa82) as in SELENBP1, would enable the protein to show a significant thioredoxin-like activity. The CxxC motif has also been reported as a highly conserved metal-binding motif in proteins such as copper chaperones or copper-transporting P-type ATPases (Opella et al. 2002; Voskoboinik et al. 1999).

It was proposed that the histidine metal-binding motifs HxH and HxxH might be an important feature of SELENBP1 for selenium binding (Flemetakis et al. 2002). However, histidines have not been described as classical sites for selenium binding, and furthermore, there seems to be no histidine residue on the surface in close proximity to the CxxC motif or any other cysteine residue (Result: Figure 12).

1.5.3 SELENBP1 is a target of protein oxidation

Some studies suggest SELENBP1 might be relevant in aging. In muscle of elderly (48–61 years) and old (76–82 years) post-menopausal women, several apparent isoforms of SELENBP1 were detected, two of which were more abundant in old participants and one isoform which was less abundant in old participants. Size and sequence of these so-called isoforms were not evaluated but judging from the two-dimensional gel electrophoresis (2DGE) signals all three spots seemed to migrate at approximately the same molecular weight but at different pH (Gueugneau et al. 2014).

During the aging process proteins can lose their function, show decreased solubility and aggregation due to non-enzymatic protein modification. One class of modification commonly associated with this process is carbonylation (Tanase et al. 2016). Carbonylation has been classified as a major hallmark of oxidative damage. It is a rather unspecific term for modifications on lipids, proteins or DNA which can become oxidized by different sources of reactive oxygen species. Commonly used carbonyl probes like *fluorescein-5-thiosemicarbazide* (FTC), in combination with other protein detection methods like SDS-PAGE, can help to assess the extent of oxidation of proteins (Fedorova et al. 2014; Yan and Forster 2011). Using such a method, *Chaudhuri et al.* measured protein carbonylation in liver of young (4-6 months) and old (22-23 months) mice and detected a two-fold increase in total protein carbonylation in old mice. SELENBP1 was among the twelve proteins which had a two-fold or higher carbonyl content and showed an increase in carbonylation of 2.1- and 2.6-fold of two spots in the 2DGE. As in the study of *Gueugneau et al.*, these spots migrated at the same molecular weight but at different pH. The authors reported that overall protein expression was unchanged in both groups of mice (Chaudhuri et al. 2006).

Ishida et al. investigated a similar type of protein modification, so called *advanced glycation endproducts* (AGEs) in red blood cells of schizophrenic and healthy patients. AGEs are age-

associated, non-enzymatic protein modifications which occur frequently on lysine and arginine residues of proteins (Henning and Glomb 2016). They looked for amino acyl alterations such as pentosidine (PEN), carboxyethyl lysine (CEL), carboxymethyl lysine (CML), argpyrimidine (ARP) and methylglyoxal-derived hydroimidazolone (MG-H1) and found that neither healthy nor schizophrenic participants had noticeable levels of PEN, CEL, CML or MG-H1. However, both groups showed a very prominent band for ARP in the immunoblot at roughly 56 kDa, which was identified to be SELENBP1 via LC-MS/MS. They also showed that schizophrenic patients had an even higher abundance of ARP modification on SELENBP1 than healthy controls. Unfortunately, although participants of both groups were claimed to be aged-matched, no detailed information on the age was provided (Ishida et al. 2017).

1.5.4 SELENBP1 protects cells from selenite toxicity

There are several studies reporting a negative correlation between SELENBP1 and the hydrogen peroxide-scavenging selenoenzyme GPX1. In the previously mentioned study by *Huang et al.*, tissue from HCC patients with and without vascular invasion were analyzed. Interestingly, they measured significantly lower SELENBP1 protein levels and increased GPX1 activity levels in the participants with vascular invasion compared to tissue from participants with no vascular invasion (Huang et al. 2012). Likewise, comparing tissue from breast cancer patients with adjacent matched normal tissue, another study found SELENBP1 levels to be significantly higher and GPX1 significantly lower in cancerous tissue compared to healthy tissue (Wang et al. 2015).

A similar association was found in the SELENBP1-negative, GPX1-positive cancer cell line HCT116 and the SELENBP1-positive, GPX1-negative cancer cell line MCF-7. GPX1 activity significantly declined after transfection of HCT116 with SELENBP1. This was also observable in MCF-7 stably transfected with GPX1 (MCF-7-GPX1). Additionally, GPX1 transfection significantly lowered SELENBP1 protein, mRNA and promotor activity levels compared to the un-transfected control. These authors also established a dose-response relationship between SELENBP1 protein levels and selenite treatment. When treating HCT116, stably transfected with SELENBP1, with selenite up to 250 nM, SELENBP1 levels declined. The same was seen in MCF-7-GPX1 but not in un-transfected MCF-7, missing GPX1 (Fang et al. 2010).

Therefore, selenium-induced changes in SELENBP1 expression seem to be directly related to GPX1.

Wang et al. investigated this relationship further, using the same cell lines. Similar to *Fang et al.* they observed a dose dependent increase of SELENBP1 protein levels when MCF-7-GPX1 cells were treated with micromolar concentrations of selenite. This was not observable in GPX1 negative MCF-7. In a selenite cell viability assay, introduction of GPX1 into MCF-7 significantly decreased cell viability, which was directly associated with an incline of SELENBP1 levels. This association seemed to be at least partially GPX1-dependent, because treatment of GPX1-negative MCF-7 with *selenbp1* shRNA also resulted in a dose-dependent decline of cell viability after selenite treatment. However, SELENBP1 seemed to be involved as well. In SELENBP1-negative HCT116 cells, neither overexpression nor depletion of GPX1 resulted in a decline of cell viability compared to the respective control treatment. This was verified when SELENBP1 was introduced into HCT116 cells via transfection. Then, the decreased cell viability caused by selenite treatment was significantly attenuated compared to the un-transfected control (Wang et al. 2015). Collectively, there is evidence suggesting that SELENBP1 interacts with GPX1 in a yet unknown way and that SELENBP1/GPX1 interaction might be important in the maintenance of cell viability against toxic selenium concentrations.

1.5.5 Functional role of SELENBP1 in cancer

The most striking clinical observation regarding SELENBP1 might be the reduced expression of SELENBP1 in many cancerous tissues compared to healthy tissues. This includes liver, kidney, prostate, ovaries, colon, female breast, esophagus, stomach, lung and thyroid glands. Additionally, reduced levels of SELENBP1 often correlated with poor clinical outcome. In fact, some studies proposed SELENBP1 as a possible predictive marker for certain types of cancer (Ansong et al. 2015; Brown et al. 2006; Chen et al. 2004; Ha et al. 2014; He et al. 2004; Huang et al. 2012, 2006; Jerome-Morais et al. 2012; Kim et al. 2006; Stasio et al. 2011; Zhang et al. 2013b). A study by *Ying et al.* even demonstrated that SELENBP1 expression could suppress tumor growth. They injected human colon cancer cells (HCT-116) carrying a doxycycline-inducible vector encoding the transcript of human SELENBP1 and HCT-116 cells with a control vector, on the right and left side of each animal, respectively. Tumors that originated from cells with induced levels of SELENBP1 had a lower tumor volume and tumor mass compared to tumors originating from injection with the control vector. They also demonstrated that induction of

SELENBP1 resulted in fewer lung metastases compared to animals with control-vector injection (Ying et al. 2015a).

Using a very similar setup, a *Pohl et al.* were able to show a comparable effect of SELENBP1 overexpression on tumor size and mass of colon cancer (Pohl et al. 2009). They further analyzed downstream targets of SELENBP1 using a proteomic approach and identified many targets associated with glucose or lipid metabolism like *fatty acid-binding protein 4*, *mitochondrial aldehyde dehydrogenase*, *UDP-glucose 6-dehydrogenase*, *glyceraldehyde-3-phosphate dehydrogenase*, *beta-enolase* or *lysophosphatidylcholine acyltransferase 2* and proteins involved in redox homeostasis such as *thioredoxin* or *glutathione peroxidase,* or *dickkopf-related protein 1*, a negative regulator of the canonical Wnt-β-catenin pathway (Bao et al. 2012; Ying et al. 2015a).

Some studies suggest that also the subcellular localization of SELENBP1 might play a role in cancer progression. SELENBP1 is usually localized in the cytoplasm, although nuclear shuttling has been shown to occur under conditions of increased oxidative stress (Chen et al. 2004; Glatt et al. 2005; Huang et al. 2012). A study analyzing 168 case-control pairs with prostate cancer, reported that the ratio of nuclear to cytoplasmic localization of SELENBP1 was inversely correlated with a measure of prostate cancer morphology, used to grade the aggressiveness of the malignant tissue (Gleason score): patients with a more aggressive stage of prostate cancer, hence with poorly differentiated prostate tissue (high Gleason score) had lower nuclear SELENBP1 (Ansong et al. 2015). Nuclear shuttling might indeed be an important function of SELENBP1 because, as *Huang et al.* demonstrated in the HeLa-derived cell line SMMC7721 (falsely used as hepatocellular cancer cell line; RRID:CVCL_0534), treatment with 50 mmol/L hydrogen peroxide for 12 hours led to the formation of very clear nuclear SELENBP1 bodies while cytoplasmic expression seemed to be unchanged. Interestingly, they observed the same behavior for the selenoprotein GPX1. Additionally, some of the observed nuclear bodies of SELENBP1 and GPX1 were localized in close proximity to one another, some with overlapping signals (Huang et al. 2012).

1.5.6 The role of DNA methylation in the transcriptional regulation of SELENBP1

DNA analysis of tumor tissue of patients and adjacent healthy tissue revealed that tumors seemed to have a higher DNA methylation state. Analysis of different cancer cells lines showed a clear association between the abundance of methylation on the SELENBP1 promotor

and SELENBP1 protein levels, with HCT-116 having the highest degree of methylation and no measurable SELENBP1 expression. Treatment of HCT-116 with the demethylating agent 5-Aza-29-deoxycytidine significantly improved promotor activity, mRNA and protein levels of SELENBP1 (Pohl et al. 2009). Interestingly, a higher degree of DNA methylation of the highly homologous SELENBP2 was likewise associated with reduced transcriptional levels (Orozco et al. 2014).

1.5.7 SELENBP1 is associated with the regulation of cell differentiation

Recently, a positive correlation between SELENBP1 abundance and the differentiation state of preadipose cells to mature adipocytes was reported. During a 14-day differentiation period of 3T3-L1 cells, strongly increasing markers for adipocyte differentiation and lipid accumulation (*anti-peroxisomal proliferator-activated receptor gamma* (PPAR-γ) and *perilipin 1*) were measured. SELENBP1 positively correlated with the differentiation stage but did not seem to take active part in the transcriptional regulation during differentiation because immunoblotting and immunostaining only showed a cytoplasmic signal for SELENBP1. Interestingly, factors such as rapamycin or the *tumor necrosis factor-α* (TNF-α), which impaired adipocyte differentiation, also strongly suppressed SELENBP1 levels. Unfortunately, the causal relationship of this scenario remained unclear (Steinbrenner et al. 2019).

Ying et al. demonstrated how SELENBP1 might regulate cellular differentiation and proliferation in more detail. Tumor tissues of mice expressing human SELENBP1 or a control vector were analyzed regarding their protein expression profile. As mentioned before, they found *dickkopf-related protein 1* (DKK1) to be significantly more abundant in SELENBP1 expressing tumors. DKK1 is known to negatively regulate Wnt signaling – a central pathway during cell proliferation and differentiation (Bao et al. 2012; Reya and Clevers 2005). Via immunoblotting they were able to validate the dampening of the Wnt pathway when they showed that downstream targets like β-catenin and cyclin D1 were less abundant in tumors transfected with SELENBP1. They also discovered another set of proteins that are involved in cell differentiation, proliferation and apoptosis, and are linked to SELENBP, namely *c-Jun N-terminal kinases* (JNK) and downstream effectors thereof. They measured increased phosphorylation of JNK but also of downstream targets like c-Jun and p53 and a greater abundance of p21 in SELENBP1 expressing tumors compared to tumors which were originally transfected with the control vector (Ying et al. 2015a). The phosphorylation of p53 elicited by

SELENBP1 expression was also demonstrated elsewhere (Ansong et al. 2015). The induction of JNK by SELENBP1 is difficult to interpret in terms of the hypothesis of SELENBP1 being involved in tumor suppression. JNK are generally recognized as a pro-apoptotic factors and could therefore potentially be regarded as a tumor suppressor. The role of JNK in cancer is still discussed controversially, though. JNK may act differently in healthy and tumor tissue. A recent comprehensive review suggested that the pro-survival functions of JNK outweigh their pro-apoptotic functions in cancer development (Weston and Davis 2007; Wu et al. 2019). Similarly, c-Jun is regarded as a proto-oncogene product, but some evidence suggests that c-Jun might also elicit tumor suppressive functions (Mariani et al. 2007; Shaulian 2010). Arguably, despite all controversy, the strong evidence for the negative correlation of SELENBP1 levels and cancer progression are evidence that activation of the JNK-c-Jun pathway can indeed be associated with tumor suppression. Also, *Wang et al.* provided further evidence for the validity of these findings. Similar to *Ying et al.*, they demonstrated that increased SELENBP1 levels were associated with increased JNK1 phosphorylation, decreased cyclin D1 phosphorylation and decreased β-catenin abundance in tumor cells (Wang et al. 2015).

Evidence of SELENBP1 taking part in cell proliferation and apoptosis was further shown in SMMC7721 HeLa-derived cells. Depletion of SELENBP1 via siRNA strongly increased the rate of cell migration using transwell- and wound healing assays. Moreover, it also resulted in better cell proliferation and less apoptosis under conditions of elevated oxidative stress (Huang et al. 2012). Experiments in HCT-116 cancer cells showed similar results. Overexpression of SELENBP1 resulted in diminished cell proliferation and increased apoptosis with H_2O_2 treatment as well as reduced cell migration under normal culture conditions (Pohl et al. 2009).

Even in simpler organisms, SELENBP1 might be involved in tissue differentiation and development. In the plant *Lotus japonicus*, a SELENBP1 homolog is abundantly expressed and was found to be highest in developing tissue (Flemetakis et al. 2002). Moreover, *Feng et al.* reported a shift in spatial expression of SELENBP1 expression during embryonic development in zebrafish, but unfortunately did not provide further evidence on the direct contribution of SELENBP1 (Feng et al. 2018).

Collectively, it seems that SELENBP1 abundance in healthy tissue is associated with a higher degree of differentiation, whereas in cancer, low abundance of SELENBP1 suppresses markers of cellular differentiation, which might arguably be a mechanism for cancer cells to de-differentiate further and to grow more invasive.

1.5.8 SELENBP1 participates in stress response and inflammation

An extensive study on the participation of SELENBP1 in inflammation and stress response was performed by *Bai et al.*. They first identified miRNA-122 as a negative regulator of

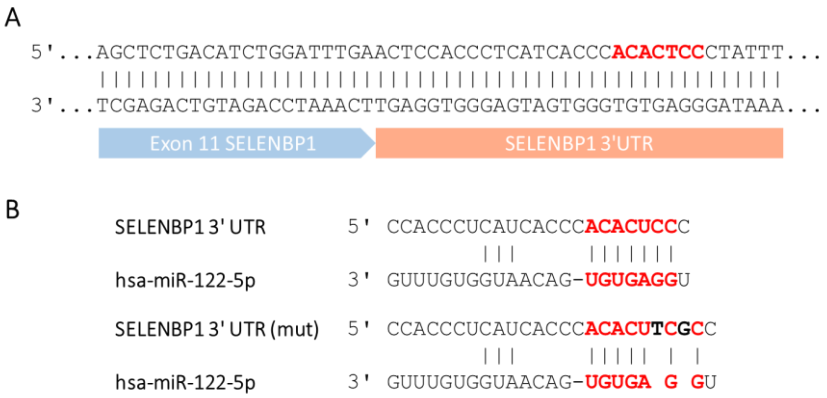

Figure 2 Binding site of hsa-miR-122-5p micro RNAi to the genomic locus of SELENBP1
(A) Human (hsa) miR-122-5p binds to a seven base pair sequence in the 3'UTR of SELENBP1 coding sequence (red). (B) Figure shows the predicted binding site of SELENBP1 and hsa-miR-122-5p using *TargetScan* and the effect of insertion of thymin (T) and guanine (G) at position six and eight of the predicted binding sequence on 3'UTR of SELENBP1. Figure was adapted from (Bai et al. 2019).

SELENBP1, diminishing protein and mRNA levels compared to the control treatment and validated its predicted binding site to be in position 19-25 of the SELENBP1 3'UTR. They measured SELENBP1 luciferase activity of a mutated versus a non-mutated version of SELENBP1 3'UTR and showed that the predicted binding site was responsible for the regulation of SELENBP1 by miRNA-122. (Figure 2) (Bai et al. 2019).

Regarding stress response, they demonstrated a strong, negative correlation of SELENBP1 levels with markers of inflammation and oxidative stress. SELENBP1 was higher in inflamed intestine of patients with Crohn's disease compared to patients with no inflammation, which was comparable to intestine of healthy controls. In the human intestinal epithelial cell line HT-29, SELENBP1 protein levels were positively associated with increased ROS levels caused by H_2O_2 treatment and declining levels of *manganese-dependent superoxide dismutase* (SOD2). A similar correlation was shown between the antioxidant enzyme GPX1 and SELENBP1 (see 1.5.4). Depletion of SELENBP1 attenuated the expression of pro-inflammatory cytokines (IL-6,

IL-8), the abundance of markers for oxidative stress (malondialdehyde, 8-hydroxydeoxyguanosine) as well as ROS levels, caused by H_2O_2 treatment. They further showed that SELENBP1 depletion significantly dampened the activation of the *nuclear factor 'kappa-light-chain-enhancer' of activated B-cells* (NF-κB) pathway caused by H_2O_2 treatment. Moreover, protein levels and phosphorylation of the NF-κB subunit p65 were strongly attenuated after SELENBP1 siRNA treatment and also measured elevated levels of the NF-κB inhibitor IκB and decreased levels of the NF-κB target gene ICAM. Pretreatment with miRNA-122 alone, performed very similarly and a combination of both, *SELENBP1* RNAi and miRNA-122, amplified these effects, further validating SELENBP1 as a target of miRNA-122. Analogous results were obtained studying mice intestine with trinitrobenzene sulfonic acid-induced colitis. Treatment with the miRNA-122 inhibitor, elevated SELENBP1 levels and was associated with a greater abundance of the same markers of inflammation and oxidative stress as before, as well as reduced glutathione levels (GSH).

In another study, depletion of *SELENBP1* RNAi showed a protective effect against ROS in HeLa cells. Untreated and hydrogen peroxide-treated cells had lower levels of oxidative stress if they were treated with *SELENBP1* RNAi before, compared to cells treated with control RNAi. Moreover, SELENBP1 depleted cells showed a better survival in the presence of three toxic compounds (paraquat, H_2O_2, camptothecin), compared to control cells (Zhao et al. 2016).

In summary, these data clearly demonstrate an important role of SELENBP1 in the production of reactive oxygen species, generated by different sources, and the onset of inflammation triggered thereby. Furthermore, this demonstrates that SELENBP1 seems to be under constant regulation of miRNA-122 and that these two act antagonistically in a pro-inflammatory context (Bai et al. 2019).

1.5.9 Dysregulation of SELENBP1 expression in patients with schizophrenia

Schizophrenia is a complex of symptoms affecting perception, thinking or affectivity and is classified as a kind of psychosis. The underlying biological mechanisms remain unclear to this date. A leading hypothesis in the pathophysiology is the disturbance of dopaminergic or glutamatergic neurotransmission involving NMDA receptors. Inflammation was recently discussed as being an important factor in schizophrenia as well. Type 1 cytokines, mediating the immune response against intracellular pathogens, have been found to be decreased in

schizophrenic patients (*interleukin 2*, *interferon-gamma*) whereas type 2 cytokines (*interleukin 6*, *interleukin 10*), involved in B cell maturation and extracellular pathogens, were measured more abundantly in schizophrenic patients (Brisch et al. 2014; Müller et al. 2015; Müller and Schwarz 2006).

As reported before, SELENBP1 was shown to be involved in inflammatory responses (Bai et al. 2019). Also, some studies report a dysregulation of SELENBP1 in schizophrenic patients. *SELENBP1* gene expression was increased in peripheral blood cells and tissue from dorsal prefrontal cortex of schizophrenic patients compared to subjects with no psychiatric disorder. Being the highest regulated gene in brain tissue, antibody staining of four case-control sets showed an increased intra-glial and a decreased intra-neuronal staining for SELENBP1. However, the possible implications for brain function remain unclear (Glatt et al. 2005). SELENBP1 protein levels were among the highest upregulated proteins in red blood cells of schizophrenic patients in another study. This was associated with the modulation of other proteins involved in oxidative stress (PRDX-5, glutathione-S-transferase, heat-shock protein 70). Interestingly, in liver samples from the same patients, SELENBP1 was one of the most down-regulated proteins together with copper-dependent superoxide dismutase and heat-shock protein 60 kDa, possibly indicating different modes of action in brain and peripheral organs in schizophrenia (Prabakaran et al. 2007). Similarly *Udawela et al.* showed that SELENBP1 expression was increased in several parts of the cerebral cortex of schizophrenic patients (Udawela et al. 2015).

Up to now, there is no causal relationship of SELENBP1 expression and the onset of schizophrenia. However, the increased expression of SELENBP1 in the brains of patients with schizophrenia and the dysregulation of reactive oxygen species and inflammation by SELENBP1 in other tissues, leave room for the hypothesis that elevated SELENBP1 levels might contribute to a pro-inflammatory milieu in the brain, fostering the onset of schizophrenia.

1.6 The model organism Caenorhabditis elegans

Caenorhabditis elegans (*C. elegans*) is an invertebrate eukaryote, classified as a nematode and belongs to the family of rhabditidae. It was first used as a model organism to study neuronal development by Sydney Brenner in 1963. It is one millimeter in length, a soil living organism

and mainly found on organic material, rich in microorganisms. Under laboratory conditions, *C. elegans* is usually cultivated at temperatures between 15–25 °C on the nutrient-rich agarose *nematode growth medium* (NGM) and supplied with *E. coli* OP50 as standard food source. At 20 °C, it develops in a matter of three to four days from an egg to adulthood and has an average lifespan of approximately 20 days, once fully developed. It reproduces as hermaphrodite, each worm generating a progeny consisting of a total of around 300 worms, making it possible to investigate large populations at the same time. In its life cycle, the nematode develops through four different larval stages, L1–L4, before reaching adulthood. *C. elegans* begins its life at the L1 larval stage after hatching from the fertilized egg. If worms hatch in the absence of food, they go into L1 arrest. In this stage, no morphological or developmental changes occur, and worms will develop further into L2 larvae once food is available. If, during the development of L1 to L2 larvae, worms experience severe stress, e.g. heat, limited food or live in a very crowded area, worms will develop to dauer larvae through the L2d larval stage. Morphological changes in the cuticle occur and intracellular stress resistance rises to adapt to harsh conditions and worms stop to consume food. In this stage they can survive up to four months, about four times longer than the average lifespan of the nematodes. Once conditions

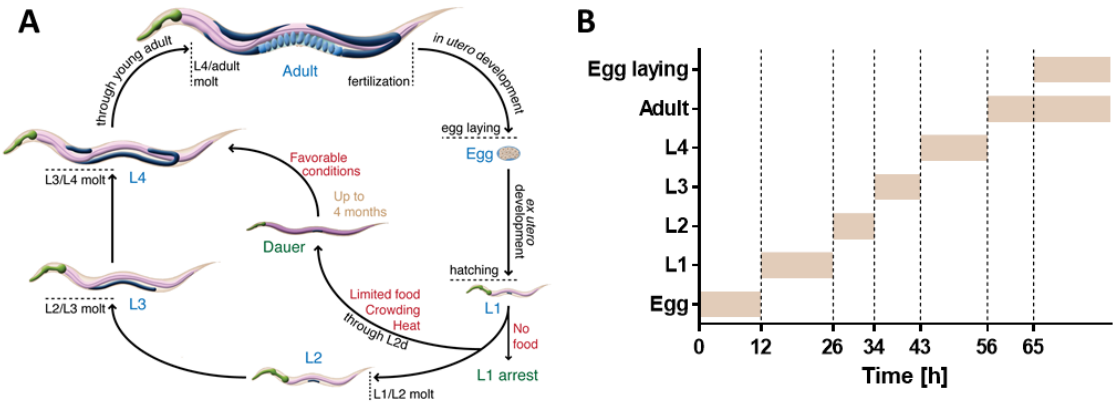

Figure 3 *C. elegans* life cycle and period of each larval state
(A) Life cycle of *C. elegans* according to (Altun and Hall, 2006). Figure adapted from (Erkut, 2014). **(B)** Diagram of the periods of the different larval stages starting from the laid egg as timepoint zero, based on data from (Byerly et al., 1976).

become more favorable, worms develop further into L4 larvae, skipping the L3 larval stage (Altun and Hall 2006; Byerly et al. 1976; Erkut 2014; Hu 2007).

The *C. elegans* embryonic cell lineage has been fully traced, meaning the origin and fate of every cell, from zygote to the adult worm, is known (Sulston et al. 1983). Studying this was

possible because of the transparent body wall which enabled the researchers to investigate each organ and even each cell individually, using live cell imaging and fluorescent probes. All the aforementioned features make *C. elegans* a versatile model for studying many aspects of life including aging processes, metabolism, redox homeostasis or cell differentiation and development.

1.6.1 Anatomy and function of the epidermis

The epidermis (old: hypodermis) is a multicellular epithelium which surrounds the worm and covers almost the entire length of the worm. In the adult worm it is mainly made up of two adjacent multinuclear cells (syncytia), the epidermal cell 7 (hyp7, 139 nuclei) and the seam cells (16 nuclei), which run along the lateral sides of the worm and are engulfed by the hyp7 syncytium. Proximally, the epidermis is covered by a basal lamina which is bounded by the pseudocoelom, a fluid-filled space which fills the *C. elegans* body cavity and thereby also enables indirect contact between other organs like the intestine or the gonads (Altun and Hall 2002). The epidermis secretes the cuticle, a flexible exoskeleton made up of different kinds of collagens, expressing a distal glycoprotein layer. The cuticle defines the shape of the worm, protects *C. elegans* from the environment and enables locomotion through its attachment to body wall muscles. The epidermis itself is important for early developmental processes, for guiding cell migration or for regulating cell fate and has been regarded as an important organ for nutrient storage. It was also reported to be involved in innate immune response and wound healing. It therefore seems unsurprising that, despite its function as the skin of *C. elegans*, transcriptome analysis showed that its gene expression pattern correlated better with blood plasma than with human skin and also well with human liver, T-cells and neutrophils (Kaletsky et al. 2018; Taffoni and Pujol 2015; Zhang et al. 2015).

Epidermal cells descend from AB founder cells which also give rise to seam and neuronal cells (Figure 4). The close phylogenetic relationship between epidermal and neuronal cells was demonstrated by *Labouesse el a.* in a *lin-26(n156)* allele – lin-26 is regarded as a cell-fate regulator – and showed that epidermal cells of *lin-26(n156)* mutants, developed a neuron-like morphology and produced neuron-like cells after division (Altun and Hall 2002; Labouesse et al. 1994, 1996). There is also increasing evidence that the epidermis can affect neuronal function, potentially by affecting ion homeostasis or by providing yet unidentified signals (Chisholm and Xu 2012). Moreover, it was demonstrated that a non-canonical DBL-1/TGFβ

pathway is activated in the epidermis upon pathogenic infection. Strikingly, the DBL-1 ligand is mainly expressed in the nervous system and only at low levels in the intestine, suggesting that there might be a paracrine signaling pathway from the nervous system to the epidermis (Zugasti and Ewbank 2009).

1.6.2 *C. elegans* neurons

Three hundred two out of 959 cells in the adult worm are neurons, making it the biggest group of cells in the nematode. As seen in Figure 4, neurons, like epidermal cells, arise mostly from the AB lineage. Except for pharyngeal neurons, which have direct contact to the body muscles, somatic neurons are mostly bounded from the muscles by the epidermal basal membrane. They can be categorized into three functionally different classes. First of all, motor neurons, which have synaptic contact to the body wall muscles and control locomotion. Most of the motor neurons posterior of the pharynx are positioned longitudinally along the ventral side of the *C. elegans* body, in the ventral nerve cord and send commissures to the dorsal cord. Secondly, interneurons, which receive and send signals to other neurons and lastly, sensory neurons. With them, *C. elegans* is able detect several different types of stimuli. Among them are chemicals (taste), odors (smell), oxygen and carbon dioxide, pain (nociception), mechanical force, temperature and osmolarity.

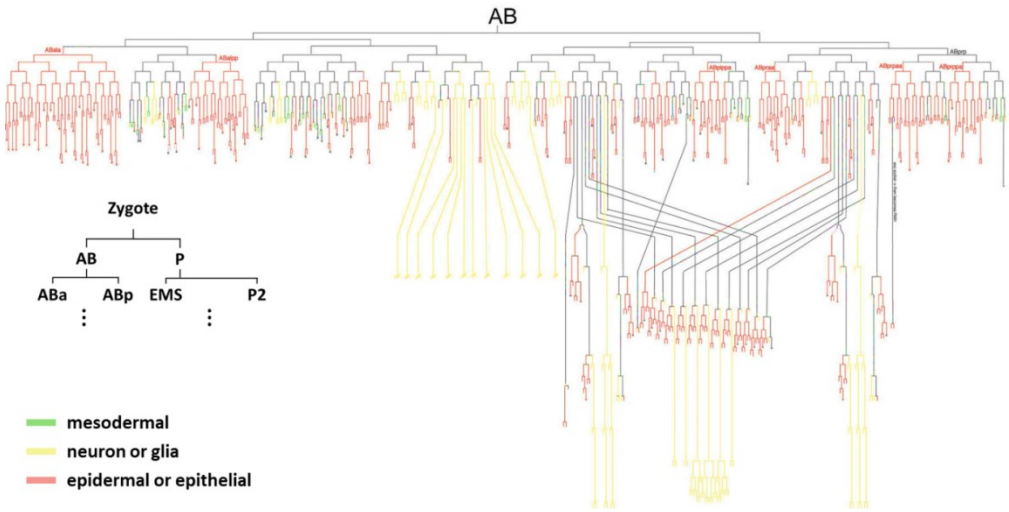

Figure 4 Lineage of the AB founder cell during embryonic development of *C. elegans*
The AB founder cell, which arises from the first division from the zygote, divides and differentiates to mainly to epidermal of epithelial (red), neuronal (yellow) and mesodermal cells (green). Modified and adapted from (Hobert, 2010).

This is collectively accomplished by neurons which belong to a sensillum (sensillar) and by those which function separately (non-sensillar). In *C. elegans*, the sensillum is a sensory organ,

each comprised of one or more sensory neurons, which projects a ciliated dendrite to the tip of the mouth, with its endings surrounded by glia-like socket- and a sheath cells. The sensillar neurons are mainly located in the head e.g. amphid neurons (posterior to the nerve ring) or the tail (phasmid neurons). The socket cell is connected to the epidermis and the sheath cell and creates a torus-shaped pore for the cilia to reach the environment. An exception of this are for example the AFD sensilla. Their dendrites end in the sheath cell near the tip of the mouth

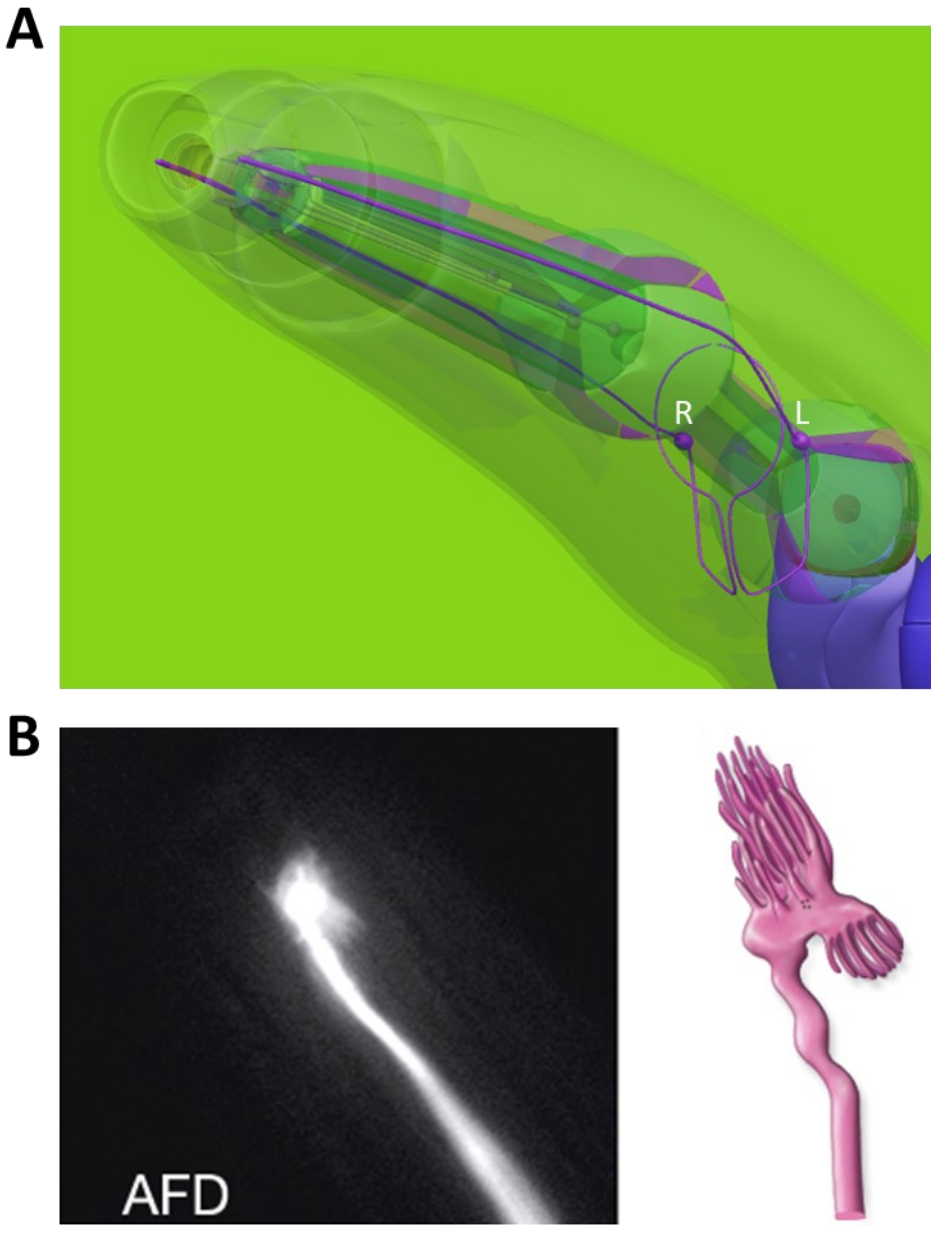

Figure 5 AFD neurons and cilia morphology
(A) 3D model of the head region of *C. elegans* showing AFD neurons in purple. AFDL (L), AFDR (R). Model adapted from the "OpenWorm project" (Szigeti et al. 2014)
(B) Left picture shows epifluorescent image of the ciliated dendrite of one AFD neuron using a *gcy-8*::GFP reporter. Right picture shows schematic of AFD cilia. Pictures are based on (Ward et al., 1975) and modified from (Altun and Hall, 2003).

but do not reach the outside. Instead, they terminate in a cilium which is surrounded by many villi and a sheath cell (Altun and Hall 2003).

1.6.2.1 AFD neurons

AFD neurons are the *C. elegans* primary thermo-sensors. They belong to the amphid neurons and are located anteriorly to the nerve ring. Their axons travel to the ventral nerve cord through the amphid commissure to the nerve ring, where they meet each other at the dorsal midline (Szigeti et al. 2014) (Figure 5A). Their dendritic endings are ciliated and are covered in microvilli, which give it a characteristic, bush-like appearance (Figure 5B).

Proteins for transduction of thermo-signals include AFD-specific guanylate cyclases (GCY-8, GCY-18, GCY-23) and cation channels (TAX-2, TAX-4), which are also present on other ciliated neurons. Temperature shifts are believed to activate guanylate cyclases which produce cGMP from GTP. This then triggers a calcium influx and cellular depolarization, mediated by the activation of the cGMP-gated cation channels TAX-2 or TAX-4. This is believed to activate post-synaptic neurons like AIY to trigger thermotaxis behavior for avoidance of noxious temperatures and to trigger a heat shock response in the soma (Goodman and Sengupta 2018; Prahlad et al. 2008). Signals in AFD neurons involving GCY-8 have been shown to trigger a heat shock response in the germ line and the soma, where heat shock proteins are expressed upon activation of the major transcription factor in heat shock response, HSF-1 (Prahlad et al. 2008; Tatum et al. 2015; Vihervaara and Sistonen 2014).

This may be linked to the influence of AFD neurons on *C. elegans* lifespan, as demonstrated by *Lee and Kenyon*. They showed that HSF-1 depletion resulted in a dramatic shortening of lifespan, but only at low temperatures (15 °C). At high temperatures (25 °C) or after ablation of AFD neurons, lifespan of *C. elegans* was shortened. This did not require functional DAF-2/DAF-16 signaling but was mediated by the *cytochrome P450* DAF-9 and the *nuclear hormone receptor* DAF-12. As hypothesized by *Lee and Kenyon*, high temperatures decrease the levels of daf-9. This in turn lowers the production of dafachronic acids produced by DAF-9, which are considered DAF-12 ligands. Thereby the activity of DAF-12 is lowered, which normally promotes premature aging at high temperatures after binding of dafachronic acids (Jeong et al. 2012; Lee and Kenyon 2009). DAF-9 however, is not expressed in AFD neurons or other sensory neurons but is strongly expressed in the epidermis, and in spermatheca of hermaphrodites (Gerisch et al. 2001). It is believed that temperature sensing neurons send

signals to interneurons like AIY, which in turn affect *DAF-9* expression in the epidermis by a yet unknown mechanism (Lin et al. 2017).

1.6.2.2 BAG neurons

BAG neurons are part of the oxygen and carbon dioxide detecting machinery. They are, however, not part of the amphid sensillum. They project dendrites which travel mouth-wards and end near the lateral lips in a bag-like structure, not reaching the outside (Figure 6B). BAG

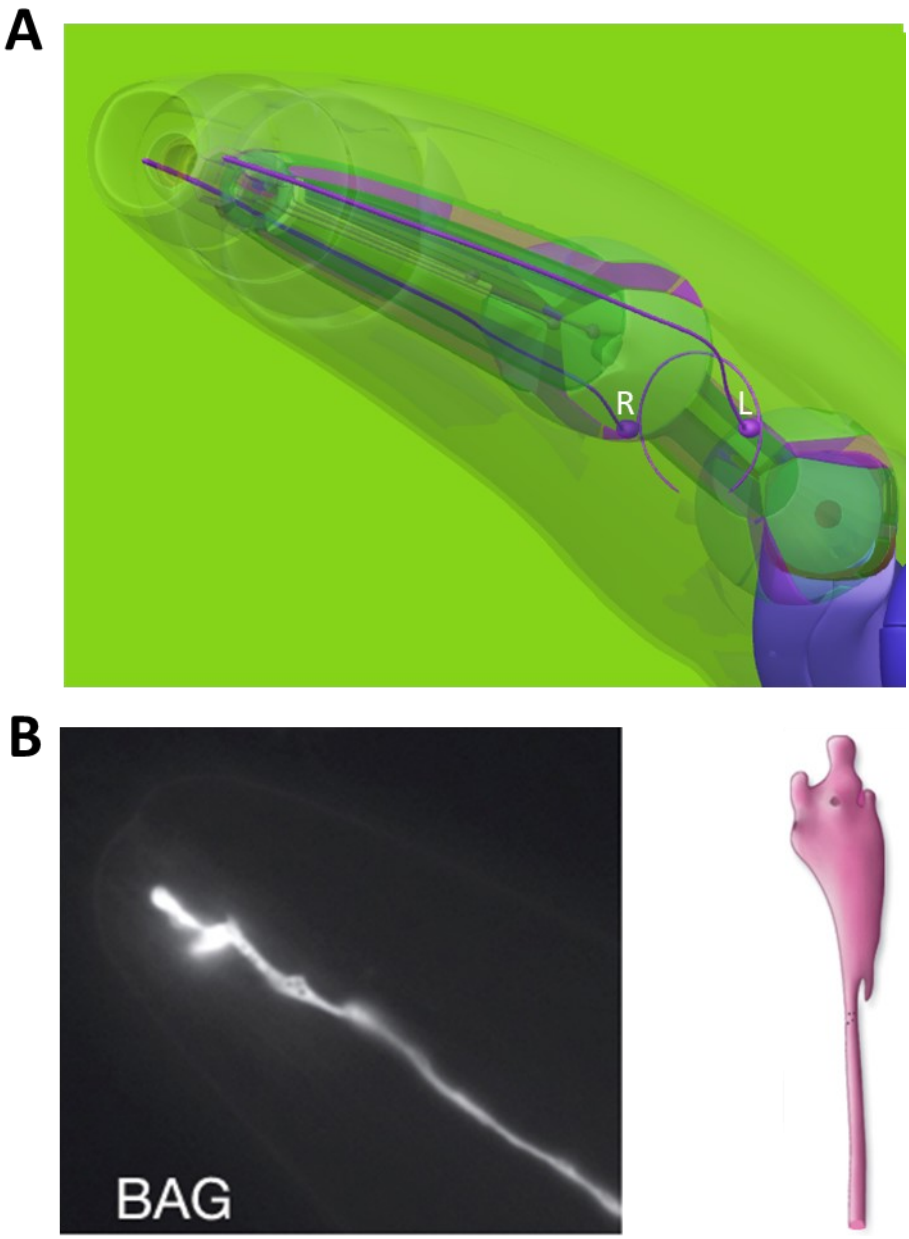

Figure 6 BAG neurons and cilia morphology
(A) 3D model of the head region of *C. elegans* showing BAG neurons in purple. BAGL (L), BAGR (R). Model adapted from the "OpenWorm project" (Szigeti et al. 2014)
(B) Left picture shows epifluorescent image of the ciliated dendrite of one BAG neuron using a *gcy-33*::GFP reporter. Right picture shows schematic of BAG cilia. Pictures are based on (Ward et al., 1975) and modified from (Altun and Hall, 2003).

neurons are located anteriorly to the nerve ring, more distally than AFD neurons (Figure 6A) (Szigeti et al. 2014).

For the perception of atmospheric O_2 levels, BAG neurons work closely together with URX neurons. At normal atmospheric oxygen levels (21 %), URX are held constantly active via the soluble guanylate cyclase GCY-36. At low oxygen levels (10 %) *Hussey et al.* demonstrated that activation of GCY-33 in BAG neurons was important for signal transduction, increasing the release of the neuropeptide NLP-17 in BAG neurons. This was reported to activate the receptor EGL-6 on URX neurons, which in turn repressed GCY-36 via the g-protein GPA-8 (Hussey et al. 2018).

Additionally, BAG neurons are involved in carbon dioxide avoidance; however, little is known about the mechanism behind the process. It was suggested that other neurons such as AFD, ASH, AWB, ADL and possibly more, work together to help *C. elegans* avoid elevated atmospheric CO_2 levels (Fenk and de Bono, 2015; Hallem and Sternberg, 2008). Among others, the cation channels TAX-2 and TAX-4 seem to be essential for the signal transduction. However, CO_2 avoidance seems to be more complex, since modulations in energy status, insulin- or TGFβ signaling also alter the ability of *C. elegans* to sense changes in CO_2 levels (Fenk and de Bono 2015; Hallem and Sternberg 2008).

BAG neurons are also able to modulate lifespan as was demonstrated by *Liu and Cai*. They showed that ablation of BAG neurons or inhibition or the guanylate cyclases GCY-31 and GCY-33 prolonged lifespan, whereas ablation of URX neurons or inhibition of GCY-35 or GCY-36 decreased lifespan. Furthermore, inhibition of URX neurons completely abolished the lifespan extension of *gcy-31* and *gcy-33* RNAi, demonstrating the importance of the BAG/URX network for lifespan regulation. Moreover, oxygen lower than atmospheric levels increased lifespan, whereas oxygen higher than atmospheric levels decreased lifespan. The effect of oxygen levels on lifespan, however, seems to be independent of BAG and URX neurons, since the lifespan phenotype of BAG or URX inactivation was still present at different oxygen levels. Interestingly, as demonstrated for AFD neurons, BAG and URX neurons modulated lifespan independent of DAF-2/DAF-16 pathway (Liu and Cai 2013).

1.6.3 Regulation of lifespan and stress response in *C. elegans*

Being a soil living organism, *C. elegans* needs to be able to protect itself against many kinds of environmental stressors. For this, well conserved cellular defense mechanisms are activated. One of the major pathways to improve resistance against environmental stress is the DAF-2/DAF-16 pathway. The signal transduction resembles the InsR/FoxO of mammals very closely, where the activation of InsR promotes a phosphorylation cascade, which at the end inhibits FOXO by phosphorylation and leads to its nuclear exclusion. Inactivation of InsR, inhibits the phosphorylation of FOXO, which leads to its nuclear accumulation and triggers the expression of genes which promote stress resistance and longevity (Klotz et al. 2015). DAF-16 is expressed in many tissues including muscle, intestine, neurons and the epidermis. In fact, the epidermis has been proposed to be the major site of DAF-16 activity, because 50 % of all DAF-16 target genes are expressed in the epidermis and 13 % are exclusively expressed there (Kaletsky et al. 2018). DAF-16 mostly regulates gene expression cell-autonomously, meaning in the cell in which DAF-16 is expressed in. However, another important transcription factor for normal lifespan and lipid homeostasis, MDT-15, was hypothesized to provide lipid-based signals by which DAF-16 can influence downstream targets in different tissues (Zhang et al. 2013a). *Rogers at al.* hypothesized that MDT-15 might be essential for DAF-16 dependent lifespan extension, because *mdt-15* RNAi reduced lifespan of long-lived IGF-1 mutants back to that of wildtype animals (Rogers et al. 2011).

GATA transcription factors seem to play a major role in controlling *C. elegans* lifespan and development. The GATA transcription factors ELT-3 and EGL-27 were shown to have little impact on lifespan by themselves; lifespan and stress resistance were shown to be only slightly attenuated in worms depleted of EGL-3 or ELT-27. However, loss of either of those almost completely abolished the strong lifespan extension of long-lived *daf-2* mutants. It was also shown, that GATA motifs are highly enriched in promotors of age-regulated genes, associated to lifespan modulation by the DAF-2/DAF-16 axis. Furthermore, many 'EGL' GATA transcription factors have, in one way or another, been reported to be important for embryonic or larval development. EGL-27 was demonstrated to control cell polarity and cell migration during development (Herman et al. 1999) and mutants, which had a loss of *egl-27*, were shown to exhibit temperature dependent embryonic lethality (Xu and Kim 2012). ELT-5 and ELT-6 controlled ELT-3 expression (Budovskaya et al. 2008) and were also shown to be necessary for

the correct differentiation of epidermal cells (Koh and Rothman 2001). Furthermore, ELT-3 was likewise suggested for being important in embryonic development (Gilleard et al. 1999). Therefore, GATA transcription factors do not only play an important role in development but also take a key role in some aspects of aging in the worm.

1.6.4 Crosstalk between lipid and energy metabolism, and redox homeostasis

The transcriptional co-regulator MDT-15 has been shown to link lipid and energy metabolism with redox homeostasis. In yeast-two-hybrid assays, MDT-15 was shown to bind to several key proteins of these processes such as NHR-49 (Taubert et al. 2006), one of the master regulators of lipid and energy homeostasis in *C. elegans* and SKN-1 (Goh et al. 2014), one of the master regulators of stress response, and was shown to be important for the expression of their target genes. Together with MDT-15, NHR-49 regulates the expression of several key enzymes of lipid desaturation and mitochondrial as well as peroxisomal beta-oxidation (van Gilst et al. 2005). MDT-15 or NHR-49 depletion resulted in accumulation of saturated fatty acids (van Gilst et al. 2005; Taubert et al. 2006). However, different lipid staining methods showed mixed results regarding the accumulation of excess lipid stores (Lee et al. 2016; Taubert et al. 2006). Both MDT-15 and NHR-49 were shown to be modulated by activation of the energy sensor AMPK (AAK-2). Loss of MDT-15 or NHR-49 dampened the AAK-2-dependent increase of oxidative metabolism and the mobilization of lipid stores by lowering the activatability of AAK-2 (Moreno-Arriola et al. 2016).

Both NHR-49 and MDT-15 were shown to be required for normal lifespan in *C. elegans* and were even able to dramatically extend normal lifespan when constitutively active (Lee et al. 2016, 2016; Taubert et al. 2006). This might be due to their contribution in stress response. Both proteins have been shown to be required for normal stress response. Loss of *mdt-15* greatly reduced the survival rate against different sources of oxidative stress (Goh et al. 2014) and loss of either NHR-49 or MDT-15 reduced the basal expression of the important stress response factor GST-4 and inhibited its activation by oxidative stress. It is believed that MDT-15, NHR-49 and SKN-1 together bind the promotor of GST-4 and SKN-1 to trigger and enhance the response to oxidative stress (Hu et al., 2018).

1.6.5 Biological relevance of selenium in *C. elegans*

Whether selenium can be regarded as essential for the nematode *C. elegans* is questionable. Unlike humans, the *C. elegans* genome only encodes a single selenoprotein, TRXR-1. The *C. elegans* TRXR-2, a selenoprotein in humans, has as cysteine in place of selenocysteine, and the remaining mammalian thioredoxin reductase, *trxr-3, C. elegans* does not have. Studies analyzing the effects of selenium on *C. elegans* have tried to measure the outcome of beneficial and toxic concentrations. Despite that, little is known on the minimum requirement of selenium for the nematode. Additionally, different treatment regimens of selenium supplementation make it difficult to draw conclusions on the precise concentration at which selenium elicits its beneficial and toxic effects.

In one study, worms were treated with sodium selenite for 12 h in liquid medium, showing that concentrations below one micromolar did not cause a reduction in survival, whereas treatment with five millimolar resulted in almost no surviving worms. The importance of the mode of selenium administration was demonstrated in the same study, in which worms living on selenium-containing agarose, containing five millimolar selenite, were still almost completely motile after 24 h (Morgan et al. 2010). Nevertheless, treating worms with 5 mM selenite *Estevez et al.* showed that this resulted in neuronal but not muscular damage (Estevez et al. 2012). In a different setup, L1 larvae were treated with selenite for 30 min followed by 48 h recovery. Thereby, they were able to show a dose dependent decline of survival using 10 mM (~30-50 % survival), 20 mM (~10-30 % survival) and 30 mM (~5-15 % survival) selenite. Paradoxically, organic selenium compounds such as selenomethionine (SeMet) and methylselenocysteine (MeSeCys) were taken up more readily by the worms but were far less toxic than selenite. The half-lethal dose of selenite (LD_{50}) was calculated to be roughly 13 mM, whereas the treatment with the organic selenium compounds only resulted in a decline of survival of around 20 % using 50 mM SeMet or MeSeCys (Rohn et al. 2019).

Regarding the contribution of the sole selenoprotein TRXR-1 in the toxicity of selenium, congruent with the results of *Boehler et al.*, *trxr-1* mutants did neither show a reduced nor an enhanced susceptibility to selenite when compared with wildtype worms (Rohn et al. 2018). In a following publication, the group around Julia Bornhorst showed that in non-treated animals as well as in worms which were treated with 100 µM selenite or 100 µM MeSeCys, much of the selenium accumulated in the non-protein fraction, which was similar in *TRXR*-1

mutants, while selenium in the protein fraction did not change noticeably. This was reflected by TRXR-1 levels which were not different in selenium treated worms (Rohn et al. 2019). However, TRXR-1 activity was shown to be modulated by treatment with organic, not inorganic selenium compounds (Rohn et al. 2019).

In nanomolar to low micromolar concentrations, selenium was demonstrated to elicit positive effects. Pretreatment of L1 larvae with 0.01–1 μM selenite resulted in an increased survival rate following pathogenic infection. This was attributed to a much faster induction of genes related to glutathione metabolic processes such as *glutathione S-transferase* (*gst-4*) and *gamma glutamylcysteine synthetase* (*gcs-1*), which were much less expressed in worms without selenium pretreatment (Li et al. 2014a). This is supported by results of *Boehler et al.* which also showed that selenite treatment led to the modulation of glutathione-related genes such as *glutathione S-transferases*, *glutathione disulfide reductase* or *glutaredoxin* (Boehler et al. 2014). In another study, 0.01 μM selenite also improved health parameters. There, the time worms needed to develop to reach adulthood was decreased, the amount of progeny increased and the time until death induced by levamisole was also delayed in the 0.01 μM selenite treatment group (Li et al. 2011). Later, the same lab demonstrated that a similar treatment rendered worms more resistant to different kinds of stressors like juglone, paraquat, H_2O_2 or heat and that selenite-treated worms accumulated fewer oxidants under non-stressful conditions. They showed that the selenite-induced resistance against juglone was dependent on trxr-1 as well as the FOXO3 ortholog DAF-16. Treatment with 0.01 μM selenite led to an increased transcriptional activity of DAF-16, indicated by an increased nuclear accumulation and more abundantly expressed DAF-16 target genes (*SOD-3*, *HSP-16.2*) (Li et al. 2014b). Similarly, *Rohn et al.* showed that pretreatment with different selenium compounds (100 μM), especially organic selenium compounds, ameliorated the production of tert-butyl-hydroperoxide-induced reactive oxygen and nitrogen species (as assessed using Carboxy-DCFH-DA) (Rohn et al. 2019).

In summary, it seems that, depending on the time point of administration and the nature of the selenium compound, low nanomolar to micromolar concentrations of selenium can be regarded as beneficial doses for *C. elegans*, scavenging reactive oxygen species and stimulating redox signaling processes. Acutely toxic effects seem to manifest at high micromolar to low millimolar concentrations. However, these concentrations are unlikely to be reached in natural

environments with an average selenium content in soil of 0,4 mg/kg to 20 mg/kg (Floor and Román-Ross 2012). Furthermore, the sole selenoprotein TRXR-1 does not seem to participate in the protection from selenium accumulation or its toxic effects but shows an increased activity under moderate exposure with organic selenium compounds.

1.7 Hydrogen sulfide production *in vivo*

The recovery of cysteine from homocysteine is achieved by transsulfuration in which the thiol group of homocysteine is transferred to serine to yield cysteine. The first step in this reaction, the fusion of homocysteine and serine to cystathionine, is catalyzed by *cystathionine-β-synthase* (human: CBS). The subsequent cleavage of cystathionine to α-ketobutyrate and cysteine is performed by *cystathionine-γ-lyase* (human: CTH). Both enzymes need pyridoxal phosphate (PLP) as a co-factor to perform this reaction.

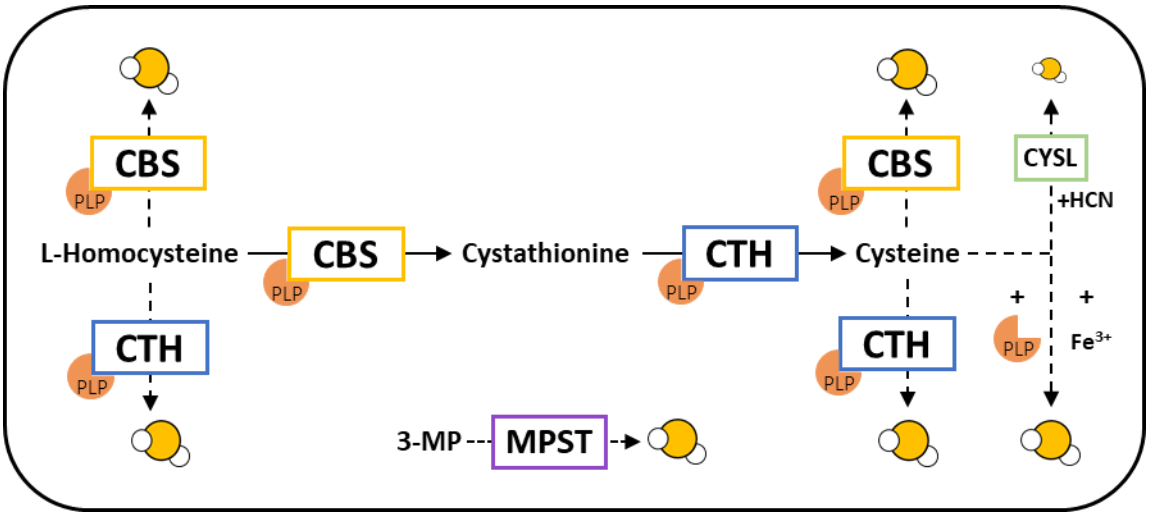

Figure 7 Major contributors to hydrogen sulfide production
The main contributors to hydrogen sulfide ( ) production *in vivo* are enzymes of the transsulfuration pathway, *cystathionine-γ-lyase* (human: CTH) *cystathionine-β-synthase* (human: CBS), needing pyridoxal phosphate ( ) as co-factor. These enzymes are also the main contributors to H_2S production and use cysteine or homocysteine as substrates. The cleavage of H_2S from cysteine can also be catalyzed by the bifunctional *L-3-cyanoalanine synthase/cysteine synthase* enzyme (*C. elegans*: CYSL) using hydrogen cyanide (HCN) or non-enzymatically by Fe^{3+} and PLP. Another major contributor to endogenous H_2S production is *mercaptopyruvate sulfurtransferase* (human: MPST), producing H_2S from 3-mercaptopyruvate (3-MP). Adapted from (Hine et al., 2015; Yang et al., 2019).

These enzymes have also been recognized as major contributors to hydrogen sulfide (H_2S) production *in vivo*, mainly using cysteine and homocysteine as substrates. H_2S is a small sulfur-containing molecule which is reported to be involved in cell signaling, in neuroprotection and exerting anti-oxidant activity, and has been shown to be able to dramatically improve the lifespan of *C. elegans* (Han et al. 2019; Miller and Roth 2007). There are some other enzymes

contributing to H_2S production; the bifunctional *L-3-cyanoalanine synthase/cysteine synthase* enzyme (*C. elegans*: CYSL), which also is able to produce H_2S from cysteine but is not expressed in humans and *mercaptopyruvate sulfurtransferase* (human: MPST), generating H_2S from 3-mercaptopyruvate (3-MP). Moreover, a non-enzymatic reaction involving pyridoxal phosphate and Fe^{3+} was also recognized as another major source of hydrogen sulfide production (Figure 7) (Hine et al. 2015; Kabil and Banerjee 2014; Yang et al. 2019).

1.8 SELENBP1 orthologs Y37A1B.5 and R11G10.2 are modulators of *C. elegans* lifespan

Y37A1B.5 and R11G10.2 were previously shown to be negative regulators of *C. elegans* lifespan because depletion via RNAi resulted in an increase of mean and maximum lifespan, as well as an improved resistance to oxidative stress (Figure 8). Furthermore, using *daf-16* or *skn-1*-deficient strains, it was shown that the lifespan extension was still present (not shown), which

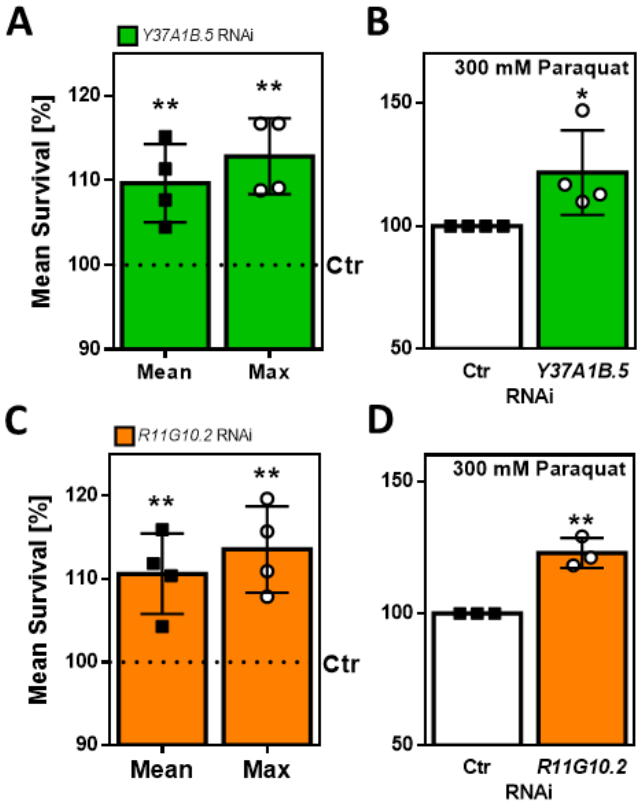

Figure 8 The SELENBP1 homologs Y37A1B.5 and R11G10.2 regulate *C. elegans* lifespan and stress resistance
(A) *Y37A1B.5* RNAi increased mean and maximum lifespan of wildtype *C. elegans*. **(B)** Pretreatment of worms with *Y37A1B.5* RNAi increased the resistance against oxidative stress induced by paraquat. **(C)** *R11G10.2* RNAi increased mean and maximum lifespan of wildtype worms. **(D)** Pretreatment with *R11G10.2* RNAi increased the resistance against oxidative stress induced by paraquat. Mean lifespan: 50 % survival, max lifespan: day of last living worm. Data are means ± SD of three to four independent experiments. Data adapted from (Köhnlein 2016, Köhnlein et al. 2020).

indicated that the lifespan modulation by Y37A1B.5 and R11G10.2 might be mediated by a non-canonical stress response pathway (Köhnlein 2016).

1.9 Objectives

Selenium is associated with the onset of metabolic disorders and is controversially discussed as a therapeutic in the prevention of cancer. SELENBP1 has emerged as a factor possibly explaining these associations. The strong negative correlation between SELENBP1 abundance in cancer tissue and the clinical outcome of cancer patients as well as the increased progression of cancers with low SELENBP1 levels, have made it a target of recent studies in search for biomarkers of cancer disease. Aside from that, SELENBP1 seems to be involved in the onset of inflammation and cellular redox balance. Moreover, SELENBP1 is dysregulated in different tissues of schizophrenic persons, which leaves room for the hypothesis that SELENBP1 might be involved in the development of schizophrenia by contributing to inflammation.

In *C. elegans,* SELENBP1 orthologs have been established as negative regulators of lifespan and oxidative stress resistance. It can be hypothesized that this displays a mechanism by which cancer cells render themselves more resistant to therapy and might ultimately be a hint as to why cancer cells often show a low abundance of SELENBP1. Therefore, the aim of this study was to determine the function of these proteins and analyze the underlying mechanism regarding the modulation of lifespan and stress resistance of SELENBP1 orthologs in *C. elegans*. The goal was (1) to define the tissue these orthologs are expressed in, (2) to analyze changes in expression during the aging process, (3) to assess the role in redox and selenium homeostasis. Moreover, the goal of this work was to (4) identify genetic regulators of expression as well as (5) downstream targets using transcriptome analysis. Finally (6) genetic null mutants were to be generated to identify the role of the two *C. elegans* proteins in development and tissue differentiation.

2 Materials and Methods

Detailed information about bacterial- or *C. elegans* strains as well as recipes for buffers and media are listed in the appendix of this thesis.

2.1 3D modelling of protein sequences

SELENBP1 as well as Y37A1B.5 and R11G10.2 were modelled using *Protein Homology/analogY Recognition Engine V 2.0* (Phyre²; http://www.sbg.bio.ic.ac.uk/phyre2/html/page.cgi?id=index) (Kelley et al. 2015). In short, the Phyre² algorithm predicts a 3D model by multiple sequence alignment with a number of selected sequences and also predicts the secondary structure using PSIPRED, building a model using the results of both algorithms. This is compared and aligned to proteins of known structure by which the protein backbone is generated. After adding the amino acid side chains, different regions of the model are compared to highly confident existing models. From that, α-carbon distances are calculated after which the new protein is 'synthesized' by a virtual ribosome. The generated .pdb file was modified using ChimeraX (0.9.1; https://www.cgl.ucsf.edu/chimerax/download.html).

2.2 *C. elegans*

Caenorhabditis elegans (*C. elegans*), an invertebrate eukaryote, is classified as a nematode strain and belongs to the family of rhabditidae. In the following, the terms 'worm' or 'nematode' are used as synonyms for *C. elegans*. The wildtype strain N2 Bristol was obtained from the *Caenorhabditis Genetics Center* (CGC) of the University of Minnesota, USA. Y37A1B.5 and R11G10.2 null mutants (PHX2066, PHY2078; see appendix Table 1) were provided by SunyBiotech (Fuzhou, China). Transgenic GFP reporters of Y37A1B.5 (LOK158) and R11G10.2 (LOK128) were generated by David Guerrero-Gómez and Dr. Antonio Miranda-Vizuete (Instituto de Biomedicina de Sevilla (IBIS), Hospital Universitario Virgen del Rocío/CSIC/Universidad de Sevilla, Sevilla, Spain) using plasmids generated by Dr. Pavel Urbánek from the Nutrigenomics lab (Prof. Klotz). All used transgenic strains were made from N2 Bristol.

For cultivation, *C. elegans* was kept on Nematode Growth Medium (NGM Agar) and received an *E. coli* OP50 suspension as standard food source (for all bacterial strains used in this work,

see appendix, Table 2). When RNA interference was performed, dsRNA was delivered by the *E. coli* strain HT115(DE3) harboring a T7-inducible plasmid (L4440) (Figure 11).

To transport the worms between NGM plates for preservation or analysis of stress resistance, a specially prepared platinum spatula was used, which was connected to a glass pipette. In technical jargon, this is often referred to as a *worm pick*.

C. elegans was cultivated at a constant temperature of 20°C. To ensure sterility, all buffers and media used, were sterilized beforehand. The transfer of large amounts of worms by buffer took place in proximity to a propane gas flame. Small number of worms for example during lifespan analyses or stress resistance assays, were transferred manually using the worm pick. To ensure sterility, the platinum spatula was heated with an ethanol flame and cooled by placing it on a worm-free part of the NGM agar before touching the worm.

Maintenance

C. elegans was maintained on NGM agar (see Table 5). In order to keep one strain in culture, five worms of the L4 larval stage (Figure 9) were transferred from an NGM agar plate with a mixed population to an unpopulated agar plate with fresh bacterial lawn. According to the life cycle at 20 °C (see Introduction 1.6.1) worms could be maintained at intervals of four to five days.

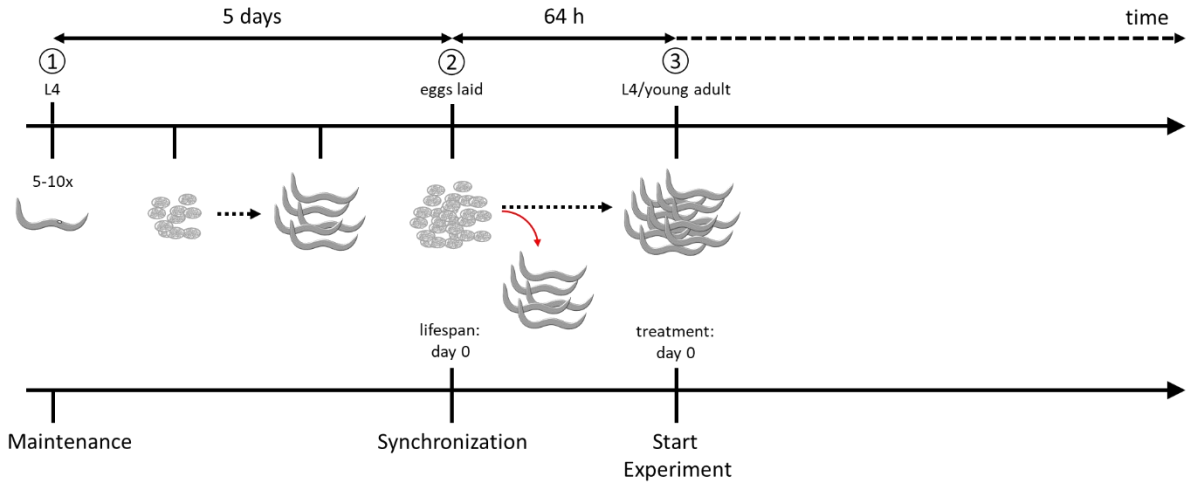

Figure 9 Time course of experiments
At the beginning of each experiment, 5-10 larvae of the L4 larval stage were placed on an NGM plate **(1)**. In the course of five days worms laid eggs, from which further worms developed. Eggs of this were then collected for synchronization which was performed at the beginning of each experiment. The eggs were distributed to fresh NGM plates. This marked day zero for life span analyses **(2)**. Usually, treatment of the worms began 64 h after synchronization **(3)**. Dashed arrow: development to, red arrow: discarded.

Synchronization

In order to ensure that the population was at the same stage of development during each experiment, worms were synchronized. For this purpose, a worm culture five days after maintenance was used. First, all worms were removed from the agar plates. The remaining eggs were then separated from the NGM plate using an L-shaped glass pipette and collected in a reaction vessel. Several washing steps were performed, consisting of centrifugation (1300 g) and exchange of the medium. The eggs, now cleaned of bacteria, were finally spotted on NGM agar. 64 hours after synchronization, worms had reached the young adult larvae stage and were usually used for the experiments. Ultrapure water was used for the collection and washing of the eggs.

For the observation of worm morphology during different larval stages, worms were synchronized by inducing L1-arrest. Eggs were prepared as described before and were pipetted into 25 ml M9 medium in a 50 ml reaction vessel. Worms were allowed to hatch overnight and were distributed to NGM plates spotted with bacteria after confirming that all worms were at the L1 larval stage.

Cryopreservation

C. elegans is suitable for long-term storage at a temperature of -80 °C in a medium containing 15 % glycerol (see Appendix Table 5). This made it possible to store different strains when not needed. For freezing, an NGM plate containing many L1 and L2 stage and which almost depleted the bacterial lawn was used. Worms were collected in a reaction vessel with S-basal and washed once. The supernatant was removed, leaving 3 ml of suspension and mixed with freezing medium containing 30 % glycerol at a ratio of 1:1. The freezing medium, containing the worms, was then aliquoted to 1 ml each, into cryogenic tubes. Slow freezing was ensured by placing the cryogenic tubes in a polystyrene box at -80 °C.

When needed, a cryopreserved strain was thawed quickly and then washed once in S-Basal at 20 °C. The thawed worms were transferred to NGM agar and screened for alive worms during a period of several days.

Bleaching

In order to remove any bacterial contamination during synchronization the worm suspension, which had been collected during synchronization, was treated with a bleaching solution (see

Appendix Table 5) for 30 seconds. Several washing steps were then performed to reduce the concentration of the bleach to a minimum, after which the eggs were transferred to NGM agar plates.

Liquid transfer

For the analysis of protein or RNA fractions, large amounts of worms were required. These were cultivated on multiple 90 mm NGM agar dishes. In order to avoid starvation of the experimental population and to remove offspring, worms were transferred to fresh plates daily, using S-Basal buffer. First, the worms were separated from the plates and collected in a 15 ml reaction vessel. Several washing steps were carried out in which the smaller and lighter offspring were separated and discarded by gravity from the initial population. Finally, the buffer was removed, leaving a few hundred microliters of suspension, and the nematodes were distributed to fresh NGM plates, spotted with bacteria.

Harvest

To analyze biochemical parameters, worms were collected (harvested) at certain times during an experiment. The harvesting process was performed similarly to the regular liquid transfer but was carried out at 4 °C in order to slow down the metabolism of the nematodes and prevent possible changes in gene expression during the process. After removal of bacteria and offspring, worms were transferred to an ice-cooled 1.5 ml reaction vessel. The supernatant buffer was removed, and the reaction vessel was frozen in liquid nitrogen and finally stored at -80 °C.

Selenite resistance assay

To evaluate the toxicity of selenite and the effect of RNAi treatments on the susceptibility of nematodes towards selenite, worms were treated with RNAi for 72 h starting at the egg stage. For treatment of the worms, each well of a sterile, 96-well plate was filled with 100 µl of a "10x" suspension of heat-inactivated bacteria (see 2.3). Roughly 50 worms were transferred to each well manually using a worm pick. Then, 50 µl of 10x heat inactivated bacteria suspension containing the appropriate amount of selenite (i.e. three times higher than final concentration; Sigma Aldrich, #S5261) was pipetted into each well. Worms were exposed to sodium selenite for 17 h while shaking at 900 rpm on an orbital shaker. Following treatment, worms were transferred to NGM plates without bacteria. The liquid was allowed to dry (5–10 min) and

worms scored directly afterwards. Each treatment, as well as each experiment, was performed in triplicates.

Heat resistance assay

Worms were pre-treated with RNAi for five days starting at young adult. On day five, a closable polystyrene box containing several 'hot-cold packs' and a 55 mm NGM agar plate with 100 µl 10x heat inactivated bacteria for each treatment was pre-heated to 37 °C in a microbiological incubator (Heraeus B6) for several hours. About 50 worms were then transferred to a pre-heated plate, immediately transferred back to the polystyrene box and placed in back into the incubator at 37 °C for three hours. Afterwards, worms were transferred back to 20 °C for 40 h before being scored.

Microscopy

The inversion microscope (Nikon, Eclipse Ti2) together with the software NIS-Element 4.6 (Nikon) was used to record microscopic and fluorescent images of *C. elegans*. Within one experiment, the settings for exposure time and gain were kept constant. The images were converted into common image formats (.tif, .png) to be displayed in this work.

Preparation of objective slides

In order to analyze *C. elegans* microscopically, the nematodes were mounted an agarose pad containing objective slide (Figure 10). Agarpads were made using a 3 % agarose solution (Thermo Scientific, #15510) in ultrapure water. Objective slides were placed between two so-called 'spacers' – slides which were covered with a transparent adhesive strip lengthwise. One

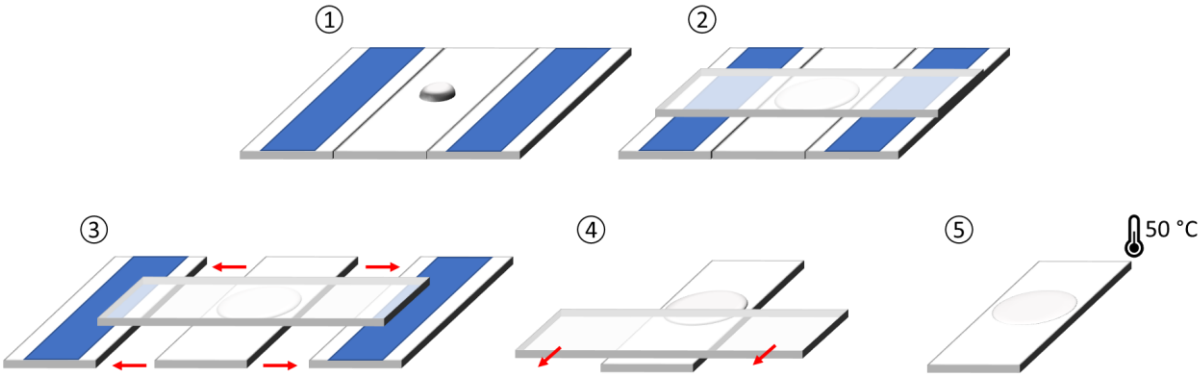

Figure 10 Preparation of objective slides for fluorescent microscopy
(1) An objective slide is placed two spacers taped with adhesive strips (blue). Then a drop of liquid agarose (3 %) is dripped onto the slide. **(2)** The agarose drop is covered with another slide. **(3)** After a short cooling, the spacers are removed. **(4)** The upper slide is gently removed to avoid formation of air bubbles. **(5)** The prepared slide is heated so that excess water would evaporate from the agar pad.

drop of hot agarose was put on the objective slide and covered by another slide. After removing the spacers and the cover, the prepared slide was dried at 50 °C for 1–2 min. The resulting agar pad had a low thickness, suitable for fluorescence imaging.

Measurement of expression using fluorescence microscopy

To analyze the expression of fluorescent nematodes, they were placed on a prepared microscope slide, anaesthetized with 10 mM sodium azide and covered by a coverslip. Pictures of individual worms were taken using brightfield and GFP (ex. 472±30 nm, em. 520±35 nm) channels. For quantification of the GFP signal, fluorescent worms were marked as regions of interest (ROI) using the binary threshold of the GFP signal or manually using the overlaid brightfield image. The total GFP intensity (SumIntensity) and the area of each ROI was then measured. Afterwards, the GFP intensity was normalized to the worm area and subtracted from the background signal to obtain the relative GFP fluorescence intensity for each worm.

Assessment of hydrogen sulfide production

Hydrogen sulfide production was estimated in crude worm lysates using lead acetate-containing agarose (lead acetate: Sigma Aldrich, #215902) and a reaction mixture containing 10 mM L-cysteine (Carl Roth, #1693) as substrate and 1 mM pyridoxal phosphate (Sigma Aldrich, #P9255) as co-factor. This method was adapted from (Hine and Mitchell 2017). To reduce changes of the pH, cysteine was dissolved in 50 mM potassium phosphate buffer (pH 7.4) and pyridoxal phosphate in PBS (Sigma Aldrich, #D8537). The pyridoxal phosphate stock solution was prepared beforehand, stored at -20 °C and thawed when needed. The L-cysteine solution was prepared freshly, every time. Worms were lysed by grinding in liquid nitrogen, using mortar and pestle, together with 50 mM potassium phosphate buffer (pH 7.4), containing protease inhibitors (Carl Roth, #3751). The lysates were collected in a 1.5 ml reaction vessel and allowed to thaw on ice. Afterwards, lysates were sonicated (Sonoplus HD 2070) on ice for three times (power: 50 %, 10s, 3 cycles) and centrifuged (4 °C, 20 min, 12000 rcf). The supernatant was collected, and the protein content was estimated via BCA assay (Thermo Scientific, #23227). Hydrogen sulfide production was determined in a 96-well plate on the same day. For this, 100 µg of protein was mixed with L-cysteine and pyridoxal phosphate to a final volume of 150 µl. The plate was covered with a lid containing 100 mM lead acetate in agarose and incubated for four hours at 37 °C. Afterwards, the amount of lead sulfide

precipitate, which had formed in a reaction of H_2S and lead acetate, was assessed by an imaging system (Biorad, Chemidoc MP) using the built-in volume tool to quantify the pixel intensity per area. Each sample was measured in triplicates.

HPLC analysis of GSH content

Levels of reduced glutathione (GSH) were measured using HPLC and o-phthaldialdehyde (OPA) derivatization. First, worms were collected and frozen. Afterwards, the worms were lysed by grinding in liquid nitrogen, using mortar and pestle, together with using 0.01 N HCl, containing protease inhibitors (Carl Roth, #3751) and sonicated 3-times (settings: 50 % power, 10s, 3 cycles, on ice). After centrifugation, (4 °C, 20 min, 12000 rcf) the supernatant was collected and the protein content was estimated using a BCA assay (Thermo Scientific, #23227). For GSH measurement via HPLC, 50 µl of worm lysate was used. Proteins were precipitated by adding 25 µl 2N $HClO_4$ and was incubated for 10 min on ice. Afterwards 200 µl 0.5M sodium phosphate buffer (pH 7.0) was added for neutralization. The samples were centrifuged for 10 min, 18.000 rcf, 4 °C and 50 µl of that was used for OPA derivatization. 15 µl H_2O and 50 µl OPA (2 % (w/v) in 0.1 M sodium borate, pH 9) were added to the mixture. 20 µl of that were then injected into the HPLC machine (for details, see Table 11). GSH levels were normalized to the protein content of each sample. For each sample, three independent experiments were analyzed. The analysis of the HPLC chromatograms was performed by Katrin Erler from the Klotz laboratory.

RNA isolation

RNA isolation was performed by guanidinium thiocyanate-phenol-chloroform extraction using Trizol® reagent (Thermo Scientific, #15596026). Before isolation, worms (≳1000) were collected and frozen in S-basal (4 °C) and stored at -80 °C until lysis.

At the beginning of the extraction, the frozen worm pellet (≅50 mg) was lysed using 1 ml Trizol® reagent and 0.3 g 1.0 mm zirconia beads (Biospec Products #11079110zx) in a swinging mill (Retsch MM 400; 3 x 1 min, 30 oscillations s^{-1}). Between the milling steps, samples were stored on ice for one minute. Then, chloroform (VWR #83626320) was added, followed by repeated inversion of the reaction vessel and incubation for three minutes at room temperature. After the centrifugation, the upper clear phase, containing the RNA, was transferred to a new reaction vessel and mixed with 1.1x isopropanol and 0.16x 2 M sodium

acetate and centrifuged (12000 rcf, 20 min, 4 °C). The precipitated RNA was washed three times with 80 % ethanol. After the final washing step, the ethanol was removed, and the pellet was dried at room temperature for 5-10 min. The RNA was then dissolved in nuclease-free H_2O (Carl-Roth, #T143) and heated to 65 °C for five minutes to dissolve RNA, put back on ice and was used for cDNA synthesis afterwards.

Isolation of genomic DNA

For isolation of genomic DNA, one plate of adult worms was collected in S-Basal and frozen. For DNA isolation, the worm pellet was thawed on ice and mixed with lysis buffer in a 1:10 ratio, containing 200 mM NaCl (Carl Roth, #3957), 100 mM Tris- HCl (pH 8.0) (Carl Roth, #5429), 50 mM EDTA (Carl Roth, #8043), 0.5 % SDS (Carl Roth, #CN30) and 0.2 mg/ml proteinase K (vivantis, #7037). The mixture was incubated at 65 °C for 30 min and cooled to 37° C. RNAse A (Thermo Fischer, #EN0531) was added to a final concentration of 0.1 mg/ml and the mixture was incubated for another 45 min at 37 °C. Using phenol:chloroform:isoamylalcohol (Carl Roth, #A156) for extraction, the DNA was isolated, and precipitated overnight by adding 2 volumes of 100 % ethanol at 4 °C. After multiple washing steps using 80 % ethanol, the DNA was dried and resuspended in 10 mM Tris-HCL pH 8.0.

RNA quantification

To assess the quantity/concentration of isolated RNA, the absorption value of 2 µl RNA at 260 nm was determined using an LVis Plate (BMG Labtech) in a microplate reader (SPECTROstar® Nano, BMG Labtech) and used to determine the concentration of nucleic acid.

cDNA synthesis

To study mRNA levels, total RNA was first reverse transcribed into cDNA. For this, one microgram RNA was mixed with 25 ng Oligo(dT)18 (Thermo Scientific #SO132) and 10 ng Random Hexamer primers (Thermo Fischer Scientific #SO142). The mixture was then heated with a Mastercycler Ep gradient S (Eppendorf) for annealing of the primers to the RNA (5 min/70 °C, 5 min/4 °C). Subsequently, nuclease-free H_2O (Carl Roth #T143), Reaction Buffer (Thermo Fischer, #K1621), PCR Nucleotide Mix (Thermo Fischer, #R0192) and RevertAid Reverse Transcriptase (Thermo Fischer, #EP0441) were added to the reaction mixture. Reverse transcription was performed as follows: 10 min/ 25 °C, 90 min/ 42 °C, 15 min/ 70 °C. The

obtained cDNA was then diluted with nuclease-free H_2O to 4 ng/µl of the original RNA concentration and stored at -20 °C.

Quantitative reverse transcription polymerase chain reaction (qRT-PCR)

To determine relative gene expression, cDNA amplification was measured via real-time (quantitative) PCR (qPCR). For this, the cDNA was mixed with 200 nm primers for the respective gene and amplified using the program in (Table 10). The amplification of cDNA was followed using *SsoAdvanced Universal SYBR Green Supermix* (Biorad, #1725275) in a CFX Connect Real-Time PCR Detection System (Biorad). To calculate the relative expression differences, the delta-delta-Cq value was calculated (see below). To do so, the Cq value of the treated sample, determined by the program, was subtracted from the Cq value of the reference gene, resulting in the delta Cq value. The delta Cq value of the treatment was then subtracted from the delta Cq value of the respective control treatment to obtain the delt-delta-Cq value. Subsequently, this value was multiplied by -1 and powered by a factor of two to obtain the relative mRNA levels [fold].

$$Relative\ mRNA\ level = \left(\left(\left(Cq_{treatment} - Cq_{reference\ gene}\right) - \left(Cq_{control} - Cq_{reference\ gene}\right)\right) * (-1)\right)^2$$

Calculation of relative mRNA levels from Cq values

Single-worm PCR

To validate the genomic knockouts, single-worm PCR was performed. For this, one adult worm was placed outside the bacterial lawn to remove excess bacteria. The worm was then placed into a drop of worm lysis buffer containing 5mM Tris pH 8.0, 0,5 % Triton X-100 (Carl Roth, #3051), 0,5 % Tween 20 (Carl Roth, #9127), 0,25 mM EDTA, 1 µg/µl proteinase K (20 mg/ml) and was transferred to a 200 µl reaction tube together with one microliter of lysis buffer and spun down using a tabletop centrifuge. The reaction tube was heated to 65 °C for 15 min to activate proteinase K for lysis, followed by an inactivation step at 85 °C for 5 min. For mRNA analysis, one microliter cDNA synthesis-mix (see Appendix Table 8) was added and cDNA synthesis was performed using the following program (25 °C for 10 min, 55 °C for 30 min, 85 °C for 5 min). Afterwards, the cDNA was diluted to 20 µl and one microliter of that was used for PCR. PCR was performed according to the manufacturer's instructions (Q5 DNA polymerase; NEB, #M0491) (PCR program: see Appendix Table 9).

Agarose gel electrophoresis

For agarose gel electrophoresis, agarose (Invitrogen, #15510) was dissolved in 1x TAE buffer (recipe see appendix Table 7) using a microwave oven. The nucleic acid dye GelRed (GeneON, #S420) was added in a 1:50,000 dilution, afterwards. Agarose gels were cast using and electrophoresis was run using a BlueMarine™ 100 Horizontal Submarine Electrophoresis Unit (SERVA Electrophoresis GmbH, # 5442243) with 40-70 V, at constant voltage.

RNA sequencing

Transcriptome analysis was performed in collaboration with Philipp Koch, Marco Groth and Karol Szafranski from the FLI Core-Facilities *DNA Sequencing* and *Life Science Computing*. Briefly, 1 µg of total RNA was prepared using the Agilent Bioanalyzer 2100 and sequenced via an Ilumina HiSeq2500. The acquired reads were processed and mapped to the *C. elegans* genome. The obtained raw data was further processed to test for differential expression between RNAi and control treatment. Philipp Koch processed the raw data, computed the differential expressed genes and the Venn analysis thereof. For further details see (Köhnlein et al. 2020).

Gene enrichment analysis

To identify pathways and processes involved in the respective treatment, the web platform *WebGestalt* (WEB-based GEne SeT AnaLysis Toolkit, http://www.webgestalt.org/) was used (Liao et al. 2019) for gene enrichment. For analysis, the list of significantly regulated genes of each treatment was taken and fed into the Webgestalt search algorithm. WormBase IDs were used as gene identifiers and fold-change as the rank of each gene. Advanced parameters were left unchanged for the analysis. To reduce redundancy, the built-in algorithm *weighted set cover* was used. For display of the enriched terms the total number of up- or downregulated genes was set to 100 % and the fraction of each gene set was calculated proportionally. The total number of genes in each gene set is displayed (100 %).

Parameters for the enrichment analysis: (i) Minimum number of IDs in the category: 5 (ii) Maximum number of IDs in the category: 2000 (iii) Significance Level: Top 10 (iv) Number of permutations: 1000.

2.3 Bacterial culture

Two different bacterial strains (see below) were used for culturing *C. elegans*, which served as food source or additionally to deliver dsRNA for RNA interference. The *E. coli* strain OP50 served as the main food source for non-RNAi experiments. Bacteria were grown at 37 °C for 15–16 h. After successful growth, the culture was centrifuged for 20 min at 3200 g, 4 °C and concentrated two- or ten-fold (e.g. 2x: 50 ml → 25 ml, 10x 50 ml → 5 ml).

E. coli OP50

The Escherichia coli strain OP50 is derived from *E. coli* B, also known as *E. coli* wildtype strain (Brooks 2004; Daegelen et al. 2009). For use as the *C. elegans* food source, the cryopreserved bacteria were first streaked on LB agar containing no antibiotics (LB agar lennox; Table 6). Subsequently, a single colony was inoculated in dYT medium and grown overnight. 15–16 h later, the bacteria were usually 2x concentrated, as described above.

E. coli HT115(DE3)

For the depletion of certain genes via RNA interference, *C. elegans* was fed *E. coli* HT115(DE3), containing the plasmid for dsRNA expression of the respective gene. HT115(DE3) is commonly used for the transformation with plasmids for RNA interference. Strains were

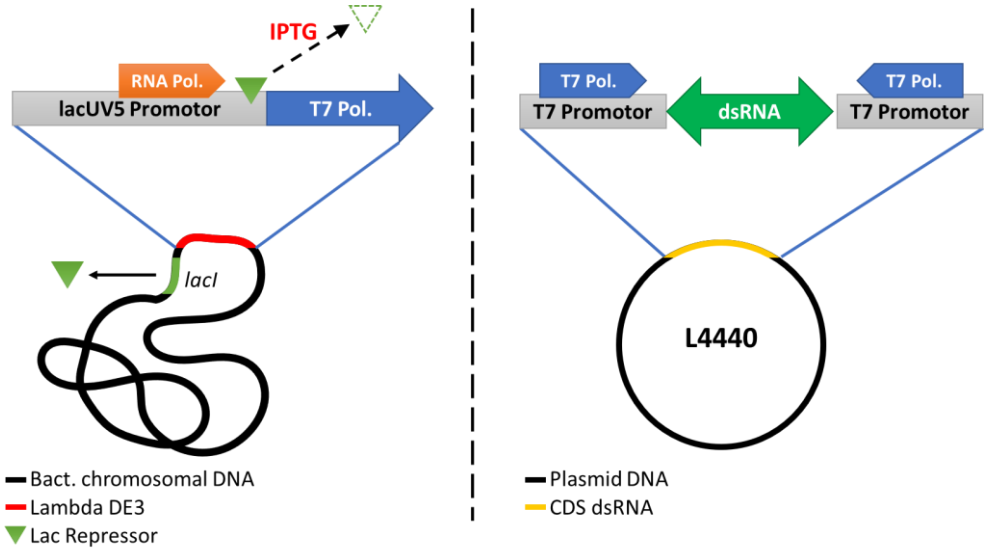

Figure 11 Induction of dsRNA expression by IPTG in HT115(DE3)
In the absence of IPTG or lactose, the Lac repressor binds to the LacUV5 promotor of the T7 polymerase gene (T7 Pol.) and prevents its transcription. The lacI gene on the bacterial genome encodes the Lac repressor. In the presence of IPTG, the Lac repressor detaches from the Lac promotor. Then transcription and translation of the T7 polymerase can occur, which initiates transcription of the dsRNA by binding to the T7 promotor on each side of the gene (Kamath and Ahringer 2003; Studier and Moffatt 1986). Scheme is not true to scale. Adapted from Novagen pET expression manual.

positively selected using ampicillin and carbenicillin on LB agar plates, followed by inoculation of a single colony in LB medium containing carbenicillin. The expression of dsRNA was induced using 1 mM isopropyl β-d-1-thiogalactopyranoside (IPTG) containing NGM agar.

For the induction of dsRNA in *E. coli* (DE3), strains contained a plasmid under the control of a T7 promotor. DE3 strains contain the lambda-DE3 lysogen which expresses the T7 RNA polymerase under the control of the lacUV5 promotor. They also encoded for the *lacI* gene in their genome producing a repressor of the lac promotor, suppressing the expression of the target dsRNA when no lactose or IPTG is present. IPGT acts as de-repressor of the lac promotor, causing transcription of the T7 polymerase gene. Once T7 polymerase is produced it can bind to each side the T7 promotor on the L4440 expression vector, flanking the dsRNA for the respective gene, upon which the dsRNA gets produced (Kamath and Ahringer 2003; Studier and Moffatt 1986) (Figure 11).

2.4 Statistical analysis

Data are presented as means ± SD unless otherwise stated. Calculation of relative means and standard deviations were performed using *GraphPad Prism* (GraphPad Software, San Diego, California, USA). Statistical analysis of lifespan data was carried out using *JMP* software (SAS Institute Inc., Cary, NC, USA) using the log rank test. Observations with a significance level of $p<0.05$ were considered statistically significant. Student's t-test or one-way ANOVA were used when appropriate. When F-test indicated differences in variances using t-test, Welch's correction was applied.

3 Results

3.1 Structural modeling of human SELENBP1

Several amino acids of SELENBP1 have been hypothesized to contribute to the binding of selenium. As proposed by *Raucii et al.*, Cys57 seems to be the most promising residue, since it was predicted to be the most accessible cysteine at neutral pH. However, judging from the 3D-Phyre²-model of SELENBP1 in Figure 12, the cysteines of the CSSC motif of SELENBP1, Cys80 and Cys83, as well as Cys5, Cys8 and Cys141 seem to be available on the surface as well, whereas Cys57 appears to be difficult to access.

Looking closer at the CSSC motif, it can be observed that only the thiol group of Cys80 sticks out to the surface, while the thiol group of Cys83 is pointed inwards. Arguably, this might indicate that these two would not form a disulfide bridge, which selenium could interact with. However, Cys141, visible in a pocket close to Cys80 and Cys83, has its thiol group in close proximity to the thiol group of Cys80. Therefore, these two might interact as well and be important for selenium binding. The enzymatic activity of bacterial SELENBP1 was shown to be copper-dependent (1.5.1). Therefore, it was important to highlight the histidine residues, which are often involved in binding divalent metal ions (Eom and Song 2019). Several histidine residues are displayed at the surface and could therefore mediate copper binding of SELENBP1. These include His61, His119, His128, His196, His227 and His236. However, none of the classical metal binding motifs (His137xxHis140; His329xAsp) seem to be present on the surface. His137xxHis140is located on a beta-strand whereas His329 is located on a loop, however both are buried in the inside of the protein.

In order to assess whether SELENBP1 might be posttranslationally modified, SELENBP1 was assessed according to parameters laid out by Fichtner et al. (2020). Figure 12 shows the amino acids of SELENBP1 which are predicted to be modified by carbonylation. Comparing this to the abundance of lysine and arginine residues on the surface, which are often highly modified, suggests that SELENBP1 might indeed be highly prone to non-enzymatic modifications, which might explain the high abundance of argpyrimidine detected on SELENBP1 (see Introduction 1.5.3).

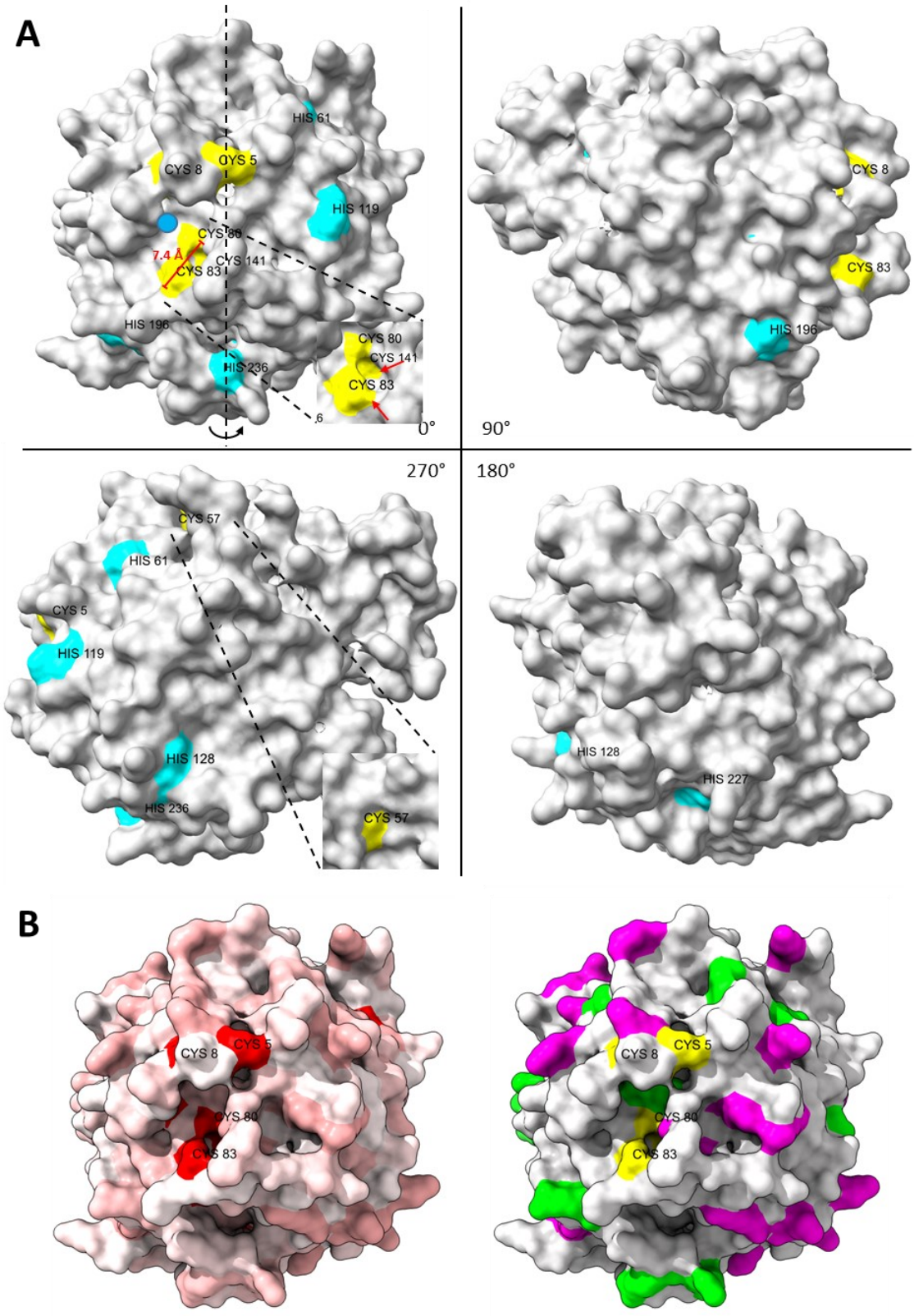

Figure 12 Structural analysis of a 3D model of human SELENBP1
3D surface model of human SELENBP1 constructed using *Protein Homology/analogY Recognition Engine V 2.0* (*Phyre*[2]; Kelley et al., 2015) and edited using *ChimeraX* Software (0.91). **(A)** Beginning at the top left panel, the protein was rotated clockwise 90 °C around the y-axis (dashed line: approx. rotation axis). Using *ChimeraX,* the distance between the two carboxyl groups of Cys80 and Cys83 was estimated to be approx. 7.4 Å. Accordingly, selenite (SeO_3^{2-}) was drawn with the size of 2.4 Å (●). Inset of top left panel: CSSC motif, red arrows point to sulfur groups of Cys80 and Cys141. Inset of bottom left panel: top section of the protein showing Cys57. Yellow: cysteine (Cys), cyan: histidine (His).

(B) Left picture shows amino acid residues, predicted to be most susceptible for protein carbonylation in red, according to parameters laid out by Fichtner et al. (2020). Intensity of the red color correlates with the susceptibility for the amino acid to be carbonylated. Right picture shows the same model, with colored amino acids, historically known to be heavily modified non-enzymatically: yellow: cysteine, purple: lysine, green: arginine. Cys5, 8, 80 and 83 are labeled.

3.2 Investigation of the *C. elegans* SELENBP1 ortholog Y37A1B.5

Previously generated results revealed that depletion of the SELENBP1 ortholog Y37A1B.5 via bacterial dsRNA lead to an increase of mean (109.6 ± 4.6 %) and maximum (112.8 ± 4.5 %) lifespan and an improved resistance to the oxidative stress inducing redox cycler, *methyl viologen* (paraquat) (121.6 ± 17.1 %) (see Figure 8).

3.2.1 Y37A1B.5 is an ortholog of SELENBP1

BLASTP alignment (Altschul et al. 1997) of human SELENBP1 (accession: CAG33133) with *C. elegans* non-redundant protein sequences revealed that Y37A1B.5 (accession: NP_001255777.1) shares 52 % identical amino acid residues and 69 % chemically similar amino acids with SELENBP1. To put this into perspective, the functional FOXO ortholog DAF-16, shares 65 % similar and 51 % identical amino acids with FOXO3. Thus, it seems likely that biological functions between SELENBP1 and Y37A1B.5 might be conserved.

Furthermore, the cysteine residue at position 57 (Cys57) of SELENBP1, which *in silico* analyses predicted to be important for biological function, and of which *in vitro* experiments demonstrated the importance for cells to resist selenium-induced toxicity (see 1.5.2), is conserved in Y37A1B.5. Although seemingly hard to access in SELENBP1, the 3D structure shows that Cys57 is also presented on the surface of the protein, as shown for SELENBP1 (Figure 13). Other structures such as the putative thioredoxin motif CxxC and the putative metal binding histidine motifs (HxD, HxxH) are also well conserved in Y37A1B.5. The CxxC motif appears to be structured differently than in SELENBP1. The thiol groups of Cys80 and Cys83 seem to be in very close proximity to one another, thus it seems plausible that these would be able to form a disulfide bridge. Furthermore, the equivalent of Cys141 in SELENBP1, Cys139, is in close proximity to Cys80 and Cys83, but buried inside the protein. As demonstrated for SELENBP1, the HxxH motif is not present on the surface.

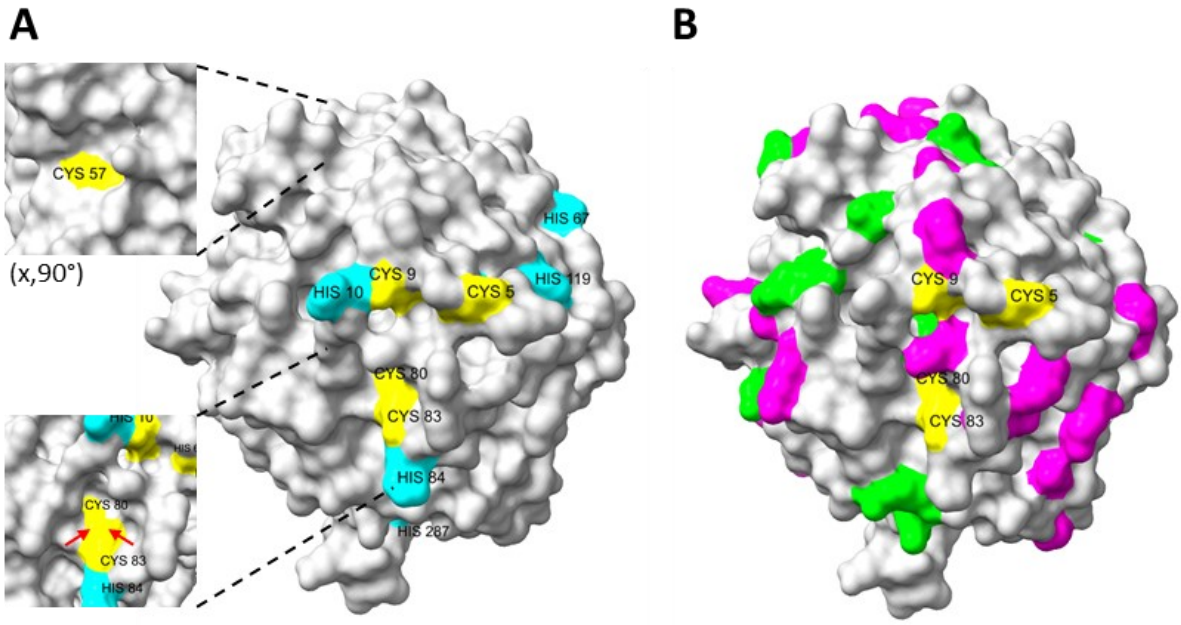

Figure 13 3D protein model of Y37A1B.5
3D surface model of Y37A1B.5, constructed using *Protein Homology/analogY Recognition Engine V 2.0* (*Phyre*[2]; Kelley et al., 2015). **(A)** Model with cysteines (Cys, yellow) and histidines (His, cyan) highlighted. Top left segment: Model was rotated 90° around the x-axis to show Cys57. Bottom left Segment: Cys80 and Cys83 are focused. Red arrow shows approx. position of thiols groups of Cys80 and Cys83. (B) Amino acid residues easily modifiable by carbonylation according to (Fichtner et al., 2020) are highlighted: cysteines (Cys, yellow), lysine (purple), arginine (green).

3.2.2 Y37A1B.5 is a cytoplasmic protein expressed in the epidermis

To address possible biological functions of Y37A1B.5, strains carrying transcriptional or translational reporters, were constructed. To this end, genomic fragments, 2989 bp of the Y37A1B.5 3'UTR region (for the transcriptional reporter, LOK157) and additionally (in the case of the translational reporter, LOK158; Figure 14) the open-reading frame, were cloned into a GFP vector by Dr. Pavel Urbánek from the Klotz laboratory and injected into *C. elegans*. This was done in collaboration with the lab of Dr. Antonio Miranda Vizuete. In accordance to the localization of Y37A1B.5 gene expression site as reported by McKay et al., a mainly epidermal signal was observed for the protein localization using the LOK158 reporter (Figure 14) (Mckay et al. 2003). As expected for somatic tissue, Y37A1B.5 dsRNA treatment was very effective in the transcriptional (not shown) and translational reporter and was comparable to mRNA levels measured via qRT-PCR at day three (2,10 % ± 0,93 %) or day five (34,25 % ± 10,98 %) of dsRNA treatment compared to control (Figure 14).

SELENBP1 was reported to be abundant in human blood plasma (Chau et al. 2018), which suggests the existence of some sort of export mechanism. Thus, it seemed plausible that extracellular localization might also be observable for Y37A1B.5. However, analysis of LOK158

revealed an exclusively intracellular signal. Furthermore, under non-stressed conditions, Y37A1B.5 localization was found primarily in the cytoplasmic region while the nuclei seemed to be omitted (Figure 14).

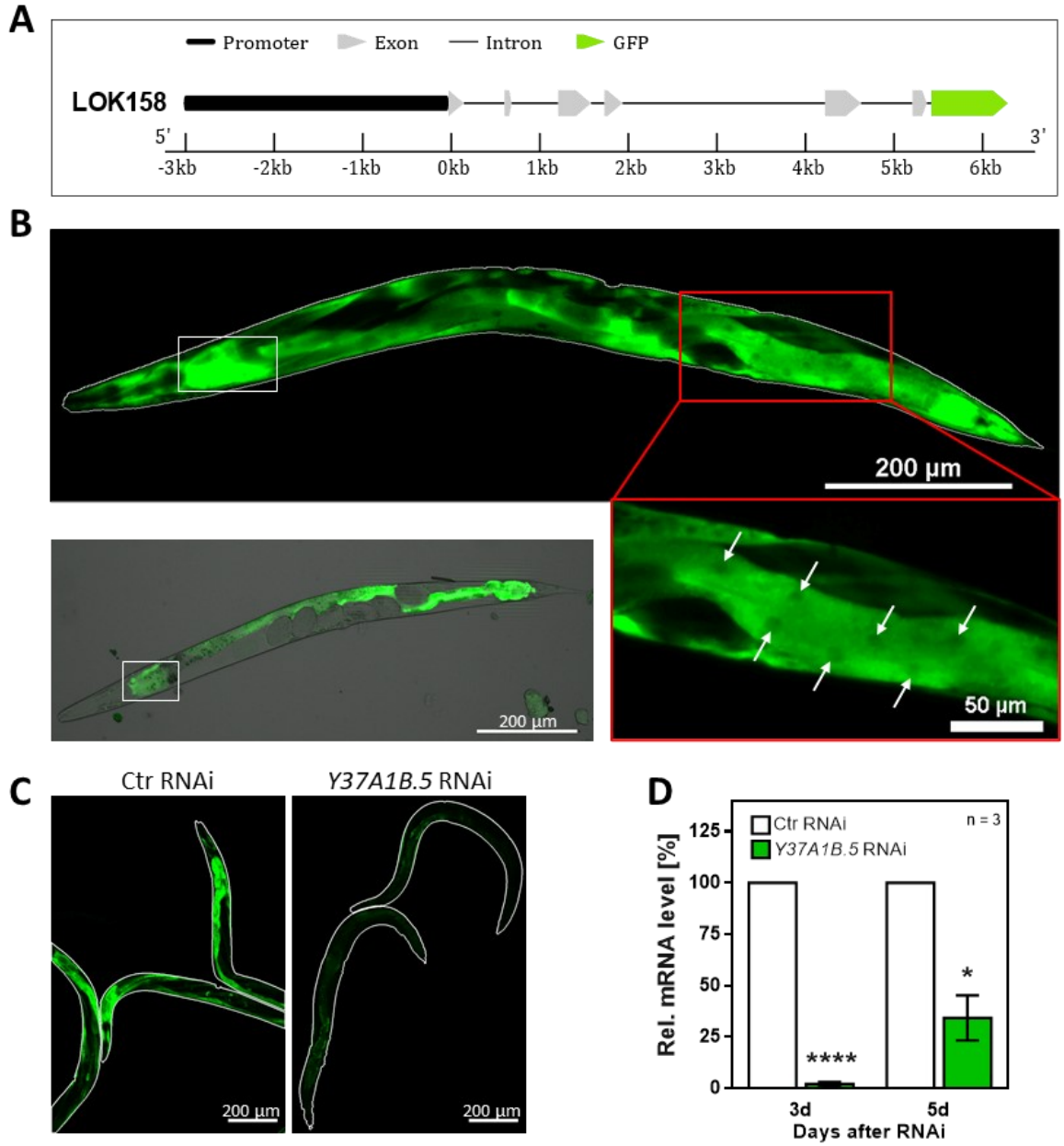

Figure 14 Y37A1B.5 is an epidermal protein, predominantly localized in the cytoplasm.
(A) Schematic representation of the translational reporter construct (LOK158) used in this study. A genomic fragment containing a 3kb region of the *Y37A1B.5* 5'UTR as promoter, together with the Y37A1B.5 open-reading frame was cloned into the GFP plasmid pPD95.77 and injected into *C. elegans* wildtype. **(B)** Localization of Y37A1B.5 is predominantly epidermal. Comparison to the intestinally expressed protein klo-2 (panel: left corner; LOK182, klo-2::GFP) shows that except for a region proximal of the pharynx (boxed white), the GFP pattern does not resemble intestinal expression. Y37A1B.5 is mainly localized in the cytoplasm (red box). White arrows show nuclei of hyp7 syncytia (for comparison see Altun and Hall 2009). **(C)** Effectiveness of *Y37A1B.5* RNAi in LOK158. GFP signal is strongly reduced after *Y37A1B.5* RNAi for five days compared to control RNAi treated worms. Reduction is comparable to the effect of RNAi on mRNA levels after treatment for three or five days (D). **(D)** Relative mRNA levels of *Y37A1B.5* after knockdown for three or five days. Data was normalized to *tba-1* expression as housekeeping gene and to ctr RNAi treatment of each day. Data is presented as mean ± SD.*p<0,05, ****p<0.0001, t-test with Welch's correction

3.2.3 Cellular localization of Y37A1B.5 under stressful stimuli

As reported before (see 1.5.6, 1.5.8), nuclear shuttling of SELENBP1 was observed under stressful conditions. Therefore, it was analyzed whether nuclear accumulation of the Y37A1B.5-GFP signal could be observed after treatment with different ROS inducing agents. However, analyzing LOK158 after treatment with paraquat (5 mM, 10 mM), selenite (0.01 µM – 1 mM) or arsenite (1 µM – 100 µM), no apparent nuclear localization could be observed (Figure 16, Figure 17). This seems to be evidence that Y37A1B.5 does not seem to function as a transcription factor.

3.2.4 Y37A1B.5 is a pro-aging factor

Because it was previously shown that depletion of Y37A1B.5 delayed aging in *C. elegans* (Köhnlein et al. 2020), mRNA levels of *Y37A1B.5* were measured from young to aged worms at different time points (Figure 15). Y37A1B.5 expression declined exponentially during aging (R^2: 0.88), further suggesting a link between Y37 expression and the aging process. Relative expression at day 20 of adulthood was reduced to 8.9 % ± 5.7 %, compared to the first day of adulthood. This is comparable to mRNA levels achieved via siRNA of *Y37A1B.5* (Figure 14). This could either mean that Y37A1B.5 becomes dispensable after reaching adulthood, or that its expression is reduced as a means to defend the nematodes from accumulation of reactive oxygen species during age, as seen similarly after *Y37A1B.5* RNAi (see: Introduction Figure 8B).

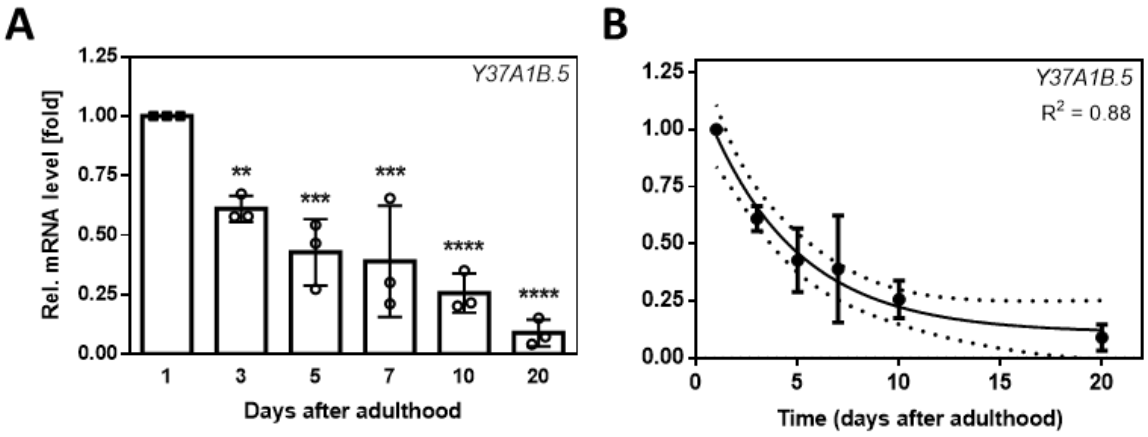

Figure 15 Y37A1B.5 expression declines exponentially during aging.
(A) mRNA levels of *Y37A1B.5* in wildtype worms at day one, three, five, seven, ten and twenty after adulthood, measured via qRT-PCR. Data was normalized to *tba-1* expression as housekeeping gene, and to the expression at day one to calculate the relative fold-change of *Y37A1B.5* expression. **p<0.01, ***p<0.001, ****p<0.0001 compared to day 1; One-way ANOVA with Bonferroni correction for multiple comparisons. **(B)** Non-linear regression revealed a highly confident (R^2 = 0.88) exponential decline (right). Data are presented as means ± SD, dashed line shows 95 % confidence interval.

3.2.5 The role of Y37A1B.5 in redox homeostasis

To address the role of Y37A1B.5 in the context of reactive oxygen species, LOK158 were treated with two different substances which are known to generate reactive oxygen species but have different modes of action. First, arsenite was used, which was shown to induce the formation of reactive oxygen and nitrogen species (Sattar et al. 2016) and interacts with thiols, especially glutathione (Spuches et al. 2005). Secondly, paraquat was used, a redox cycler that causes the generation of superoxide anions (Bonneh-Barkay et al. 2005).

Treatment of fully developed young adult worms with different concentrations of sodium arsenite revealed a dose-dependent decline of Y37A1B.5 protein abundance (Figure 16A). With the highest concentration of arsenite, Y37A1B.5 abundance was decreased by roughly 40 % compared to the vehicle-treated control. The effect of depletion of Y37A1B.5 on glutathione levels was tested. As expected, worms after treatment with *Y37A1B.5* RNAi showed a tendency of increased GSH levels and showed an increased expression of most of the *C. elegans* glutaredoxins (Figure 16B,C), enzymes involved in protein regeneration using glutathione.

Treatment with the redox cycler paraquat, on the other hand, did not alter the abundance of Y37A1B.5 (Figure 16D). One hypothesis explaining this might be that paraquat does not directly interact with thiols and therefore does not modulate Y37A1B.5, or that Y37A1B.5 simply is not responsive to superoxide anions. Of note, *Y37A1B.5* RNAi depletion also largely failed to robustly upregulate the superoxide dismutase system (Figure 16E), which is responsible for catalyzing the reaction from superoxide to hydrogen peroxide.

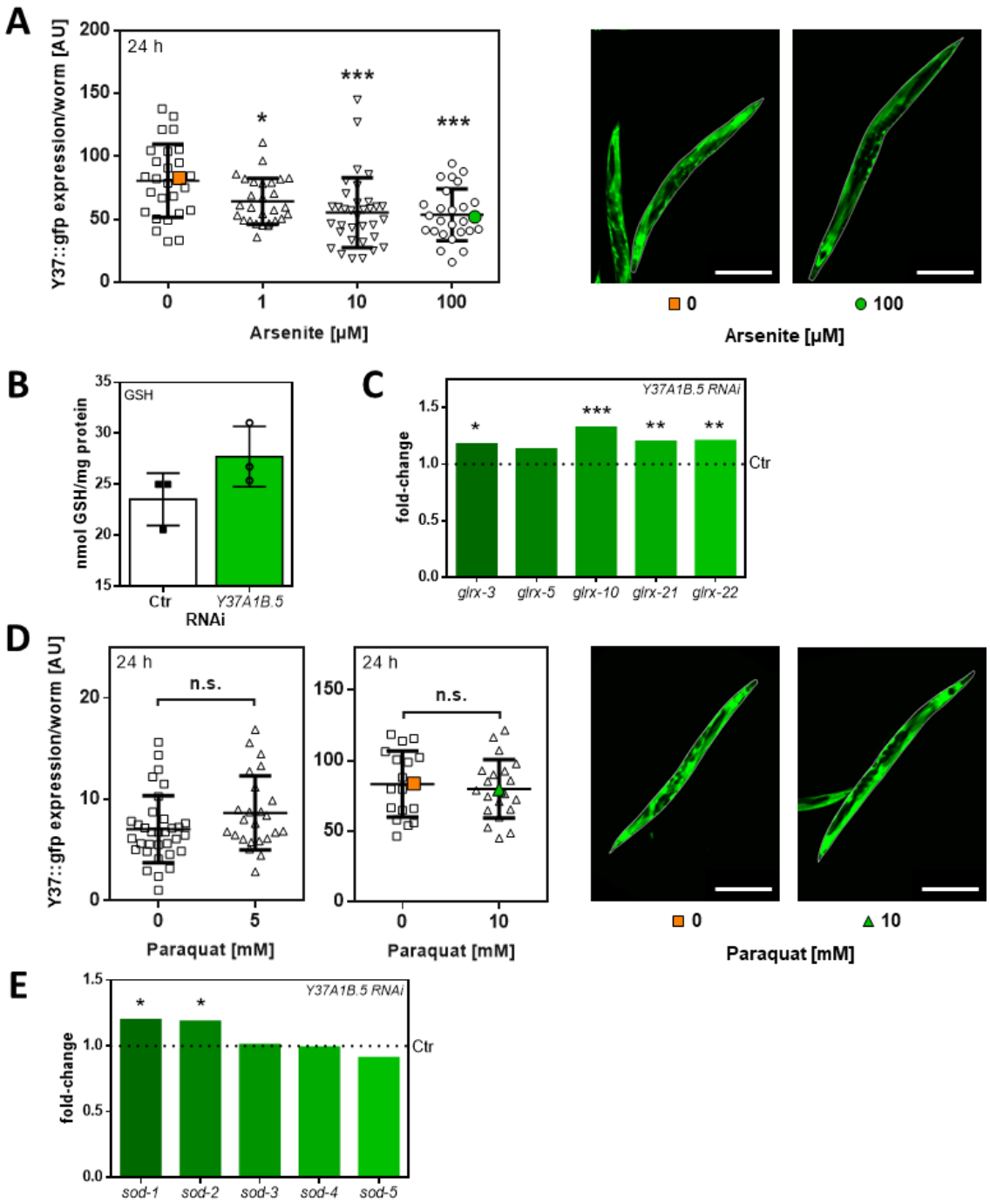

Figure 16 Y37A1B.5 abundance is reduced in response to arsenite but not to oxidative stress in general.
(A) LOK158 young adult worms were treated with different concentrations of sodium arsenite for 24 h. Worms were then mounted on objective slides for analysis of the GFP signal. Datapoints are GFP expression of individual worms and means ± SD. p>0.05, ***p<0.001, ANOVA with Bonferroni for multiple comparisons. Right panel shows exemplary pictures of worms treated with 0 µM or 100 µM arsenite. **(B)** GSH measurement via HPLC method of wildtype worms after treatment with *Y37A1B.5* RNAi for five days. Data is and means ± SD **(C)** Gene expression of *C. elegans glutaredoxins* (*glrx*) from transcriptome analysis of wildtype worms treated with *Y37A1B.5* RNAi for five days compared to control RNAi. **(D)** LOK158 young adult worms treated with different concentrations of paraquat for 24 h. Data shows GFP expression of individual worms as datapoints and means ± SD. n.s., p≥0.05; unpaired t-test. Right panel shows exemplary pictures of worms treated with 0 µM or 10 mM paraquat. **(E)** Gene expression of *C. elegans superoxide dismutases* (*sod*) from transcriptome analysis of wildtype worms treated with *Y37A1B.5* RNAi for five days compared to control RNAi. Data is presented as mean ± SD. *p<0.05. Scale bars are 250 µm

3.2.6 Y37A1B.5 is important for the protection against selenite

To address the hypothesis of Y37A1B.5 being a potential selenium binding protein, worms were treated with a wide range of sodium selenite concentrations to evaluate if there would be a modulation of Y37A1B.5 abundance in response to a selenium stimulus. The range of selenite concentrations used spanned from hormetic and subtoxic concentrations (0.01 µM, 1 µM) to toxic concentrations (100 µM, 1 mM) (see 1.6.5). Subtoxic concentrations did not seem to induce Y37A1B.5 expression. However, at 100 µM, Y37A1B.5 expression was induced strongly and even more so with exposure to 1 mM selenite. This points towards a mechanism, where Y37A1B.5, as potential selenium binding protein, is expressed more abundantly in response to selenite to protect *C. elegans* from a selenium overload. To test this, worms were treated with lethal concentrations of sodium selenite after pretreatment with *Y37A1B.5* siRNA. It was shown that worms which were depleted of Y37A1B.5 before, were significantly less

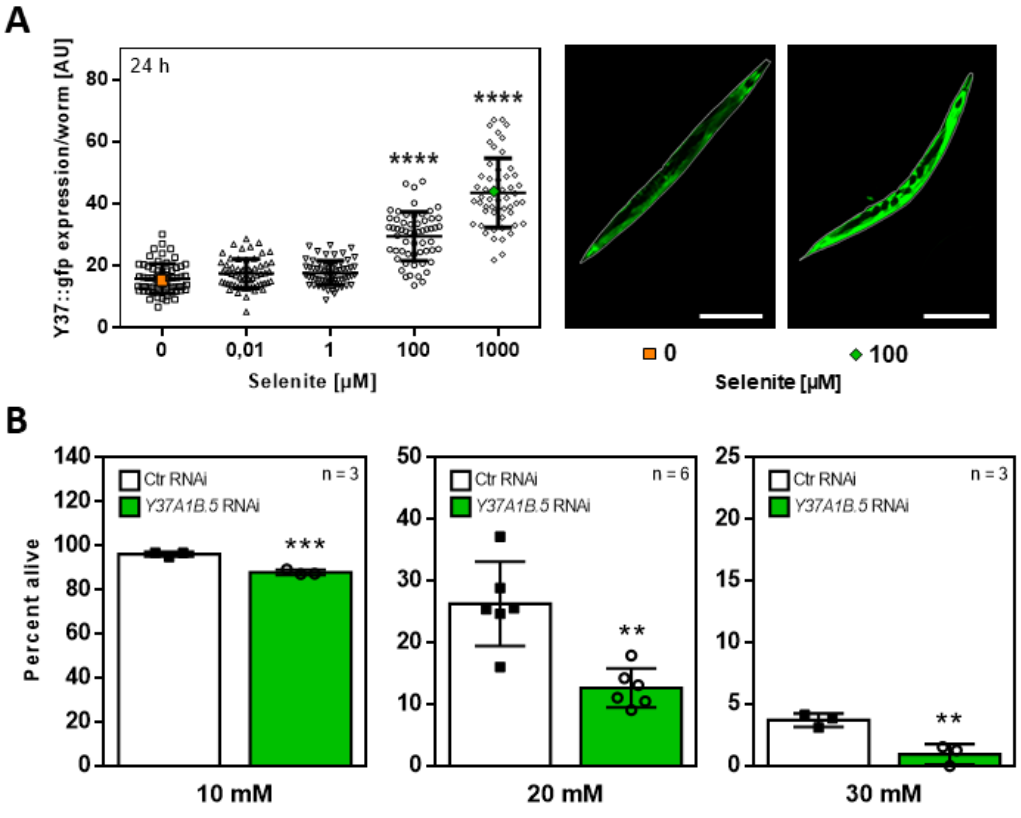

Figure 17 Y37A1B.5 protects against selenite-induced toxicity.
(A) LOK158 young adult worms were treated with different concentrations of sodium selenite for 24 h. Worms were then mounted on objective slides for the GFP signal to be analyzed under a fluorescent microscope. Right panel shows exemplary pictures of worms treated with 0 µM or 1 mM sodium selenite. Data points are GFP expression of individual worms and means ± SD. ****p<0.0001, ANOVA with Bonferroni correction for multiple comparisons. **(B)** Wildtype worms were pretreated with Y37A1B.5 RNAi before being subjected to different concentrations of sodium selenite. Data are presented as means ± SD. **p>0.01, ***p<0.001; unpaired t-test. Scale bars are 250 µM.

resistant to selenite, from mildly, to highly lethal concentrations, compared to worms treated with control RNAi (Figure 17). These results confirm the hypothesis that Y37A1B.5 is important for the protection against selenite and strengthen the possibility that Y37A1B.5 might be a selenium-binding protein ortholog.

3.2.7 MDT-15 and EGL-27 are regulators of Y37A1B.5

In search for transcriptional regulators of Y37A1B.5, MDT-15 and EGL-27 seemed to be good candidates. As described before, MDT-15 was shown to be involved in stress response and EGL-27 was also described as a transcription factor promoting stress resistance (Xu and Kim

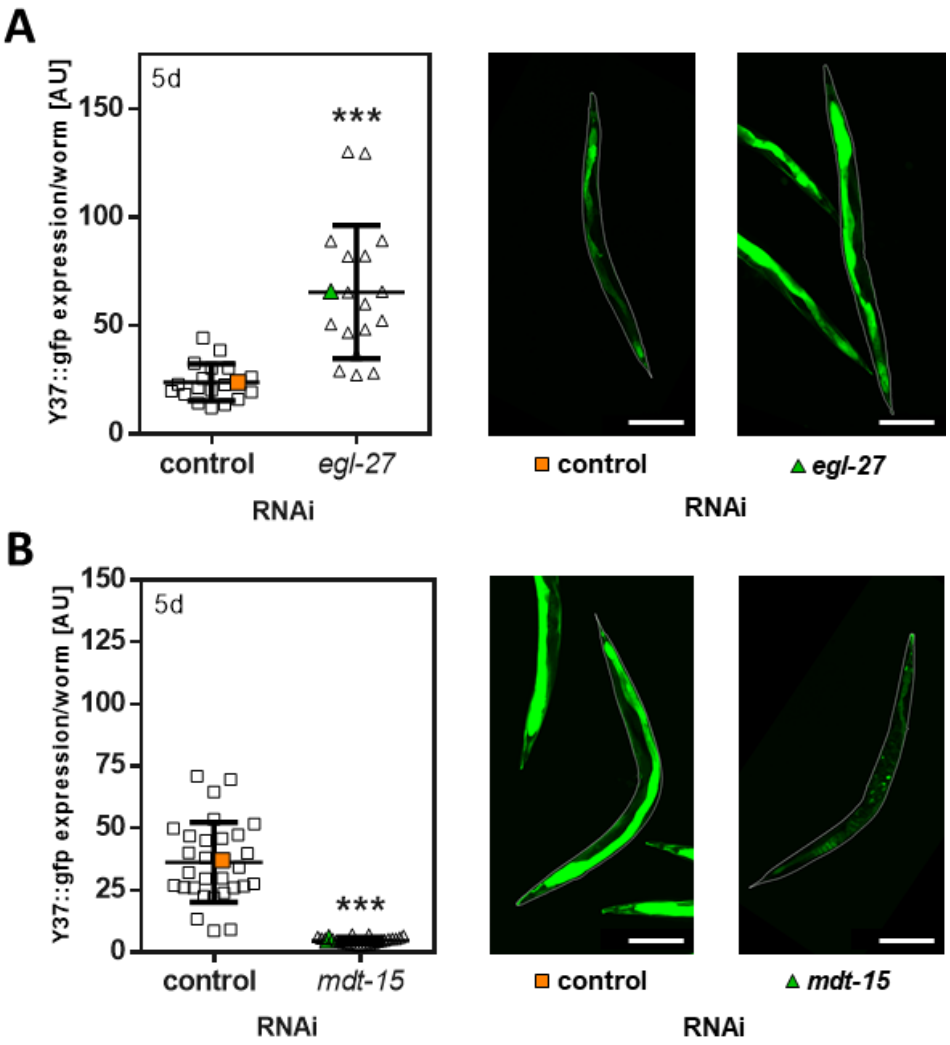

Figure 18 MDT-15 and EGL-27 are regulators of Y37A1B.5
LOK158 young adult worms were treated with siRNA against either *egl-27* or *mdt-15* and control plasmid for five days and GFP intensity of single worms was measured afterwards **(A)** Treatment with *egl-27* or control RNAi. GFP expression of individual worms is given as data points, as well as means ± SD. ***p<0.001, unpaired t-test with Welch's correction. Right panel: exemplary pictures of worms treated with control or *egl-27* RNAi. Individual worms are outlined in white. **(B)** RNAi treatment against *mdt-15* compared to control. Data shows GFP expression of individual worms as datapoints and means ± SD. ***p<0.001, unpaired t-test with Welch's correction. Right panel: exemplary pictures of worms treated with control or *egl-27* RNAi. Individual worms are outlined in white. Scale bars are 250 μM.

2012) regulating *Hox* genes, which are involved in cell differentiation processes of the epidermis (Ch'ng and Kenyon 1999).

To test if EGL-27 and MDT-15 are regulators of Y37A1B.5, LOK158 was subjected to *egl-27*, *mdt-15* or control RNAi. It was observed that knockdown of *egl-27* resulted in a 2.75-fold mean increase of Y37A1B.5 abundance. This fits very well to data showing that EGL-27 is a positive regulator of *C. elegans* lifespan and stress resistance (Xu and Kim 2012). Since it was shown that Y37A1B.5 is a negative regulator of lifespan (Köhnlein et al. 2020), it can be speculated that EGL-27 is part of a transcriptional network which targets Y37A1B.5 to promote stress resistance. Depletion of MDT-15, on the other hand, strongly depleted *C. elegans* from Y37A1B.5, reducing its abundance to 7.7 % compared to control RNAi-treated animals (Figure 18). As described before (1.6.4), loss of MDT-15 results in premature death and strongly attenuates resistance to different stressful stimuli. In light of that, the reduction of the pro-aging factor Y37A1B.5 by MDT-15 does not seem to fit. Possible hypotheses explaining this will be discussed in the following sections.

3.2.8 Functional association of Y37A1B.5 with MDT-15 and EGL-27

Loss of MDT-15 also resulted in a phenotype which was described before as a disruption of cellular organization and the presence of vacuoles (Taubert et al. 2006). This phenotype was not reversed after additional depletion of Y37A1B.5 via RNAi (Figure 19). Therefore, it appears that the anti-aging effects elicited by Y37A1B.5 depletion do not occur under conditions of a disturbed MDT-15 signaling. Thus, MDT-15 might be an important factor in the lifespan extension elicited by knockdown of *Y37A1B.5*.

To further clarify the relationship between Y37A1B.5, MDT-15 and EGL-27 in the promotion of stress resistance, a heat stress assay was performed in which worms were treated with either *Y37A1B.5* RNAi, *mdt-15* RNAi, *egl-27* RNAi or a double knockdown of *Y37A1B.5* and *egl-27* or *mdt-15*. This was hoped to reveal whether the depletion of Y37A1B.5 also promotes resistance to heat stress, apart from promoting resistance to oxidative stress, but also if EGL-27 or MDT-15 are involved in this process. For this, worms were pretreated with the respective RNAi for five days before being submitted to 37 °C for three hours with a subsequent recovery of 40 h. It was revealed that Y37A1B.5 indeed improved heat resistance by 33.1 ± 5.4 % compared to control RNAi. *Mdt-15* RNAi strongly diminished the survival under heat stress

to a total of 13.5 ± 7.5 % (vs. control), whereas depletion of EGL-27 did not alter the survival rate (total: 113.6 ± 23.1 %) compared to the control (Figure 19). Of special interest in the case of *mdt-15* RNAi was the fact that additional depletion of Y37A1B.5 did not show any difference

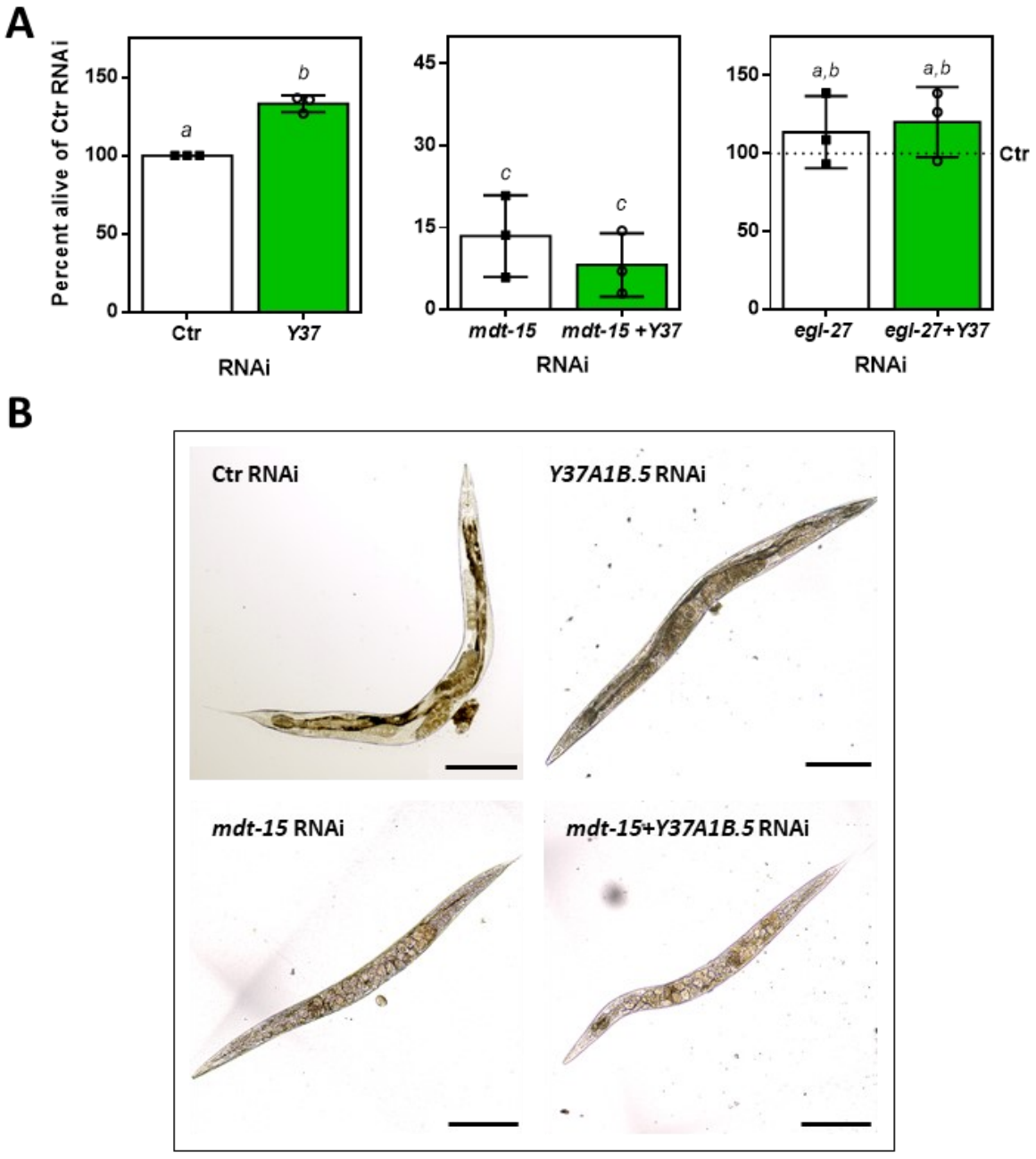

Figure 19 Depletion of Y37A1B.5 increases survival under heat stress; role of MDT-15
(A) Young adult wildtype worms were treated with RNAi against *Y37A1B.5*, *mdt-15*, *egl-27* or a combination of the latter with *Y37A1B.5* for five days. Worms were then subjected to heat stress (37 °C, 3h) with subsequent recovery for 40 h and were then scored for survival. Data are means ± SD. a vs. b: $p<0.01$, a vs. c: $p<0.01$. Groups with same letter significance did not statistically change to one another; unpaired t-test with Welch's correction **(B)** Pictures of worms after treatment with the respective RNAi. Worms depleted of Y37A1B.5 showed wildtype phenotype, organs can be distinguished from one another. Loss of MDT-15 resulted in accumulation of vacuoles and disorganized organ structure. Additional treatment RNAi of *Y37A1B.5* did change the phenotype of *mdt-15* RNAi. Scale bars are 250 μM.

compared to single RNAi of *mdt-15*, which indicated that MDT-15 was required for the improved resistance to heat stress upon *Y37A1B.5* RNAi. Further experiments will reveal if MDT-15 is also necessary for the lifespan extending and ROS protecting effects elicited by loss of Y37A1B.5.

3.2.9 Y37A1B.5 regulates targets of metabolic pathways and defense response

To identify downstream targets which may be important for the improvements of lifespan and stress resistance, transcriptomes of worms undergoing *Y37A1B.5* RNAi and control RNAi were analyzed and compared against each other. As displayed in Figure 20, gene enrichment analysis revealed that most of the positively associated genes after depletion of Y37A1B.5 belonged to the KEGG term *"Metabolic pathways"*. The positive association with *"Ribosome"* and *"Lysosome"* point toward a higher protein turnover, while *"Carbon metabolism"* and *"Fatty acid metabolism"* suggest a higher flux of sugars and lipids. The positive association with metabolic pathways was also reflected by most of the upregulated biological processes i.e. *"Organic acid metabolic process"*, *"Lipid metabolic process"* and *"Cofactor metabolic process"*.

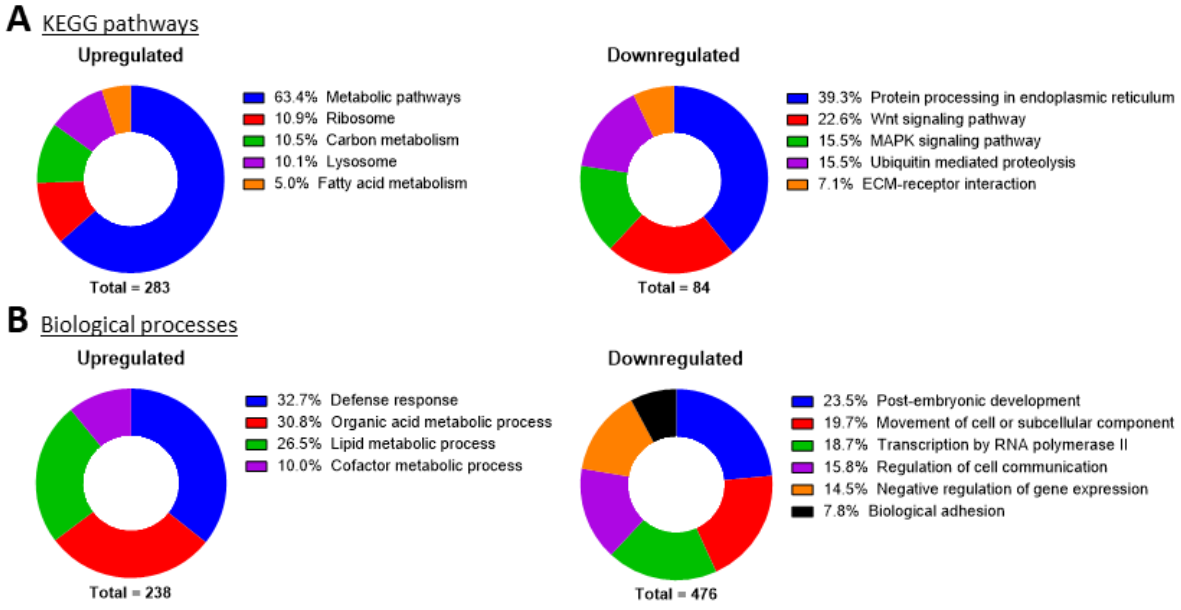

Figure 20 Defense response and metabolic pathways are upregulated after *Y37A1B.5* RNAi
Differentially expressed genes obtained by transcriptome analysis of wildtype worms treated with *Y37A1B.5* RNAi for five days were enriched for KEGG pathways **(A)** or biological processes **(B)** using WebGestalt 2019 (Liao et al. 2019). The total number of up- or downregulated genes was set to 100 % and the fraction of each gene set was calculated proportionally.

Considering the improved stress resistance elicited by *Y37A1B.5* RNAi, it is not surprising that the largest group of the positively enriched genes belonged to the term *"Defense response"*.

Since Y37A1B.5 was shown to be predominantly expressed in the epidermis, an organ heavily involved in early development, it was unsurprising that there were a number of downregulated pathways suggesting an impaired development such as "*Wnt signaling*" or "*MAPK signaling*" or biological processes like "*Cell development*", "*Regulation of developmental processes*" and "*Post-embryonic development*" (Figure 20). However, since knockdown of the samples for transcriptome analysis was performed after embryonic and larval development, this might be a remnant of Y37A1B.5 functions in earlier stages of *C. elegans* life.

3.2.10 Is Y37A1B.5 involved in the regulation of sulfur metabolism?

One set of genes, too small to appear in the gene enrichment analysis but possibly important for explaining the long-lived phenotype of *Y37A1B.5* RNAi, belongs to the transsulfuration pathway. These were already described above (chapter 1.7). Key enzymes for transsulfuration seemed to be the most important for the production of H_2S, *cystathionine-β-synthase* (CBS) and *cystathionine-γ-lyase* (CTH) as well as the *bifunctional L-3-cyanoalanine synthase/cysteine synthase* (CYSL) and the *mercaptopyruvate sulfurtransferase* (MPST). *Cth-1* was upregulated 3.4-fold and was one of the highest differentially expressed genes in the data set, while expression of *cbs-1* was reduced in comparison to control RNAi (0.8-fold). Additionally, *cysl-2* and *cysl-3* were each upregulated 1.7- and 1.2-fold while *mpst-1-7* mRNA levels were not changed. H_2S production was measured using a method described by (Hine and Mitchell 2017). In short, whole *C. elegans* extracts were supplemented with millimolar concentrations of cysteine as

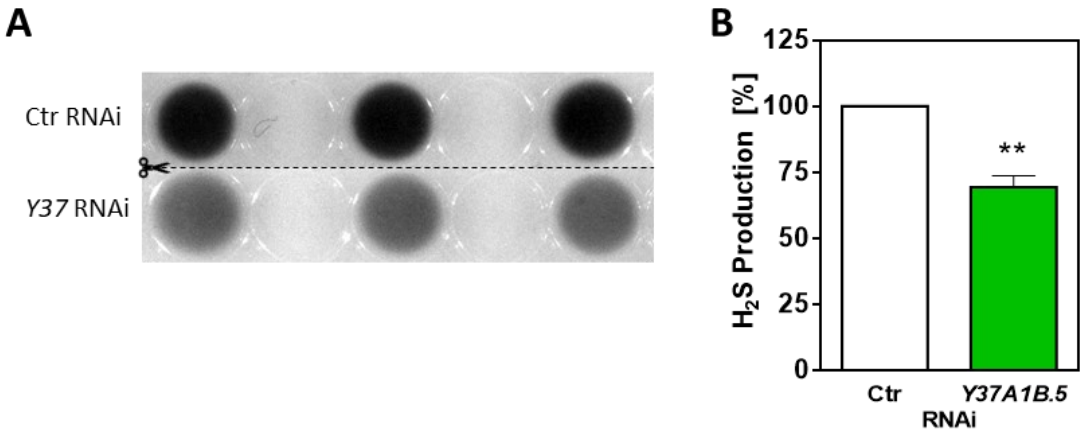

Figure 21 The capacity to produce H_2S from cysteine is reduced after *Y37A1B.5* RNAi
(A) H_2S production was assessed in a 96-well format using 100 µg of total protein lysate. 96-well plate was covered with a lid containing 100 mM lead-acetate and was incubated at 37 °C for 4 h. Image was taken in a Biorad Chemidoc MP imager. Picture shows three technical replicates of experiment #3 of Ctr or *Y37A1B.5* RNAi. **(B)** Quantification of three independent experiments of measurement shown in (A). Volume intensity of each black dot was measured using the ImageLab volume tool (Biorad). Data shows mean ± SD of fold change compared to control RNAi; **p<0.001 unpaired t-test with Welch's correction

substrate and pyridoxal phosphate as cofactor and incubated at 37° C. The gaseous H_2S emitted from the reaction was captured in lead acetate-containing agarose, covering the reaction chamber. H_2S production was estimated measuring the extent of blackening of the agar by precipitated lead sulfide. Surprisingly, the capacity to produce H_2S from cysteine was reduced by around 30 % in Y37A1B.5-depleted worms compared to the control (Figure 21). Iron and pyridoxal phosphate participate in the breakdown of cysteine to generate H_2S. Iron is stored via the protein ferritin, which is encoded twice in *C. elegans*, as FTN-1 and FTN-2; mRNAs of both were elevated after *Y37A1B.5* RNAi, 1.6-fold and 1.2-fold, respectively. This may suggest reduced levels of free iron which could have contributed to the outcome of the of H_2S assay.

3.2.11 Y37A1B.5 null mutant is morphologically indistinguishable from wildtype

To address the question if a complete loss of Y37A1B.5 would result in similar effects on lifespan and stress resistance, a null mutant (PHX2078, *Y37A1B.5(syb2078)*) was obtained, expressing only a small fragment of the original *Y37A1B.5* mRNA. The strain was validated via PCR on genomic and cDNA level. Primers were designed to detect differently sized amplicons in wildtype and PHX2078.

Since this strain was only received recently, no functional analysis could be performed. Surprisingly, phenotypical comparison of PHX2078 to wildtype animals revealed no morphological differences, the larval stages were reached at approximately the same time and animals developed normally to adulthood (Figure 22). This was very surprising because data from *Hashimshony et al.* showed a strong upregulation of Y37A1B.5 in early blastomere stages of the embryo of wildtype animals (Hashimshony et al. 2015), which suggested a high relevance of Y37A1B.5 in embryonic development. However, since no growth abnormalities were visible in PHX2078, Y37A1B.5 seems to be redundant during this process.

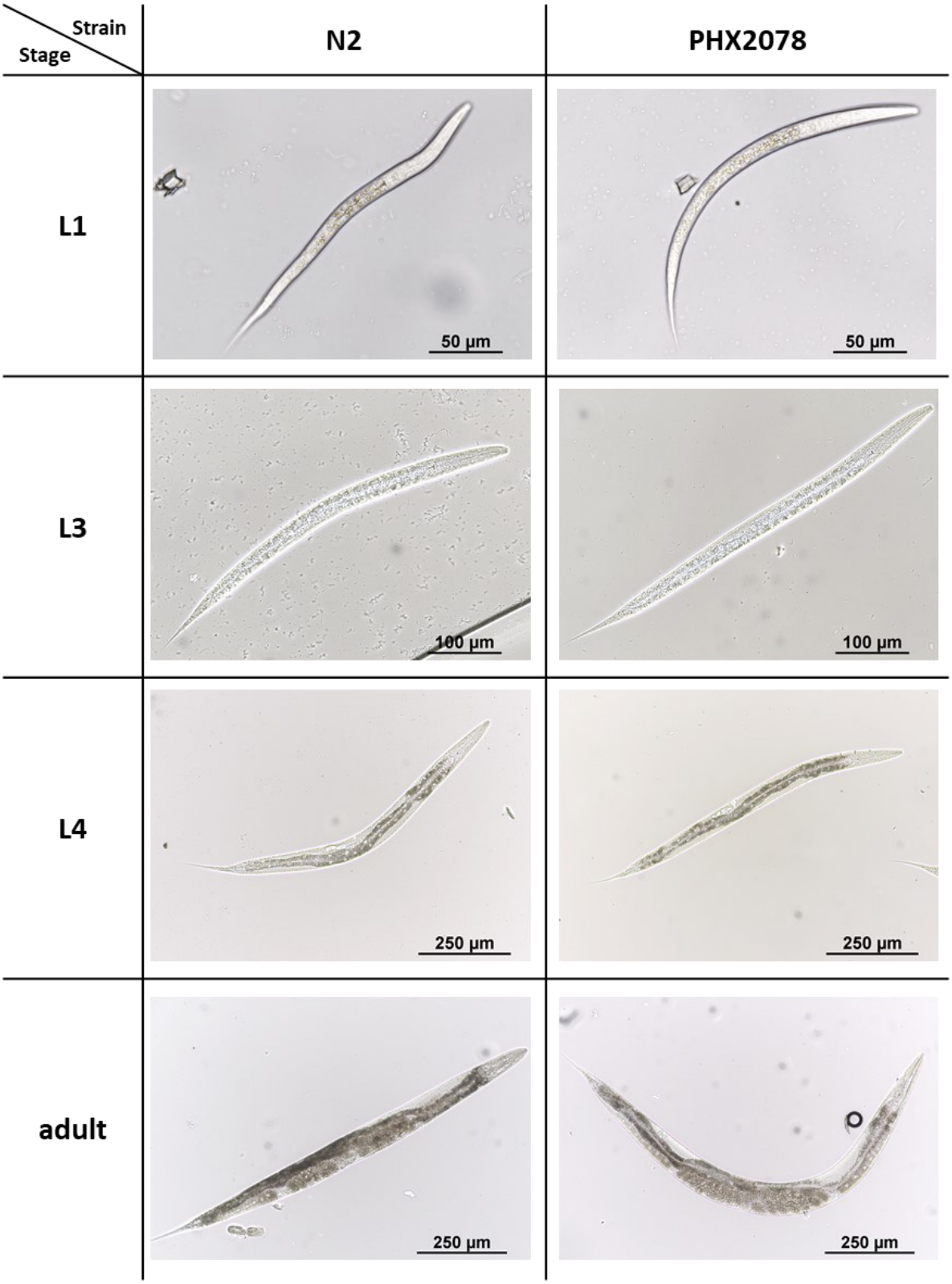

Figure 22 *Y37A1B.5* null mutant strain, PHX2078
Phenotypical analysis of *Y37A1B.5* null mutant PHX2078. PHX2078 and wildtype N2 animals were synchronized via L1 arrest. Pictures of L1 animals were taken 4 hours after refeeding. L3, L4, and adult animals were photographed at 24-hour intervals following that. No phenotypical differences were observed in the different larval stages.

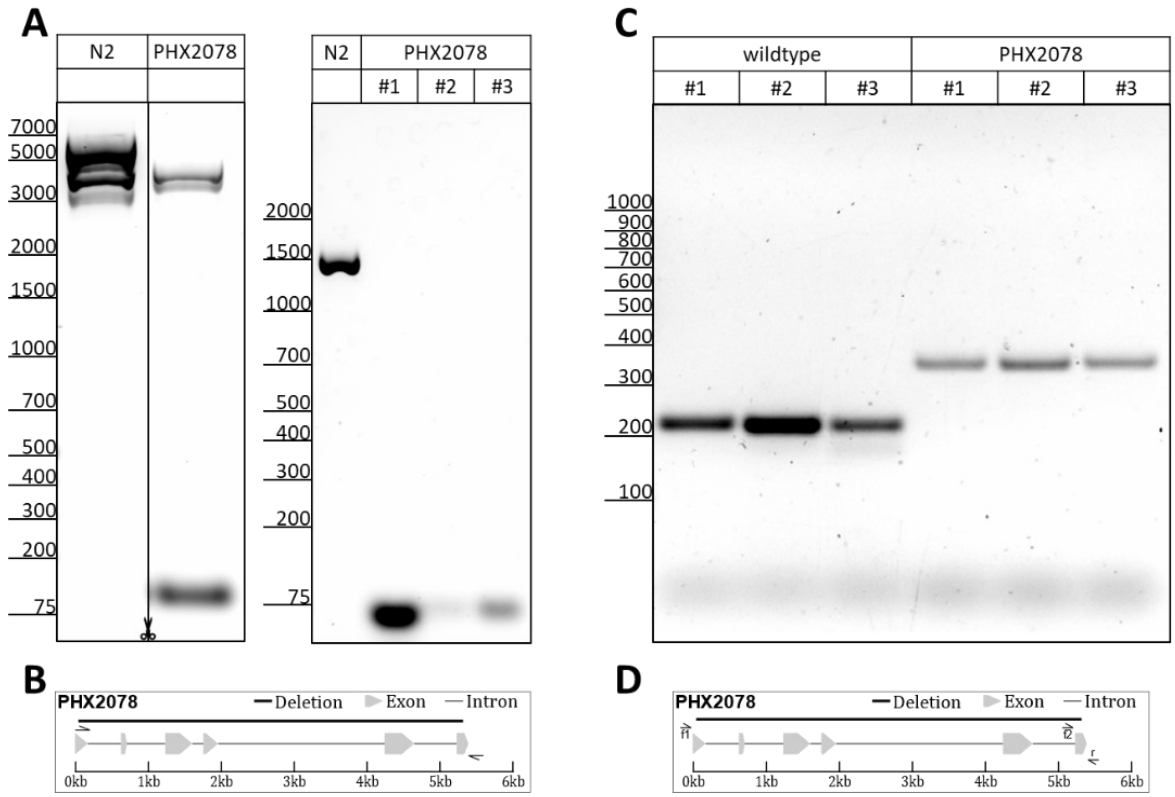

Figure 23 Genetic validation of PHX2078
Validation of PHX2078 via PCR **(A) (left). G**enomic DNA of wildtype N2 and PHX2078 mutants. Expected bands: N2: 5352 bp, PHX2078: 117 bp (Primer7+8). One main band at around 5000bp base pairs and several between 4000 and 3000 bp base pairs were amplified in wildtype worms. PCR on DNA of PHX2078 showed two bands of around 3000-4000bp base pair size and one band at the anticipated size of around 117 bp. **(right)** PCR amplifying cDNA fragments. Anticipated bands: N2 1310 bp, PHX2078 64 bp (Primer3+4). On wildtype DNA one band between 1500 and 1000 bp was visible corresponding to the expected size of 1310 bp. Single worm PCR of PHX2078 of three different specimens amplified one band at the expected size of 64 bp. **(C)** Single-worm PCR on genomic DNA of worms with a wildtype Y37A1B.5 allele and PHX2078 mutants carrying the *Y37A1B.5(syb2078)* allele. As expected animals carrying the wildtype allele showed one band at 216 bp. PHX2066 appears to be homozygous for *R11G10.2(syb2066)* because only one bands for the mutant allele (312 bp) was amplified (Primer12+13+14). For each strain three worms were analyzed. **(B+D)** Schematic depiction of *Y37A1B.5(syb2078)* allele in PHX2078. Deletion is 5235 bp of *Y37A1B.5* CDS. **(B)** Primers for PCR on genomic DNA bind on the first exon and in the 3'UTR of *Y37A1B.5* CDS. **(D)** Primers for duplex PCR on genomic DNA resulting in a 216 bp fragment on a wildtype allele (f2+r; Primer12+14) and 312 bp fragment on a Y37A1B.5*(syb2066)* allele (f1+r; Primer13+14). DNA was loaded onto a 1 % (A) or 2 % (C) agarose gel for separation via electrophoresis.

3.3 Investigation of the SELENBP1 *C. elegans* ortholog R11G10.2

In a previous work, the *putative selenium-binding protein* R11G10.2 had been described by me as regulating lifespan and resistance to oxidative stress. Depletion of the gene via RNAi resulted in an extension of mean (110.6 ± 4.8 %) and maximum (113.5 ± 5.2 %) lifespan, comparable to what was described for Y37A1B.5. Also, stress resistance following R11G10.2 RNAi was found to be comparable between the two selenium binding protein orthologs (122.9 ± 5.7 %, compared to control RNAi) (Köhnlein 2016). These results were surprising,

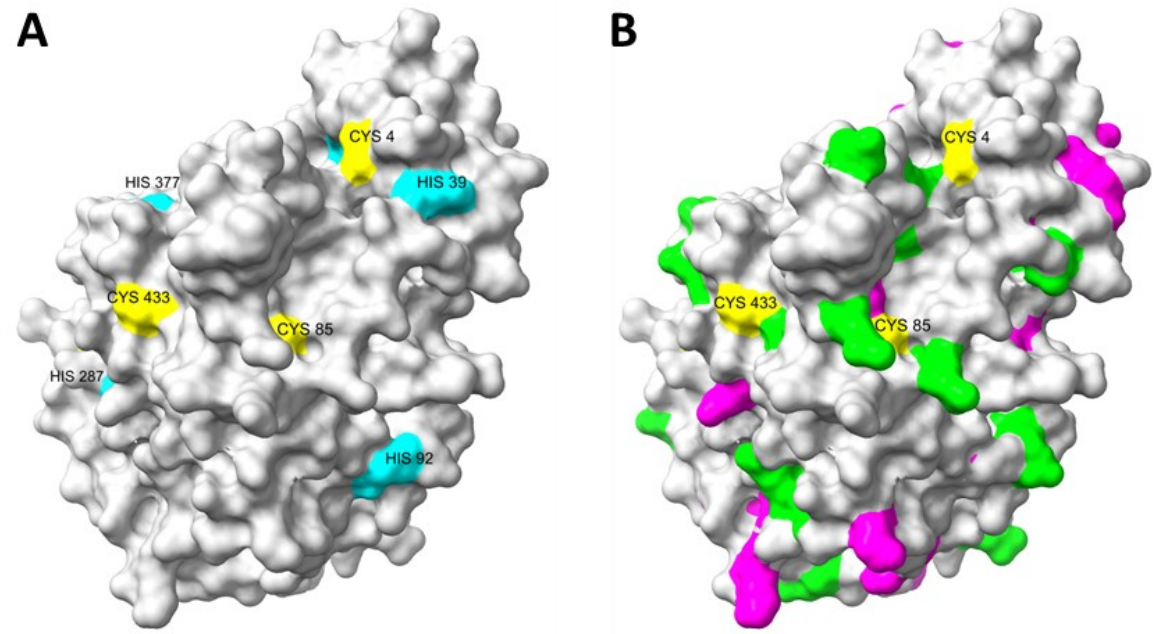

Figure 24 3D protein model of R11G10.2
3D surface model of R11G10.2 constructed using *Protein Homology/analogY Recognition Engine V 2.0* (*Phyre*²; Kelley et al., 2015). **(A)** Model with cysteines (Cys, yellow) and histidines (His, cyan) highlighted. Top left Segment: Model was rotated 90° around the x-axis to show Cys57. Bottom left Segment: Cys80 and Cys83 are focused. Red arrow shows approx. position of thiols groups of Cys80 and Cys83. (B) Amino acid residues easily modifiable by carbonylation according to (Fichtner et al., 2020) are highlighted: cysteines (Cys, yellow), lysine (purple), arginine (green).

considering the lower conservation rate of R11G10.2 compared to Y37A1B.5. Thirty five percent of the amino acids of R11G10.2 are identical to the human SELENBP1 and 56 % have similar chemical properties according to similarity criteria used in sequence homology analysis programs such as BLAST (Altschul et al. 1997). Given the relatively low sequence similarity it was not surprising that also many of the motifs proposed to be important for the function of the protein or the binding of selenium, are not present in R11G10.2. Its sequence does not include a CxxC motif, but Cys57 of SELENBP1 aligns with Cys85 of R11G10.2 and seems to be accessible and on the surface. Although the HxxH and HxD motifs of SELENBP1 are not conserved, histidines seem to present on the surface (His7, His39, His63, His92, His176, His222, His232, His287, His293, His 308, His 323, His 360 and His 377) more abundantly than shown for SELENBP1 (Figure 24).

Analysis of *R11G10.2* mRNA levels during *C. elegans* lifetime did not reveal a clear pattern. There seems to be a trend towards an increased expression with progressing age ($R^2 = 0{,}48$) (Figure 25). However, due to the large variability of the expression between the biological samples, no clear statement can be made.

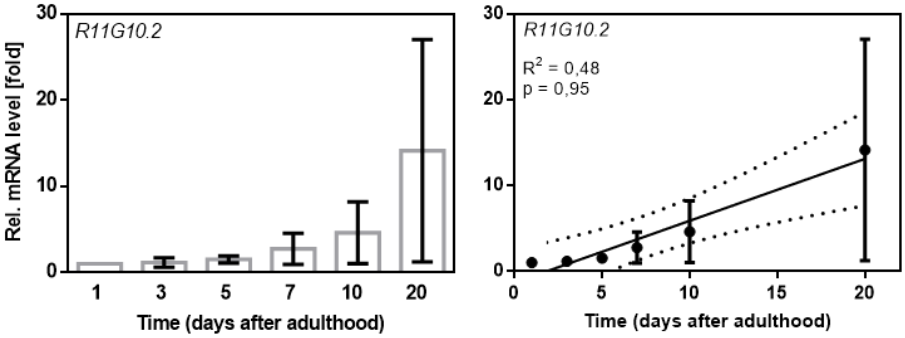

Figure 25 mRNA expression of *R11G10.2* is not strongly associated with aging.
mRNA levels of *R11G10.2* in wildtype worms at day one, three, five, seven, ten and twenty after adulthood measured via qRT-PCR. Data were normalized to tba-1 as housekeeping gene and to the expression at day one to calculate the fold-change. Linear regression revealed a weak trend ($R^2 = 0.48$) of inclining R11G10.2 levels during aging (**right**). Data are presented as means ± SD, dashed line shows 95 % confidence interval.

3.3.1 R11G10.2 is expressed in AFD and BAG neurons

Strains carrying transcriptional or translational reporters, were constructed and cloned into a GFP vector by Dr. Pavel Urbánek from the Klotz laboratory. To this end, genomic fragments, 3086 bp of the R11G10.2 3'UTR region (for the transcriptional reporter, LOK127) and additionally (in the case of the translational reporter, LOK128; Figure 26) the open-reading frame, were cloned into a GFP vector and injected into *C. elegans*. This was done in collaboration with the lab of Dr. Antonio Miranda Vizuete.

Strikingly, R11G10.2 expression was exclusively found in a set of two head neurons and the corresponding dendrites (Figure 26). Dr. Martin Srayko, University of Alberta, Edmonton, AB, Canada, identified the expressing neurons as AFD and BAG neurons. The proximal set of neurons, identified as AFD, terminate in bush-like structures in front of the tip of the mouth, not reaching the outside, which is a well-described feature of AFD neurons (see 1.6.2.1). The more distally observed neurons end near the tip but do likewise not seem to reach the outside. The structure of the dendritic endings appears to be bag-like, which would indicate BAG neurons (see 1.6.2.2). Additionally, BAG neurons are not part of a sensillum. Because no overlap between the GFP signal of these neurons and dil staining, which stains amphid and phasmid sensilla, was observed (Dr. Martin Srayko, pers. comm.), these neurons were concluded to be BAG.

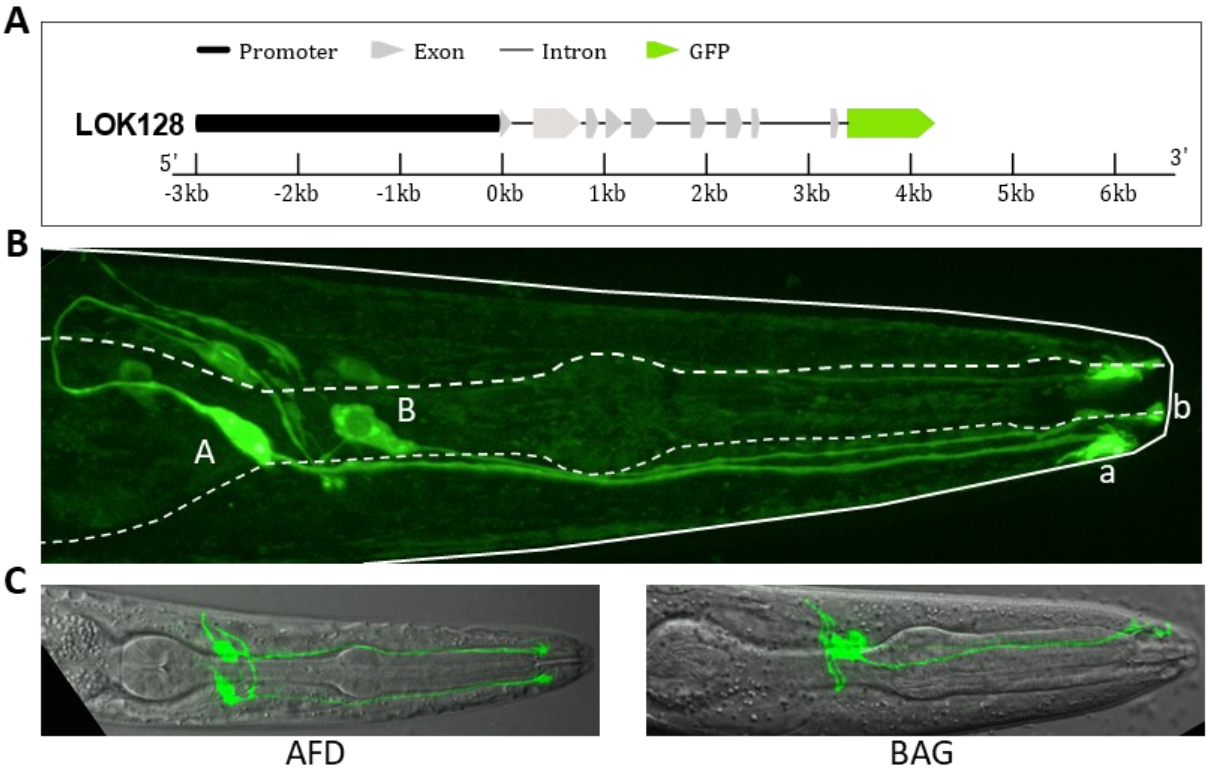

Figure 26 R11G10.2 is a neuronal protein, expressed in AFD and BAG neurons.
(A) Schematic representation of the translational reporter construct (LOK128). A genomic fragment containing a 2,978 kb region of the *R11G10.2* 5'UTR as promoter, together with the *R11G10.2* open-reading frame was cloned into the GFP plasmid pPD95.77 and injected into *C. elegans* wildtype (Dr. Miranda-Vizuete). **(B)** R11G10.2 is solely expressed in two head neurons and their dendrites, identified as AFD (A,a) and BAG (B,b) neurons (Dr. Martin Srayko). Dashed line outlines the pharynx. **(C)** Pictures show AFD (left; PY1322) and BAG (right; DA1290) reporter strains and for comparison (pictures provided by Dr. Martin Srayko).

RNAi was reported to be ineffective in the *C. elegans* nervous system (Timmons et al. 2001). This led to the initial hypothesis that the lifespan modulation after *R11G10.2* RNAi may be caused by signals of R11G10.2 neurons to somatic tissues, which might have R11G10.2 expressed at sub-detection-level, undetectable in LOK128. However, Weiye Gong from the Klotz laboratory demonstrated that the R11G10.2-GFP signal in the head neurons of LOK128 was strongly diminished after R11G10.2 siRNA treatment, which appeared to be similar to the reduction in mRNA expression of whole worm lysates, following *R11G10.2* RNAi. However, expression in the ciliated dendritic endings remained intact in most of the evaluated LOK128 worms following *R11G10.2* RNAi (Figure 27A). Depletion of R11G10.2 also triggered the elevation levels of reduced glutathione (GSH) compared to control-RNAi treated worms in whole-worm lysates (Figure 27C), which likely contributed to the lifespan extension and stress resistance elicited by *R11G10.2* RNAi.

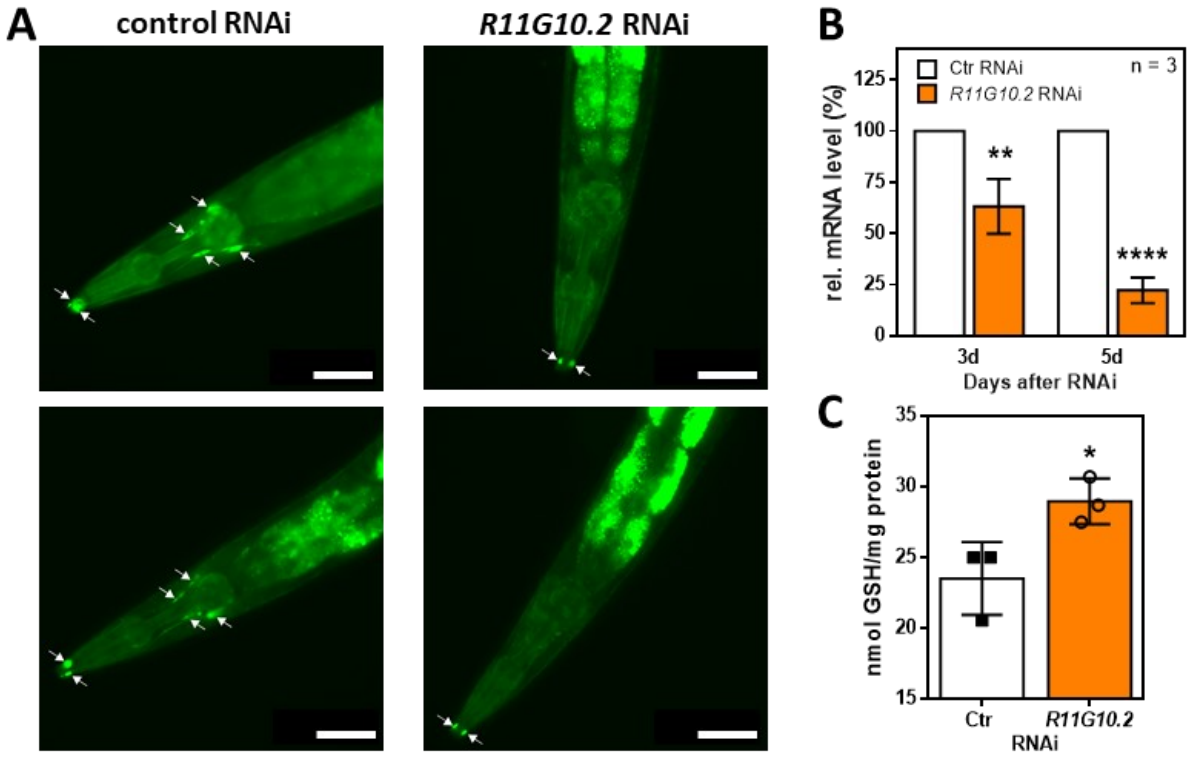

Figure 27 *R11G10.2* RNAi is effective in neurons and RNAi increases GSH levels.
(A) *R11G10.2* RNAi is effective in LOK128. Pictures kindly provided by Weiye Gong. GFP signal in neurons was strongly reduced after *R11G10.2* RNAi treatment for five days compared to control, while the signal in the dendritic endings remained intact in most analyzed worms after RNAi. Scale bar: 50 µm. Reduction of GFP signal is comparable to the effect of RNAi on mRNA levels after treatment with *R11G10.2* RNAi three or five days **(B)**. **(C)** GSH measurement via HPLC method of wildtype worms after treatment with *R11G10.2* RNAi for five days. GSH levels showed a trend of being increased after *R11G10.2* RNAi.

3.3.1.1 R11G10.2 null mutant is morphologically indistinguishable from wildtype

For *R11G10.2* a null mutant (PHX2066, *R11G10.2(syb2066)*) was obtained recently. Strains were validated via PCR, in which wildtype and mutant alleles were distinguished by differently sized amplicons on genomic DNA and the respective transcripts. Phenotypical analysis of both wildtype and PHX2066 mutant worms revealed no apparent growth defect. Mutants were morphologically indistinguishable from wildtype animals at all times and needed the same time to reach the different larval stages (Figure 28).

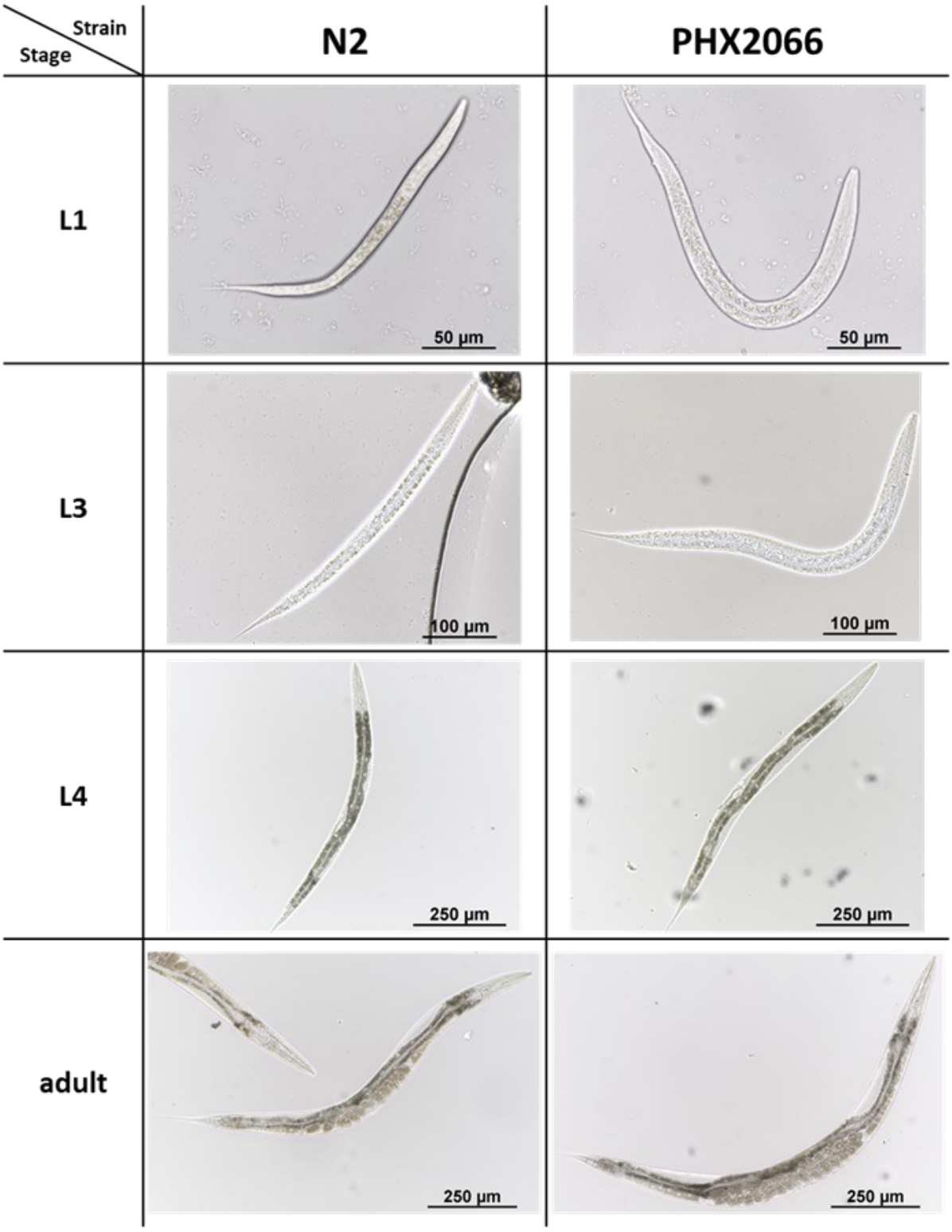

Figure 28 *R11G10.2* null mutant PHX2066
Phenotypical analysis of R11G10.2 null mutant PHX2066. PHX2066 and wildtype N2 animals were synchronized via L1 arrest. Pictures of L1 animals were taken 4 hours after refeeding. L3, L4, and adult animals were photographed at 24-hour intervals following that (details see introduction). No phenotypical differences were observed in the different larval stages.

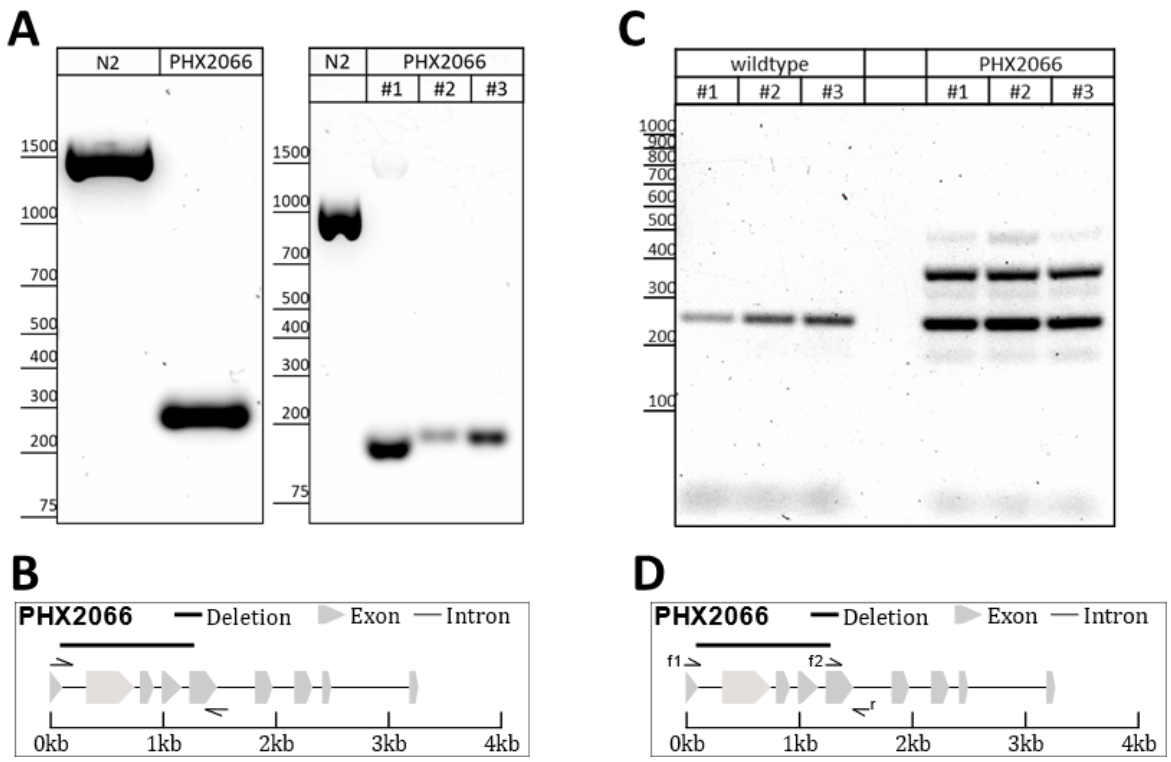

Figure 29 Genetic validation of PHX2066
Validation of PHX2066 via PCR**. (A) (left)** Genomic DNA of wildtype N2 and PHX2066 mutants. Expected bands: N2 1450 bp, PHX2066 268 bp. One main band below 1500 bp was amplified in wildtype worms. showed one band at the anticipated size of around 268 bp in PHX2066 (Primer5+6). **(right)** cDNA of wildtype and PHX2066. Anticipated bands: N2 959 bp, PHX2066 165 bp (Primer 1+2). In wildtype only one band between below 1000 bp was visible, which corresponds to the expected size of 959 bp. Single-worm PCR of three different specimens of PHX2066 amplified one band at the expected size of approx. 165 bp size. The faint band in worm #1 is presumably an unspecific amplicon because it does not appear in worms #2 and #3. **(C)** Single-worm PCR on genomic DNA of worms with a wildtype R11G10.2 allele and PHX2066 mutants carrying the *R11G10.2(syb2066)* allele. As expected animals with the wildtype allele showed one band at 268 bp. PHX2066 appears to be heterozygous for *R11G10.2(syb2066)* because two bands for the wildtype (480 bp) and the mutant allele (366 bp) were amplified (Primer9+10+11). For each strain three worms were analyzed. **(B, D)** Schematic depiction of *R11G10.2(syb2066)* allele in PHX2066. The genomic deletion is 1182 bp of the R11G10.2 CDS. **(B)** Primers for PCR on genomic DNA resulting in a 1450 bp fragment in wildtype and 268 bp fragment in PHX2066 animals. **(D)** Primers for duplex PCR on genomic DNA resulting in a 480 bp fragment on a wildtype allele (f2+r; Primer9+11) and 366 bp fragment on a R11G10.2(syb2066) allele (f1+r; Primer10+11). DNA was loaded onto a 1 % (A) or 3 % (C) agarose gel for separation via electrophoresis.

3.3.2 R11G10.2 regulates genes involved in nervous system development

Enrichment of genes regulated after *R11G10.2* RNAi revealed a picture similar to what was observed after *Y37A1B.5* RNAi. The treatment mainly increased genes related to metabolic pathways (*Ribosome*, *Proteasome*, *oxidative phosphorylation*, *organophosphate metabolic process*) and "*cellular defense*", while attenuating genes associated to developmental or growth-related processes (*Wnt signaling*, *ErbB/EGFR signaling*, *animal organ development*). The strong enrichment of downregulated genes related to "*nervous system development*" could arguably be regarded as a validation of the knockdown of a neuronal gene (Figure 30).

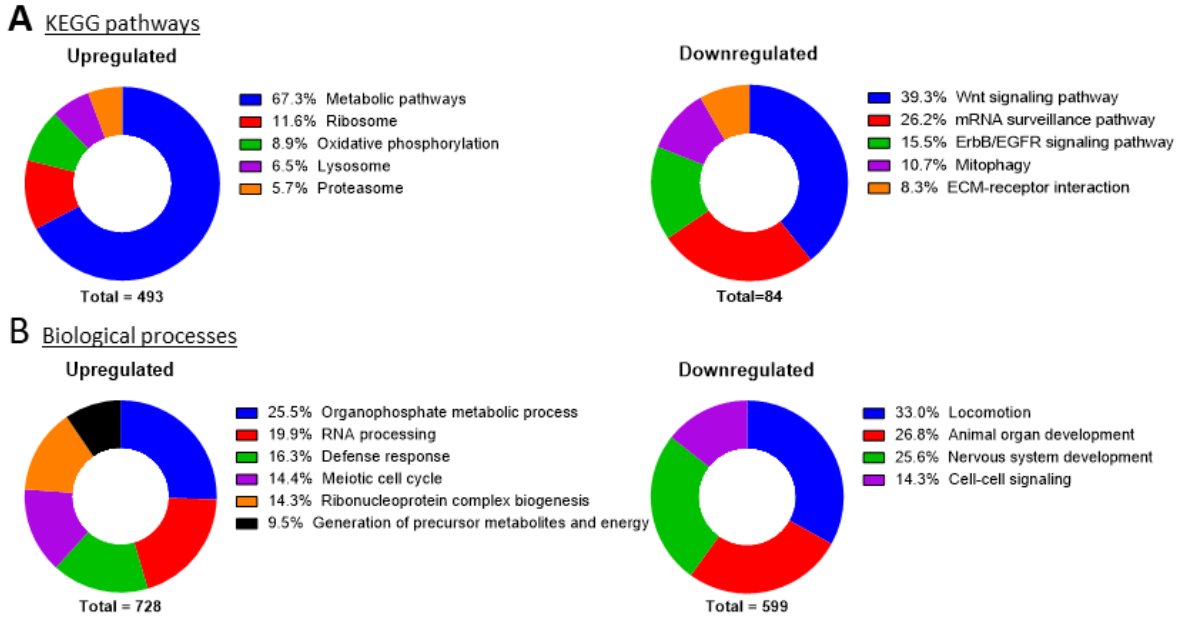

Figure 30 R11G10.2 regulates metabolic pathways and genes associated with nervous system development
Differentially expressed genes, obtained by transcriptome analysis of wildtype worms treated with *R11G10.2* siRNA for five days, were enriched for KEGG pathways **(A)** or biosocial processes **(B)** using WebGestalt 2019 (Liao et al. 2019). The total number of up- or downregulated genes was set to 100 % and the fraction of each gene set was calculated proportionally. Total displays the number of genes in each gene set (100 %).

3.3.3 Is R11G10.2 involved in the regulation of sulfur metabolism?

Additionally, a similar regulation of the genes associated to H_2S production, as seen after *Y37A1B.5* RNAi, was found after *R11G10.2* RNAi. *Cth-1* was upregulated 2.3-fold, *cbs-1* was downregulated 0.8-fold, cysl-2 and cysl-3 were upregulated 1.4- or 1.2-fold and most of the *mercaptopyruvate sulfurtransferase*s were not regulated. With regard to the effect which was observed after *Y37A1B.5* RNAi, it was unsurprising that the cysteine-based hydrogen sulfide production was diminished by around 30 % in the R11G10.2-depleted group (Figure 31, note: control lane is identical with control lane in Figure 21A). As reported for Y37A1B.5, the ferritin homologs FTN-1 and FTN-2 were elevated after *R11G10.2* RNAi, 1.9-fold and 1.2-fold, respectively.

3.4 Venn analysis of RNASeq data of R11G10.2 and Y37A1B.5 RNAi

Due to the apparent overlap of enriched pathways in worms depleted of Y37A1B.5 or R11G10.2, the genes which were exclusively regulated by either treatment, as well as the overlap of both treatments were analyzed using *Webgestalt* with the purpose of revealing functions which might be inherent to SELENBP1 and which might be organism- or tissue-

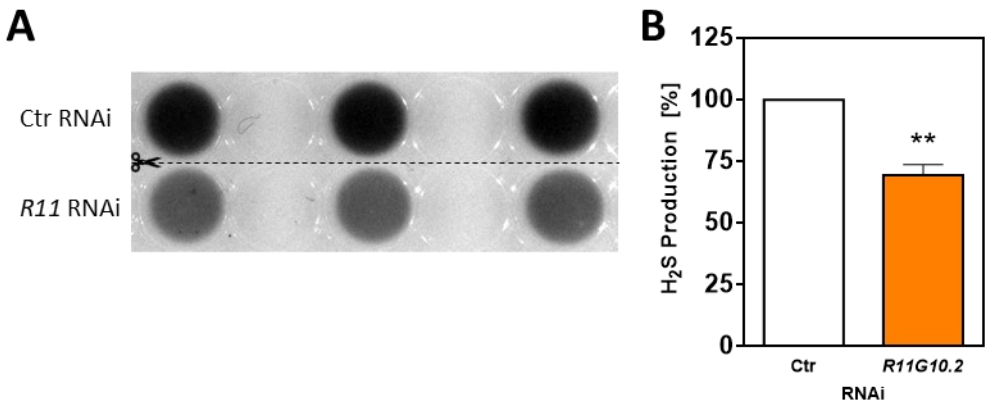

Figure 31 The capacity to produce H_2S from cysteine is reduced after *R11G10.2* RNAi
(A) H_2S production was assessed in a 96-well format using 100 µg of total protein lysate. 96-well plate was covered with a lid containing 100 mM lead acetate in agarose and was incubated at 37 °C for 4 h. Image was taken in a Biorad Chemidoc MP imager. Picture shows three technical replicates of one independent experiment of worms treated with *R11G10.2* or Ctr RNAi. Note: Control lane is identical with control lane in Figure 21A. **(B)** Quantification of three independent experiments as depicted in (A). The volume intensity of each black dot was measured using the ImageLab volume tool (Biorad). Data shows mean ± SD. **p<0.001 unpaired t-test with Welch's correction, compared to control RNAi.

specific. Regarding the long-lived and stress-resistant phenotype of each RNAi-treated worm strain, it was reassuring that genes which were upregulated by both treatments were especially related to "*defense response*" but also to lipid- and energy metabolism related processes (*lipid metabolic-*, *organophosphate metabolic process*) (Figure 32). As reported, c*th-1* and *cbs-1* were also regulated in a similar fashion by both *Y37A1B.5* and *R11G10.2* RNAi. It was surprising that genes related to nervous system development were attenuated in both treatments, which did not appear before in the enrichment of the *Y37A1B.5* RNAi (see Figure 20).

The number of genes which were exclusively regulated by Y37A1B.5 was small (384) compared to the complete list of genes regulated by both treatments (4,981). Additionally, few of the enriched biological processes could be attributed to epidermal specific functions. However, one of Y37A1B.5 exclusive regulated processes was the *"Regulation of immune system"* which could be of interest, since the epidermis is regarded as an organ of innate immunity (Taffoni and Pujol 2015).

Regarding the exclusively enriched terms of *R11G10.2* RNAi, the only process which seemed be intuitively attributable to R11G10.2 was the attenuation of genes related to "*Nervous system development*".

Figure 32 Comparison between genes regulated by *Y37A1B.5* RNAi and *R11G10.2* RNAi
(A) Venn diagram of genes regulated by Y37A1B.5 RNAi (II) and *R11G10.2* RNAi (III) or regulated by both treatments (I). **(B)** Genes of each category were enriched for biological processes using Webgestalt 2019 (Liao et al. 2019). The total number of up- or downregulated genes was set to 100 % and the fraction of each gene set was calculated proportionally. Total displays the number of genes in each gene set (100 %).

4 Discussion

With the ongoing demographic shift in many developed countries and an ever-growing population with increased age (European Commission and Eurostat 2015), more research is beginning to focus on the mechanisms of aging and age-related diseases. Aging is one of the strongest risk factors of many diseases, including cancer (Smetana et al. 2016). However, to cure such age-related diseases, one must first understand the underlying mechanisms. SELENBP1 has emerged as a major possible contributor to cancer development (Yang and Diamond 2013), which is why this study focused on identifying basic mechanisms of SELENBP1 and its involvement in aging in the model *Caenorhabditis elegans*.

4.1 Association of SELENBP1 orthologs with aging and redox homeostasis

This work established the contribution to aging by the two SELENBP1 orthologs Y37A1B.5 and R11G10.2: Depletion of SELENBP1 orthologs ameliorated the toxic effects of the redox cycler paraquat, which was associated with a prolonged lifespan and the improvement of other health parameters (Köhnlein 2016; Köhnlein et al. 2020), showing that these orthologs somehow contribute to oxidative stress homeostasis. This might be an evolutionarily conserved trait, in regard to data showing a contribution of human SELENBP1 in inflammation and stress response (Bai et al. 2019). It can be hypothesized that these features might be exploited by cancer cells to make them more resistant, which would explain why SELENBP1 abundance is so strongly reduced in many types of cancer and why this correlates negatively with clinical outcome (Elhodaky et al. 2018). It was therefore important to identify mechanisms that might be relevant for the stress resistance phenotype following RNAi of *Y37A1B.5* and *R11G10.2*.

Possible transcriptional regulation of Y37A1B.5

In this work, the expression of Y37A1B.5 was demonstrated to exponentially decline during the aging process of the worms. This raised the question: Is this a mechanism used by aging cells to protect themselves against the burden of senescence or might Y37A1B.5 just be dispensable in later life? To answer this, future experiments will address this question using a system for drug-inducible gene expression of transgenes as developed by Mao et al. or Monsalve et al. (Mao et al. 2018; Monsalve et al. 2019). With this, it is planned to induce

Y37A1B.5 expression in all stages of life to see how this will affect overall gene expression, lifespan or stress resistance.

SELENBP1 expression was shown to be heavily affected by DNA methylation (Pohl et al. 2009). *C. elegans* was speculated to be devoid of DNA methylation and DNA methyl transferases some years ago (Wenzel et al. 2011; Yi 2012). However, some studies have proven otherwise, showing adenine N6-methylation (6mA) in dependence of the DNA demethylase NMAD-1 and the DNA methyltransferase DAMT-1 (Greer et al. 2015) and also evidence of 5-methyl-2'-deoxycytidine (5-mdC) and 5-hydroxymethyl-2'-deoxycytidine (5-hmdC) (Hu et al. 2015). It was shown that 6mA affected fertility and 5-mdC was elevated in response to cadmium treatment. Additionally, it was shown that many *C. elegans* promotors have a high density of CpG, as many vertebrates have, which have been established as targets for methylation to regulate transcriptional gene expression. Furthermore, *C. elegans* expresses a *CpG-binding protein* homolog (CFP-1), an epigenetic regulator of DNA methylation, which leaves room for the hypothesis that, like in vertebrates, changes in DNA methylation might be associated with aging (Bell et al. 2019; Chen et al. 2014). Therefore, like SELENBP1, Y37A1B.5 might also be susceptible to DNA methylation and the declining levels of Y37A1B.5 during the age of the worms might be due to changes in methylation of the Y37A1B.5 promotor.

The role of Y37A1B.5 in redox homeostasis was examined, analyzing the effect of different substances known to induce reactive oxygen species on the abundance of Y37A1B.5. The hypothesis behind this was, that reactive oxygen species would trigger a reduction of Y37A1B.5, which would lead to an increase of stress resistance. However, the superoxide anion producing redox cycler paraquat (Bonneh-Barkay et al. 2005), failed to affect Y37A1B.5 expression. One hypothesis explaining this, is that Y37A1B.5 may not be responsive to superoxide anions. This would explain why *Y37A1B.5* RNAi also did not induce the expression of the superoxide dismutase system, which is responsible for catalyzing the reaction of superoxide to hydrogen peroxide. However, as shown in this work, Y37A1B.5 levels were attenuated dose dependently by arsenite, which is also known to trigger the formation of reactive oxygen species. However, as discussed before, arsenite does also actively deplete thiols, especially reduced glutathione (see Results 3.2.5). One mode of action might therefore be, that the accumulation of arsenic-glutathione complexes not arsenite itself, trigger the reduction of Y37A1B.5 in order to regenerate glutathione levels. This hypothesis is backed

up by the trend of elevated GSH elicited by *Y37A1B.5* RNAi and by the upregulation of most *C. elegans* glutaredoxins (see Results 3.2.5). The modulation of glutathione would also a plausible explanation to why depletion of Y37A1B.5 renders worms more stress resistant to oxidative stress, as shown before (Köhnlein et al. 2020).

Transcription factors affecting Y37A1B.5 expression

Searching for downstream transcription factors involved in the stress resistant and anti-aging phenotype of *Y37A1B.5* RNAi, possible candidates were the transcription factors MDT-15 and EGL-27. Similarly to what transcriptome analysis of *Y37A1B.5* RNAi suggested, MDT-15 was shown to be a transcriptional co-regulator and is an important component in the maintenance of stress response as well as energy and lipid metabolism (see Introduction 1.6.4). The GATA transcription factor EGL-27 is a positive regulator of lifespan (see Introduction 1.6.3). Regarding resistance to heat, it was demonstrated that loss of *egl-27* negatively affected the survival against noxious temperatures (Xu and Kim 2012).

To test the hypothesis that the expression of Y37A1B.5 target genes responsible for the elevated stress resistance might be dependent on MDT-15, a stress resistance assay was performed in which the effect of *Y37A1B.5* RNAi, as well as *mdt-15* RNAi on heat resistance, was analyzed. This was not only done to test for the contribution of MDT-15 in the Y37A1B.5 stress resistant phenotype, but also to see if depletion of Y37A1B.5 would confer resistance to heat. Genes responsible for resistance to heat are mainly controlled by the heat shock factor HSF-1 (Vihervaara and Sistonen 2014). An interplay of MDT-15 and HSF-1 was shown to be important for the maintenance of *C. elegans* proteostasis. Furthermore, it was shown that depletion of MDT-15 hyperactivated HSF-1 target genes like *hsp-16.2* or *hsp-4* upon heat stress. If this, however, was dependent on HSF 1 remained unclear in that study (Taubert et al. 2008). Therefore, it was hypothesized that MDT-15 might be involved in heat shock response.

The results of the heat-stress assay shown in this work (see Results 3.2.8), *mdt-15* RNAi strongly reduced the survival of *C. elegans* in response to noxious temperatures, showing that MDT-15 might not be as dispensable to heat-shock response, as concluded by (Taubert et al. 2008). As demonstrated in this work, *Y37A1B.5* RNAi increased the survival of *C. elegans* to heat stress by roughly 30 %, which was completely abolished in a *mdt-15* RNAi background. It can therefore be concluded that the resistance to heat stress demonstrated for Y37A1B.5

RNAi is dependent on MDT-15. Future experiments will show, if MDT-15 is also involved in the enhancement of lifespan and resistance to oxidative stress caused by a depletion of Y37A1B.5.

However, some things remained unclear. First, this work showed that *mdt-15* RNAi resulted in a strong depletion of Y37A1B.5, which, however, was associated with an increase in lifespan and stress resistance. Secondly, it was demonstrated in a prior publication, that depletion of Y37A1B.5 did not regulate *mdt-15*, at least not on a transcriptional level (Köhnlein et al. 2020). This begs the following questions: I. How does Y37A1B.5 influence MDT-15 to regulate lifespan and stress resistance and II. how does the downregulation of Y37A1B.5 by *mdt-15* RNAi match up with the contrasting phenotypes of *Y37A1B.5* and *mdt-15* RNAi regarding stress resistance?

One attempt to explain the first question, is that Y37A1B.5 might be located in a network of genes, which influence each other to regulate lifespan but which are tightly controlled by MDT-15 and shut off when MDT-15 is missing. This would answer both questions, since it would also explain why *Y37A1B.5* RNAi did not affect *mdt-15* expression directly. Based to this hypothesis, it would also not be surprising, why Y37A1B.5 was not able to ameliorate the phenotype caused by *mdt-15* RNAi, which was characterized by a deterioration of the intestine and the germline, and an accumulation of vacuoles throughout the body in this work and but also by Taubert et al. (2006).

Since it was shown in this work, that a common feature of Y37A1B.5 and R11G10.2 seems to be the regulation of lipid metabolic processes and genes associated with defense response, it can be speculated whether the lifespan extension and the stress resistance caused by *R11G10.2* RNAi might also dependent on MDT-15, thus similar approaches as for Y37A1B.5 will be taken to investigate their relationship. Furthermore, the regulation of metabolic processes as well the regulation of stress response, might be evolutionary conserved features of SELENBP1, since it was reported that SELENBP1 is also involved in stress response in humans (see Introduction 1.5.8) and was positively associated with the accumulation of lipids in adipocytes (Steinbrenner et al. 2019).

Regarding the role of EGL-27 in the resistance to heat, differently from what was expected, depletion of *egl-27* via RNAi did not modulate the survival to heat-stress. Likewise, a

combination of Y37A1B.5 and *egl-27* RNAi failed to alter the survival compared to control. In regard to the enhancement of heat resistance by *Y37A1B.5* RNAi, this could be interpreted, as EGL-27 being of relevance for the increased survival of Y37A1B.5 depletion. As to the different contributions of EGL-27 to heat shock in this study, compared to what was reported by Xu and Kim, there are some possible explanations. First, Xu and Kim used the *egl-27* knock out mutant *egl-27(we3)*, whereas in this thesis, *egl-27* was depleted via RNAi, which likely was not as effective as a genetic knockout. Second, looking at the graph in the study of Xu and Kim, the *egl-27(we3)* mutant seemed to slightly diminish survival only ten to twenty hours after the heat stimulus. However, at around 40 to 50 hours post heat treatment, which is similar to what was used in this work, there seemed to be not much difference in survival compared to wildtype worms. Nevertheless, since *egl-27* RNAi suppressed the positive effects of *Y37A1B.5* RNAi on heat resistance, it can be proposed that heat resistance elicited by *Y37A1B.5* RNAi seems to be somehow reliant on EGL-27. This is in accordance with the idea of EGL-27 being a factor that delays aging and promotes stress resistance as shown by Xu and Kim.

4.2 Potential role of SELENBP1 orthologs in selenium homeostasis

In order to investigate the role of Y37A1B.5 in selenium homeostasis and whether it might behave as a selenium-binding protein, experiments were performed in which the abundance of Y37A1B.5 were measured in response to a wide range of selenite concentrations. As shown in this work, only concentrations which would be regarded as highly toxic, i.e. 100 μM and above, trigger the elevation of Y37A1B.5 levels, whereas mildly toxic (1 μM) or hormetic doses (0.01 μM) did not alter the abundance of Y37A1B.5. Certain selenium compounds are also known to generate reactive oxygen species (Li et al. 2007). However, as demonstrated in this work, Y37A1B.5 does not seem to be responsive to reactive oxygen species per se, which is why this effect can be attributed to the effect of selenite itself. Further experiments revealed that Y37A1B.5 was necessary for survival in the presence of toxic environmental selenium because *Y37A1B.5* RNAi reduced the survival under such conditions. Therefore, it can be proposed that Y37A1B.5 might act as a kind of buffer for selenium which would otherwise elicit toxic effects. To answer this question, experiments using recombinantly expressed human, mouse and *C. elegans* SELENBP1 are currently being made to determine whether they

are able to bind selenium under physiological circumstances and if they share a common binding motif.

This thesis also described potentially important features of the SELENBP1 protein structure as well as of Y37A1B.5 and R11G10.2. Y37A1B.5 seemed to be similar to human SELENBP1, sequence wise, but also judging from the position of amino acid residues, which were discussed in literature to be important for the function of SELENBP1 and for selenium binding. Because the functionally important cysteine residue at position 57 in SELENBP1 as well as one of the thioredoxin motifs (CxxC) are present in Y37A1B.5, it can be proposed that these might play a role in the protective function of Y37A1B.5 against selenium. Due to the lack of these features in R11G10.2, it seems unlikely that this SELENBP1 ortholog would also participate in the protection against the toxic effects of selenium.

4.3 Regulation of sulfur metabolism by the SELENBP1 orthologs

The volatile signaling molecule hydrogen sulfide has been shown to be involved in the regulation of lifespan and the resistance to heat and oxidative. It was reported that loss of certain hydrogen sulfide producing enzymes negatively affected lifespan and stress resistance, whereas supplementation with the hydrogen sulfide releasing chemical (*p*-methoxyphenyl)morpholino-phosphinodithioic acid (GYY4137) enhanced lifespan and the resistance to noxious heat (Miller and Roth 2007; Qabazard et al. 2014). As reported in this thesis, one of the enzymes majorly contributing to endogenous hydrogen sulfide production, *cystathionine-γ-lyase* (CTH), was upregulated strongly after RNAi of *Y37A1B.5* or *R11G10.2*. Therefore, it was hypothesized that the lifespan extension elicited by RNAi of *Y37A1B.5* or *R11G10.2* might be due to elevated levels of hydrogen sulfide. However, with the lead-acetate-based method used in this work, the conversion rate of cysteine by *cystathionine-γ-lyase* and *cystathionine-β-synthase*, the only known enzymes to produce hydrogen sulfide from cysteine, was diminished by around 30 % in lysates of Y37A1B.5 or R11G10.2 depleted worms. Assuming that Y37A1B.5 and R11G10.2 might share some biochemical properties with SELENBP1, this might be explainable by several mechanisms. First, SELENBP1 is an H_2S producing enzyme itself (see Introduction 1.5.1), thus depletion of a SELENBP1 ortholog might already reduce the H_2S production. To verify this, efforts are currently being made to identify if purified R11G10.2 or Y37A1B.5 exhibit MTO activity. Second, according to *Singh et*

al., the contribution to H_2S production via the reaction of cysteine and homocysteine to cystathionine is much larger (≈95 %) than the reaction of cysteine to serine, or two cysteines to lanthionine (each ≈2,5 %) (Singh et al. 2009). Therefore, a reduction of homocysteine levels after RNAi of *R11G10.2* or *Y37A1B.5* would be a plausible explanation for the unexpected outcome. This hypothesis will be addressed by using a combination of cysteine and homocysteine as substrates in future analyses.

Furthermore, iron ions, together with pyridoxal phosphate – the latter was abundantly added to the hydrogen sulfide reaction mix used in this work – were reported to catalyze the reaction from cysteine to hydrogen sulfide in a non-enzymatic manner (Yang et al. 2019). Therefore, reduced levels of free iron ions would reduce the contribution of this reaction to overall hydrogen sulfide production. Ferritins are proteins that assemble to spherical complexes and are the most important storage for free iron in pro- and eukaryotes. In *C. elegans*, FTN-1 and FTN-2 are regarded as ferritin orthologs (Arosio et al. 2009). As shown before, the expression of FTN-1 and FTN-2 was increased after *R11G10.2* or *Y37A1B.5* RNAi (see Results 3.2.10, 3.3.3). Since iron storages are supposedly bigger but no iron was supplemented, this suggests reduced levels of free iron. If levels of free iron were reduced after *R11G10.2* or *Y37A1B.5* RNAi, this would also reduce the contribution of the non-enzymatic production of H_2S by iron and pyridoxal phosphate and would thereby be another possibility explaining the reduced hydrogen sulfide production after depletion of R11G10.2 or Y37A1B.5.

4.4 Role of SELENBP1 orthologs in differentiation and development

It was demonstrated before that *Y37A1B.5* gene expression was found mainly in the epidermis and recently, Y37A1B.5 transcriptional reporters have also been used as markers for epidermal expression (Kaletsky et al. 2018; Mckay et al. 2003). Using a Y37A1B.5-GFP fusion probe, this work demonstrated that Y37A1B.5 protein levels also occur mainly in the epidermis and it does not seem to be exported out of the cell.

Since *C. elegans* has a constant number of cells once fully developed (Sulston et al. 1983), the epidermis does not develop or differentiate any further once worms reach adulthood. Therefore, regarding the declining expression of Y37A1B.5 in aging adult worms, it seems plausible that Y37A1B.5 may be dispensable after reaching adulthood. To test the hypothesis that Y37A1B.5 might instead be important for larval or embryonic development, a Y37A1B.5

null mutant (PHX2078) was obtained by Suny Biotech (Fuzhou, China; see Results 3.2.11). Due to the involvement of the epidermis in developmental processes (Chisholm and Hsiao 2012) and the regulation of pathways associated with development (MAPK, Wtn) by Y37A1B.5, it was expected that these worms would show some form of developmental defect. However, as presented in this work, PHX2078 did not show any phenotypical difference compared to wildtype worms.

The R11G10.2 null mutant PHX2066 also did not display any morphological deficits. This was likewise surprising given the downregulation of genes related to *"animal organ-"* and *"nervous system development"* by *R11G10.2* RNAi as shown by RNASeq (see Figure 30). To reveal if R11G10.2 expressing neurons will be altered in their appearance, the R11G10.2 transcriptional reporter LOK127 reporter will be crossed with PHX2066.

4.5 Relevance of neuronal expression of R11G10.2

Despite its lower homology to SELENBP1, R11G10.2 was also shown to modulate lifespan and stress resistance to a similar extent as Y37A1B.5. However, as demonstrated, R11G10.2 was only expressed in a set of two head neurons, involved in thermotaxis and heat-shock response (AFD) as well as BAG neurons, which are involved in the detection of oxygen and carbon dioxide. SELENBP1 on the other hand was hypothesized to be involved in the pathophysiology of schizophrenia (see Introduction 1.5.9). Although there is no data verifying this, R11G10.2 could, in a more general sense, also be involved in the normal function of AFD or BAG neurons in *C. elegans*, by mechanisms which may hypothetically be similar to SELENBP1 in human brain. Therefore, future studies on R11G10.2 might help decipher the regulatory mechanisms of SELENBP1 in human brain. Unfortunately, little is known about the mechanisms of SELENBP1 in schizophrenia. However, inflammation was hypothesized to play a role in the onset of schizophrenia (see Introduction 1.5.9). In this regard, R11G10.2 could be involved in similar processes, since its depletion modulated intracellular levels of reduced glutathione, which likely contributed to an increase in stress resistance.

As described before, both sets of neurons were reported to modulate lifespan independent of DAF-2/DAF-16 signaling. This is interesting in regard that *R11G10.2* RNAi seemed to increase lifespan independent of DAF-16, as shown before (Köhnlein 2016). One of the current hypothesis is, that depletion of R11G10.2 alters the communication of AFD and BAG with

other neurons, which influence genes in other cells or tissues to modulate lifespan. Lifespan modulation by BAG neurons was reported to be mediated by the guanylate cyclase GCY-31 and GCY-33 and was dependent on a functional network with URX neurons (Liu and Cai 2013). *Lui and Cai* also demonstrated a method for genetic ablation of individual neurons which will be used in future experiments to target AFD, BAG or other signaling partners to identify the network involved in the lifespan regulation. This system works by expressing the cell-death activator EGL-1 under the control of a neuron-type specific promotor. To analyze the contribution of R11G10.2 on neuronal function, efforts are currently being made to establish a thermotaxis assay in which the behavior of the worms in a temperature gradient will be observed. Worms with an intact thermotaxis are known to memorize and stay at the temperature they were cultured at, while athermotactic animals cannot feel environmental temperatures and will spread to different temperature regions (Goodman 2014). Using such an assay is hoped to reveal if R11G10.2 participates in thermotaxis via AFD neurons and will be used to identify functional interactions with other types of neurons.

5 Conclusion

In this study, the *C. elegans* orthologs of SELENBP1, Y37A1B.5 and R11G10.2, were shown to be expressed in completely different tissues. Whereas Y37A1B.5 was demonstrated to be an epidermally expressed protein, R11G10.2 was exclusively found in two types of sensory neurons of *C. elegans*, known to be participate in detecting differences in ambient temperature (AFD) and changes in breathing gases (BAG). Despite these major differences in expression sites, both genes were shown to modulate similar aspects of worm life. Based on transcriptome analyses of worms depleted of either of the transcripts, Y37A1B.5 as well as R11G10.2 are suggested to be regulators of energy and lipid metabolism and to regulate genes of sulfur metabolism, causing the modulation of endogenous hydrogen sulfide levels. Depletion of either ortholog reduced the amount of hydrogen sulfide produced *in vitro*, to a similar extent. Because SELENBP1 itself is a hydrogen sulfide-generating enzyme, the depletion of an ortholog might be expected to decrease hydrogen sulfide production. However, whether Y37A1B.5 and R11G10.2 are indeed able to produce to hydrogen sulfide, and to which extent they modulate hydrogen sulfide metabolism, has still to be evaluated.

Y37A1B.5 was demonstrated here to be necessary for the protection of *C. elegans* against toxic concentrations of exogenous selenium. Whether this holds true for R11G10.2 has still to be evaluated. However, due to the lack of important features expected to be required for selenium binding in the modelled three-dimensional structure, this seems unlikely. The protection against selenite, however, seemed to have come at a cost. Y37A1B.5 as well as R11G10.2 behave as of pro-aging factors, because depletion of either gene increases lifespan and the resistance to oxidative stress. In line with this, R11G10.2 was shown to modulate glutathione levels, suggesting that this could be a way of affecting both lifespan and stress resistance. The elevated stress resistance, resulting from the depletion of Y37A1B.5 or R11G10.2, resembles features reported for human SELENBP1, which is known to negatively affect stress resistance and inflammation.

Two regulators of Y37A1B.5 expression were identified in this work: MDT-15 and EGL-27, which are transcriptional regulators of lifespan in *C. elegans* and are likely to be essential for the stress-resistant and long-lived phenotype elicited by knockdown of *Y37A1B.5*. Due to the often similarly demonstrated effects of both orthologs, it is hypothesized that this might hold true for R11G10.2 as well. Figure 31 summarizes the findings of this work on the *C. elegans* orthologs of SELENBP1, R11G10.2 and Y37A1B.5.

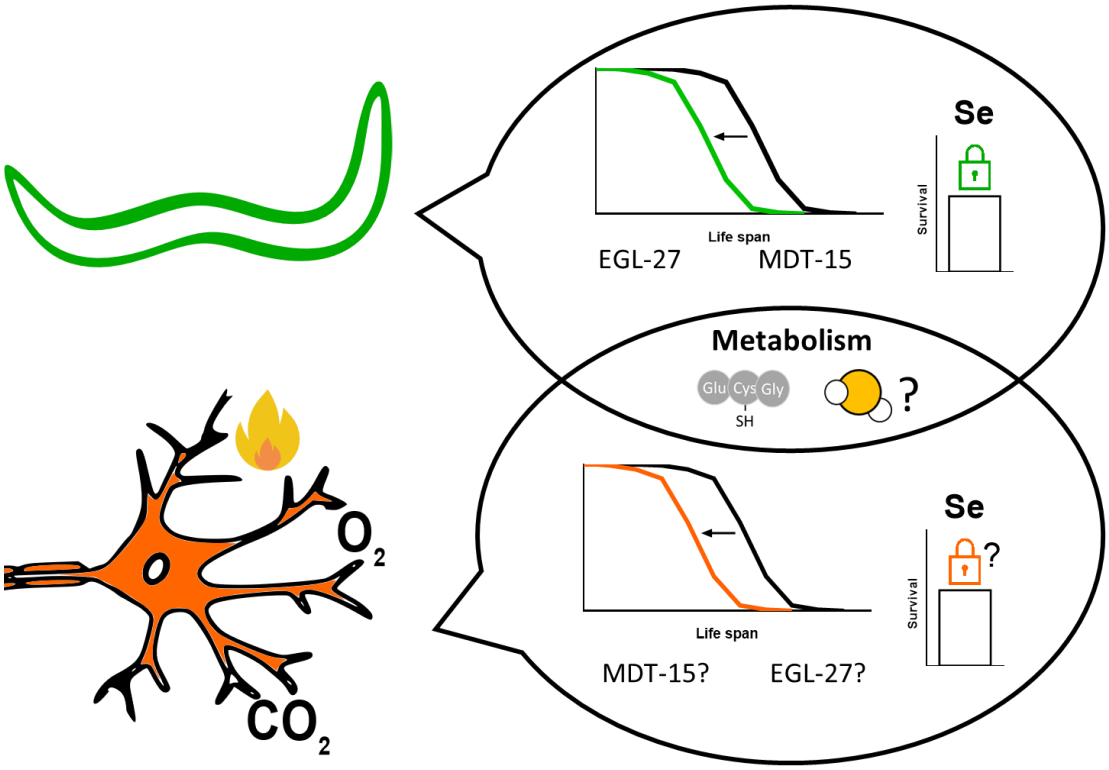

Figure 33 Functions of SELENBP1 orthologs in *C. elegans*
Y37A1B.5 (green) is expressed in the epidermis. It is a negative regulator of lifespan, protects from selenium and affects hydrogen sulfide ( ) production. It is regulated by MDT-15 and EGL-27, which are necessary for the stress resistance of Y37A1B.5-depleted worms. R11G10.2 (orange) is expressed in temperature- and O_2 and CO_2-sensitive neurons. It is a negative regulator of lifespan, regulates glutathione levels ( ) and, like Y37A1B.5, affects hydrogen sulfide production. It regulates metabolic processes, potentially together with Y37A1B.5, and, in analogy to Y37A1B.5, is hypothesized to protect from selenium.
Neuron: https://svgsilh.com/image/2022398.html CC0 1.0
Lock symbol: https://www.svgrepo.com/svg/1896/lock, CC4.0
Fire symbol: https://www.svgrepo.com/svg/11819/firewall, CC4.0

6 Summary

The selenium-binding protein 1 (SELENBP1) contains selenium probably in the form of selenite. SELENBP1 is involved in the regulation of cell proliferation and differentiation, and it is downregulated in many types of tumors. Furthermore, SELENBP1 participates in inflammatory and redox-related processes is it affects the activity of NFκB and of the major antioxidant selenoenzyme glutathione peroxidase 1 as well as cellular levels of glutathione.

To better understand principal functions of SELENBP1 *in vivo*, the aim of this work was to investigate the role and the regulation of two putative SELENBP1 orthologs, Y37A1B.5 and R11G10.2, in the model organism *C. elegans*. Knockdown of these proteins had previously been shown to increase lifespan and stress resistance of *C. elegans.*

In this thesis, it was demonstrated that Y37A1B.5 responds to redox-active compounds, such as arsenite and participates in the regulation of genes involved in cellular defense and sulfur metabolism. Two transcription factors, MDT-15 and EGL-27, regulated Y37A1B.5 abundance and influenced the stress resistance elicited by treatment with *Y37A1B.5* RNAi. Y37A1B.5 appears to protect *C. elegans* from high concentrations of selenium, as treatment selenite dose-dependently increased protein levels of Y37A1B.5 and Y37A1B.5 depletion shortened the survival of worms exposed to toxic doses of selenite.

In contrast to the hypodermal localization of Y37A1B.5, R11G10.2 was found exclusively in two head neurons, BAG and AFD, which are involved in the response to O_2 and CO_2,, in the perception of environmental temperatures as well as in lifespan regulation. It was demonstrated that depletion of R11G10.2 results in increased levels of reduced glutathione in the worms, which could contribute to the observed stress resistance upon treatment with *R11G10.2* RNAi. The neuronal expression of R11G10.2 might indicate similarities to human SELENBP1, which was discussed to be important for normal brain function.

In summary, this work identified several functions of the two SELENBP1 orthologs in the nematode *Caenorhabditis elegans*, with show similarities to the role of SELENBP1 in humans, and it elucidated molecular mechanisms underlying the observed increases in stress resistance and lifespan upon knockdown of the orthologs *Y37A1B.5* and *R11G10.2*.

7 Zusammenfassung

Das selenbindende Protein 1 (SELENBP1) enthält Selen vermutlich in Form von Selenit. SELENBP1 ist an der Regulation der Zellproliferation und -differenzierung beteiligt und zeigt im vielen Tumoren eine exprimierte Expression. Darüber hinaus ist SELENBP1 an Entzündungs- und Redox-Prozessen beteiligt: SELENBP1 beeinflusst die Aktivität von NFκB, die des wichtigsten antioxidativen Selenoenzyms Glutathionperoxidase 1, sowie den zellulären Glutathionspiegel.

Um die Funktion von SELENBP1 *in vivo* besser zu verstehen, sollte in dieser Arbeit, die Rolle und die Regulation der zwei mutmaßlichen SELENBP1-Orthologe, Y37A1B.5 und R11G10.2, im Modellorganismus *C. elegans* untersucht werden. Zuvor konnten wir bereits eine erhöhte Lebensdauer und Stressresistenz von *C. elegans* nach Depletion dieser Proteine belegen.

In dieser Arbeit wurde gezeigt, dass die Expression von Y37A1B.5 durch redox-aktive Substanzen, wie z.B. Arsenit beeinflusst wird und an der Regulation von der zellulären Abwehr sowie des Schwefelstoffwechsels beteiligt ist. Zwei Transkriptionsfaktoren, MDT-15 und EGL-27, regulierten die Expression von Y37A1B.5 und beeinflussten, die durch *Y37A1B.5* RNAi hervorgerufene Stressresistenz. Selenit steigerte dosisabhängig die Proteingehalte von Y37A1B.5, während die Depletion von Y37A1B.5 das Überleben von *C. elegans* gegenüber toxischen Konzentrationen von Selenit verkürzte.

Im Gegensatz zur hypodermalen Lokalisation von Y37A1B.5, wurde R11G10.2 ausschließlich in zwei Kopfständigen Neuronen, BAG und AFD, gefunden, die an der Reaktion auf O_2 und CO_2, an der Wahrnehmung von Umgebungstemperaturen sowie an der Regulierung der Lebensdauer beteiligt sind. Die neuronale Expression könnte auf Ähnlichkeiten mit dem menschlichen SELENBP1 hinweisen, welches als wichtig für die normale Gehirnfunktion diskutiert wurde. Nach Depletion von R11G10.2 war die Konzentration des reduzierten Glutathions erhöht, was zu der zuvor beobachteten verbesserten Stressresistenz nach Behandlung mit *R11G10.2* RNAi beitragen könnte. Die neuronale Expression von R11G10.2 könnte auf Ähnlichkeiten mit dem menschlichen SELENBP1 hinweisen, welches als wichtig für die normale Gehirnfunktion diskutiert wurde

Zusammengefasst wurden in dieser Arbeit Funktionen zweier Orthologe des humanen SELENBP1 in der Nematode *Caenorhabditis elegans* identifiziert, und molekulare Mechanismen aufgeklärt, die wahrscheinlich zur erhöhten Stressresistenz und Lebensdauer der Würmer nach Depletion der Orthologen Y37A1B.5 und R11G10.2 beitragen.

Bibliography

Altschul SF, **Madden TL**, **Schaffer AA**, **Zhang J**, **Zhang Z**, **Miller W**, **Lipman DJ**. Gapped BLAST and PSI-BLAST: a new generation of protein database search programs. *Nucleic Acids Res* 25: 3389–3402, 1997.

Altun ZF, **Hall DH**. WormAtlas Hermaphrodite Handbook - Epithelial System - Hypodermis. *WormAtlas*, 2002. doi:10.3908/wormatlas.1.13.

Altun ZF, **Hall DH**. WormAtlas Hermaphrodite Handbook - Nervous System - Neuronal Support Cells. *WormAtlas*, 2003. doi:10.3908/wormatlas.1.19.

Altun ZF, **Hall DH**. WormAtas Hermaphrodite Handbook - Introduction. *WormAtlas*, 2006. doi:10.3908/wormatlas.1.1.

Ansong E, **Ying Q**, **Ekoue DN**, **Deaton R**, **Hall AR**, **Kajdacsy-Balla A**, **Yang W**, **Gann PH**, **Am Diamond**. Evidence that selenium binding protein 1 is a tumor suppressor in prostate cancer. *PLoS One* 10: 0127295, 2015.

Arosio P, **Ingrassia R**, **Cavadini P**. Ferritins: A family of molecules for iron storage, antioxidation and more. *Biochimica et Biophysica Acta (BBA) - General Subjects* 1790: 589–599, 2009.

Bai J, **Yu J**, **Wang J**, **Xue B**, **He N**, **Tian Y**, **Yang L**, **Wang Y**, **Wang Y**, **Tang Q**. DNA Methylation of miR-122 Aggravates Oxidative Stress in Colitis Targeting SELENBP1 Partially by p65NF-κB Signaling. *Oxidative Medicine and Cellular Longevity*, 2019. doi:10.1155/2019/5294105.

Bansal MP, **Mukhopadhyay T**, **Scott J**, **Cook RG**, **Mukhopadhyay R**, **Medina D**. DNA sequencing of a mouse liver protein that binds selenium: implications for selenium's mechanism of action in cancer prevention. *Carcinogenesis* 11: 2071–3, 1990.

Bansal MP, **Oborn CJ**, **Danielson KG**, **Medina D**. Evidence for two selenium-binding proteins distinct from glutathione peroxidase in mouse liver. *Carcinogenesis* 10: 541–546, 1989.

Bao J, **Zheng JJ**, **Wu D**. The Structural Basis of DKK-Mediated Inhibition of Wnt/LRP Signaling. *Sci Signal* 5: pe22–pe22, 2012.

Bell CG, **Lowe R**, **Adams PD**, **Baccarelli AA**, **Beck S**, **Bell JT**, **Christensen BC**, **Gladyshev VN**, **Heijmans BT**, **Horvath S**, **Ideker T**, **Issa J-PJ**, **Kelsey KT**, **Marioni RE**, **Reik W**, **Relton CL**, **Schalkwyk LC**, **Teschendorff AE**, **Wagner W**, **Zhang K**, **Rakyan VK**. DNA methylation aging clocks: challenges and recommendations. *Genome Biology* 20: 249, 2019.

Bernard AR, **Wells TN**, **Cleasby A**, **Borlat F**, **Payton MA**, **Proudfoot AE**. Selenomethionine labelling of phosphomannose isomerase changes its kinetic properties. *Eur J Biochem* 230: 111–118, 1995.

Bierla K, **Bianga J**, **Ouerdane L**, **Szpunar J**, **Yiannikouris A**, **Lobinski R**. A comparative study of the Se/S substitution in methionine and cysteine in Se-enriched yeast using an inductively coupled plasma mass spectrometry (ICP MS)-assisted proteomics approach. *Journal of Proteomics* 87: 26–39, 2013.

Boehler CJ, **Raines AM**, **Sunde RA**. Toxic-selenium and low-selenium transcriptomes in Caenorhabditis elegans: toxic selenium up-regulates oxidoreductase and down-regulates cuticle-associated genes. *PLoS One* 9: 101408, 2014.

Boles JO, **Cisneros RJ**, **Weir MS**, **Odom JD**, **Villafranca JE**, **Dunlap RB**. Purification and characterization of selenomethionyl thymidylate synthase from Escherichia coli: comparison with the wild-type enzyme. *Biochemistry* 30: 11073–11080, 1991.

Bonneh-Barkay D, **Reaney SH**, **Langston WJ**, **Di Monte DA**. Redox cycling of the herbicide paraquat in microglial cultures. *Molecular Brain Research* 134: 52–56, 2005.

Brisch R, **Saniotis A**, **Wolf R**, **Bielau H**, **Bernstein H-G**, **Steiner J**, **Bogerts B**, **Braun K**, **Jankowski Z**, **Kumaratilake J**, **Henneberg M**, **Gos T**. The Role of Dopamine in Schizophrenia from a Neurobiological and Evolutionary Perspective: Old Fashioned, but Still in Vogue. *Front Psychiatry* 5, 2014.

Brooks SA. Appropriate glycosylation of recombinant proteins for human use: Implications of choice of expression system. *Mol Biotechnol* 28: 241–55, 2004.

Brown LM, **Helmke SM**, **Hunsucker SW**, **Netea-Maier RT**, **Chiang SA**, **Heinz DE**, **Shroyer KR**, **Duncan MW**, **Haugen BR**. Quantitative and qualitative differences in protein expression between papillary thyroid carcinoma and normal thyroid tissue. *Mol Carcinog* 45: 613–626, 2006.

Budovskaya YV, **Wu K**, **Southworth LK**, **Jiang M**, **Tedesco P**, **Johnson TE**, **Kim SK**. An elt-3/elt-5/elt-6 GATA Transcription Circuit Guides Aging in C. elegans. *Cell* 134: 291–303, 2008.

Burk RF. Effect of Dietary Selenium Level on 75Se Binding to Rat Plasma Proteins. *Proceedings of the Society for Experimental Biology and Medicine* 143: 719–722, 1973.

Byerly L, **Cassada RC**, **Russell RL**. The life cycle of the nematode Caenorhabditis elegans: I. Wild-type growth and reproduction. *Developmental Biology* 51: 23–33, 1976.

Chau EJ, **Mostaid MS**, **Cropley V**, **McGorry P**, **Pantelis C**, **Bousman CA**, **Everall IP**. Downregulation of plasma SELENBP1 protein in patients with recent-onset schizophrenia. *Prog Neuropsychopharmacol Biol Psychiatry* 85: 1–6, 2018.

Chaudhuri AR, **de Waal EM**, **Pierce A**, **Van Remmen H**, **Ward WF**, **Richardson A**. Detection of protein carbonyls in aging liver tissue: A fluorescence-based proteomic approach. *Mechanisms of Ageing and Development* 127: 849–861, 2006.

Chen G, **Wang H**, **Miller CT**, **Thomas DG**, **Gharib TG**, **Misek DE**, **Giordano TJ**, **Orringer MB**, **Hanash SM**, **Beer DG**. Reduced selenium-binding protein 1 expression is associated with poor outcome in lung adenocarcinomas. *The Journal of Pathology* 202: 321–329, 2004.

Chen RA-J, **Stempor P**, **Down TA**, **Zeiser E**, **Feuer SK**, **Ahringer J**. Extreme HOT regions are CpG-dense promoters in C. elegans and humans. *Genome Research* 24: 1138–1146, 2014.

Chisholm AD, **Hsiao TI**. The C. elegans epidermis as a model skin. I: development, patterning, and growth. *Wiley Interdiscip Rev Dev Biol* 1: 861–878, 2012.

Chisholm AD, **Xu S**. The C. elegans epidermis as a model skin. II: differentiation and physiological roles. *Wiley Interdiscip Rev Dev Biol* 1: 879–902, 2012.

Ch'ng Q, **Kenyon C**. egl-27 generates anteroposterior patterns of cell fusion in C. elegans by regulating Hox gene expression and Hox protein function. *Development* 126: 3303–3312, 1999.

Daegelen P, **Studier FW**, **Lenski RE**, **Cure S**, **Kim JF**. Tracing ancestors and relatives of Escherichia coli B, and the derivation of B strains REL606 and BL21(DE3). *J Mol Biol* 394: 634–43, 2009.

Elhodaky M, **Diamond AM**, **Diamond A**. Selenium-Binding Protein 1 in Human Health and Disease. *Int J Mol Sci* 19: 3437, 2018.

Eom H, **Song WJ**. Emergence of metal selectivity and promiscuity in metalloenzymes. *J Biol Inorg Chem* 24: 517–531, 2019.

Erkut C. C. elegans life cycle and developmental stages. 2014.

Estevez AO, **Mueller CL**, **Morgan KL**, **Szewczyk NJ**, **Teece L**, **Miranda-Vizuete A**, **Estevez M**. Selenium induces cholinergic motor neuron degeneration in Caenorhabditis elegans. *NeuroToxicology* 33: 1021–1032, 2012.

European Commission, **Eurostat**. People in the EU: who are we and how do we live? : 2015 edition. [Online]. Publications Office.http://bookshop.europa.eu/uri?target=EUB:NOTICE:KS0415567:EN:HTML [9 Jan. 2020].

Eyice Ö, **Myronova N**, **Pol A**, **Carrión O**, **Todd JD**, **Smith TJ**, **Gurman SJ**, **Cuthbertson A**, **Mazard S**, **Mennink-Kersten MA**, **Bugg TDH**, **Andersson KK**, **Johnston AWB**, **Camp, Huub JM Op den**, **Schäfer H**. Bacterial SBP56 identified as a Cu-dependent methanethiol oxidase widely distributed in the biosphere. *The ISME Journal* 12: 145, 2018.

Fang W, **Goldberg ML**, **Pohl NM**, **Bi X**, **Tong C**, **Xiong B**, **Koh TJ**, **Diamond AM**, **Yang W**. Functional and physical interaction between the selenium-binding protein 1 (SBP1) and the glutathione peroxidase 1 selenoprotein. *Carcinogenesis* 31: 1360–6, 2010.

Fedorova M, **Bollineni RC**, **Hoffmann R**. Protein carbonylation as a major hallmark of oxidative damage: Update of analytical strategies. *Mass Spectrometry Reviews* 33: 79–97, 2014.

Feng S, **Wang S**, **Wang Y**, **Yang Q**, **Wang D**, **Li H**. Identification and expression of carbonic anhydrase 2, myosin regulatory light chain 2 and selenium-binding protein 1 in zebrafish Danio rerio: Implication for age-related biomarkers. *Gene Expr Patterns* 29: 47–58, 2018.

Fenk LA, **de Bono M**. Environmental CO2 inhibits Caenorhabditis elegans egg-laying by modulating olfactory neurons and evokes widespread changes in neural activity. *Proc Natl Acad Sci USA* 112: E3525–E3534, 2015.

Flemetakis E, **Agalou A**, **Kavroulakis N**, **Dimou M**, **Martsikovskaya A**, **Slater A**, **Spaink HP**, **Roussis A**, **Katinakis P**. Lotus japonicus gene Ljsbp is highly conserved among plants and animals and encodes a homologue to the mammalian selenium-binding proteins. *Mol Plant Microbe Interact* 15: 313–22, 2002.

Floor GH, **Román-Ross G**. Selenium in volcanic environments: A review. *Applied Geochemistry* 27: 517–531, 2012.

Gerisch B, **Weitzel C**, **Kober-Eisermann C**, **Rottiers V**, **Antebi A**. A Hormonal Signaling Pathway Influencing C. elegans Metabolism, Reproductive Development, and Life Span. *Developmental Cell* 1: 841–851, 2001.

Gilleard JS, **Shafi Y**, **Barry JD**, **McGhee JD**. ELT-3: ACaenorhabditis elegansGATA Factor Expressed in the Embryonic Epidermis during Morphogenesis. *Developmental Biology* 208: 265–280, 1999.

van Gilst MR, **Hadjivassiliou H**, **Jolly A**, **Yamamoto KR**. Nuclear Hormone Receptor NHR-49 Controls Fat Consumption and Fatty Acid Composition in C. elegans. *PLOS Biol* 3: 53, 2005.

Glatt SJ, **Everall IP**, **Kremen WS**, **Corbeil J**, **Šášik R**, **Khanlou N**, **Han M**, **Liew C-C**, **Tsuang MT**. Comparative gene expression analysis of blood and brain provides concurrent validation of SELENBP1 up-regulation in schizophrenia. *PNAS* 102: 15533–15538, 2005.

Goh GYS, **Martelli KL**, **Parhar KS**, **Kwong AWL**, **Wong MA**, **Mah A**, **Hou NS**, **Taubert S**. The conserved Mediator subunit MDT-15 is required for oxidative stress responses in Caenorhabditis elegans. *Aging Cell* 13: 70–9, 2014.

Goodman MB. Thermotaxis navigation behavior. *WormBook* 1–10, 2014.

Goodman MB, **Sengupta P**. The extraordinary AFD thermosensor of C. elegans. *Pflugers Arch* 470: 839–849, 2018.

Goodman SR, **Kurdia A**, **Ammann L**, **Kakhniashvili D**, **Daescu O**. The Human Red Blood Cell Proteome and Interactome. *Exp Biol Med (Maywood)* 232: 1391–1408, 2007.

Greer EL, **Blanco MA**, **Gu L**, **Sendinc E**, **Liu J**, **Aristizábal-Corrales D**, **Hsu C-H**, **Aravind L**, **He C**, **Shi Y**. DNA methylation on N6-adenine in C. elegans. *Cell* 161: 868–878, 2015.

Gueugneau M, **Coudy-Gandilhon C**, **Gourbeyre O**, **Chambon C**, **Combaret L**, **Polge C**, **Taillandier D**, **Attaix D**, **Friguet B**, **Maier AB**, **Butler-Browne G**, **Béchet D**. Proteomics of muscle chronological ageing in post-menopausal women. *BMC Genomics* 15: 1165, 2014.

Ha Y-S, **Lee GT**, **Kim Y-H**, **Kwon SY**, **Choi SH**, **Kim T-H**, **Kwon TG**, **Yun SJ**, **Kim IY**, **Kim W-J**. Decreased selenium-binding protein 1 mRNA expression is associated with poor prognosis in renal cell carcinoma. *World J Surg Oncol* 12, 2014.

Hallem EA, **Sternberg PW**. Acute carbon dioxide avoidance in Caenorhabditis elegans. *PNAS* 105: 8038–8043, 2008.

Han Y, **Shang Q**, **Yao J**, **Ji Y**. Hydrogen sulfide: a gaseous signaling molecule modulates tissue homeostasis: implications in ophthalmic diseases. *Cell Death Dis* 10: 1–12, 2019.

Hashimshony T, **Feder M**, **Levin M**, **Hall BK**, **Yanai I**. Spatiotemporal transcriptomics reveals the evolutionary history of the endoderm germ layer. *Nature* 519: 219–222, 2015.

He Q-Y, **Cheung YH**, **Leung SY**, **Yuen ST**, **Chu K-M**, **Chiu J-F**. Diverse proteomic alterations in gastric adenocarcinoma. *Proteomics* 4: 3276–87, 2004.

Henning C, **Glomb MA**. Pathways of the Maillard reaction under physiological conditions. *Glycoconj J* 33: 499–512, 2016.

Herman MA, **Ch'ng Q**, **Hettenbach SM**, **Ratliff TM**, **Kenyon C**, **Herman RK**. EGL-27 is similar to a metastasis-associated factor and controls cell polarity and cell migration in C. elegans. *Development* 126: 1055–1064, 1999.

Hine C, **Harputlugil E**, **Zhang Y**, **Ruckenstuhl C**, **Lee BC**, **Brace L**, **Longchamp A**, **Treviño-Villarreal JH**, **Mejia P**, **Ozaki CK**, **Wang R**, **Gladyshev VN**, **Madeo F**, **Mair WB**, **Mitchell**

JR. Endogenous Hydrogen Sulfide Production Is Essential for Dietary Restriction Benefits. *Cell* 160: 132–144, 2015.

Hine C, **Mitchell JR**. Endpoint or Kinetic Measurement of Hydrogen Sulfide Production Capacity in Tissue Extracts. *Bio Protoc* 7, 2017.

Horibe T, **Gomi M**, **Iguchi D**, **Ito H**, **Kitamura Y**, **Masuoka T**, **Tsujimoto I**, **Kimura T**, **Kikuchi M**. Different contributions of the three CXXC motifs of human protein-disulfide isomerase-related protein to isomerase activity and oxidative refolding. *J Biol Chem* 279: 4604–11, 2004.

Hu C-W, **Chen J-L**, **Hsu Y-W**, **Yen C-C**, **Chao M-R**. Trace analysis of methylated and hydroxymethylated cytosines in DNA by isotope-dilution LC–MS/MS: first evidence of DNA methylation in Caenorhabditis elegans. *Biochem J* 465: 39–47, 2015.

Hu PJ. Dauer. *WormBook* , 2007. doi:10.1895/wormbook.1.144.1.

Huang C, **Ding G**, **Gu C**, **Zhou J**, **Kuang M**, **Ji Y**, **He Y**, **Kondo T**, **Fan J**. Decreased selenium-binding protein 1 enhances glutathione peroxidase 1 activity and downregulates HIF-1α to promote hepatocellular carcinoma invasiveness. *Clin Cancer Res* 18: 3042–53, 2012.

Huang K-C, **Park DC**, **Ng S-K**, **Lee JY**, **Ni X**, **Ng W-C**, **Bandera CA**, **Welch WR**, **Berkowitz RS**, **Mok SC**, **Ng S-W**. Selenium binding protein 1 in ovarian cancer. *Int J Cancer* 118: 2433–40, 2006.

Huber RE, **Criddle RS**. Comparison of the chemical properties of selenocysteine and selenocystine with their sulfur analogs. *Archives of Biochemistry and Biophysics* 122: 164–173, 1967.

Hussey R, **Littlejohn NK**, **Witham E**, **Vanstrum E**, **Mesgarzadeh J**, **Ratanpal H**, **Srinivasan S**. Oxygen-sensing neurons reciprocally regulate peripheral lipid metabolism via neuropeptide signaling in Caenorhabditis elegans. *PLOS Genetics* 14: e1007305, 2018.

Ishida YI, **Kayama T**, **Kibune Y**, **Nishimoto S**, **Koike S**, **Suzuki T**, **Horiuchi Y**, **Miyashita M**, **Itokawa M**, **Arai M**, **Ogasawara Y**. Identification of an argpyrimidine-modified protein in human red blood cells from schizophrenic patients: A possible biomarker for diseases involving carbonyl stress. *Biochemical and Biophysical Research Communications* 493: 573–577, 2017.

Jacob C, **Giles GI**, **Giles NM**, **Sies H**. Sulfur and selenium: The role of oxidation state in protein structure and function. *Angew Chem Int Ed Engl* 42: 4742–58, 2003.

Jeong D-E, **Artan M**, **Seo K**, **Lee S-J**. Regulation of lifespan by chemosensory and thermosensory systems: findings in invertebrates and their implications in mammalian aging. *Front Gene* 3, 2012.

Jeong J-Y, **Wang Y**, **Sytkowski AJ**. Human selenium binding protein-1 (hSP56) interacts with VDU1 in a selenium-dependent manner. *Biochem Biophys Res Commun* 379: 583–8, 2009.

Jerome-Morais A, **Wright ME**, **Liu R**, **Yang W**, **Jackson MI**, **Combs GF**, **Diamond AM**. Inverse association between glutathione peroxidase activity and both selenium-binding protein 1 levels and Gleason score in human prostate tissue. *Prostate* 72: 1006–12, 2012.

Jiang L, **Zhu H-Z**, **Xu Y-Z**, **Ni J-Z**, **Zhang Y**, **Liu Q**. Comparative selenoproteome analysis reveals a reduced utilization of selenium in parasitic platyhelminthes. *PeerJ* 1: e202, 2013.

Kabil O, **Banerjee R**. Enzymology of H2S biogenesis, decay and signaling. *Antioxidants & redox signaling* 20: 770–782, 2014.

Kaletsky R, **Yao V**, **Williams A**, **Runnels AM**, **Tadych A**, **Zhou S**, **Troyanskaya OG**, **Murphy CT**. Transcriptome analysis of adult Caenorhabditis elegans cells reveals tissue-specific gene and isoform expression. *PLOS Genetics* 14: e1007559, 2018.

Kamath RS, **Ahringer J**. Genome-wide RNAi screening in Caenorhabditis elegans. *Methods* 30: 313–321, 2003.

Kasaikina MV, **Hatfield DL**, **Gladyshev VN**. Understanding selenoprotein function and regulation through the use of rodent models. *Biochim Biophys Acta* 1823: 1633–1642, 2012.

Kelley LA, **Mezulis S**, **Yates CM**, **Wass MN**, **Sternberg MJE**. The Phyre2 web portal for protein modeling, prediction and analysis. *Nat Protoc* 10: 845–858, 2015.

Kim H, **Kang HJ**, **You KT**, **Kim SH**, **Lee KY**, **Kim TI**, **Kim C**, **Song SY**, **Kim H-J**, **Lee C**, **Kim H**. Suppression of human selenium-binding protein 1 is a late event in colorectal carcinogenesis and is associated with poor survival. *Proteomics* 6: 3466–76, 2006.

Klotz L-O, **Sánchez-Ramos C**, **Prieto-Arroyo I**, **Urbánek P**, **Steinbrenner H**, **Monsalve M**. Redox regulation of FoxO transcription factors. *Redox Biol* 6: 51–72, 2015.

Koh K, **Rothman JH**. ELT-5 and ELT-6 are required continuously to regulate epidermal seam cell differentiation and cell fusion in C. elegans. *Development* 128: 2867–2880, 2001.

Köhnlein K. Untersuchung zweier potenzieller Selenbindeprotein-1-Orthologe in Caenorhabditis elegans. Einfluss auf Lebensspanne, Stressresistenz und Energiemetabolismus. Master thesis, 2016.

Köhnlein K, **Urban N**, **Guerrero-Gómez D**, **Steinbrenner H**, **Urbánek P**, **Priebs J**, **Koch P**, **Kaether C**, **Miranda-Vizuete A**, **Klotz L-O**. A Caenorhabditis elegans ortholog of human selenium-binding protein 1 is a pro-aging factor protecting against selenite toxicity. *Redox Biology* 28: 101323, 2020.

Labouesse M, **Hartwieg E**, **Horvitz HR**. The Caenorhabditis elegans LIN-26 protein is required to specify and/or maintain all non-neuronal ectodermal cell fates. *Development* 122: 2579–2588, 1996.

Labouesse M, **Sookhareea S**, **Horvitz HR**. The Caenorhabditis elegans gene lin-26 is required to specify the fates of hypodermal cells and encodes a presumptive zinc-finger transcription factor. *Development* 120: 2359–2368, 1994.

Lee K, **Goh GYS**, **Wong MA**, **Klassen TL**, **Taubert S**. Gain-of-Function Alleles in Caenorhabditis elegans Nuclear Hormone Receptor nhr-49 Are Functionally Distinct. *PLOS ONE* 11: e0162708, 2016.

Lee S-J, **Kenyon C**. Regulation of the longevity response to temperature by thermosensory neurons in Caenorhabditis elegans. *Curr Biol* 19: 715–722, 2009.

Li G-X, **Hu H**, **Jiang C**, **Schuster T**, **Lü J**. Differential involvement of reactive oxygen species in apoptosis induced by two classes of selenium compounds in human prostate cancer cells. *International Journal of Cancer* 120: 2034–2043, 2007.

Li W-H, **Chang C-H**, **Huang C-W**, **Wei C-C**, **Liao VH-C**. Selenite Enhances Immune Response against Pseudomonas aeruginosa PA14 via SKN-1 in Caenorhabditis elegans. *PLoS One* 9: 105810, 2014a.

Li W-H, **Hsu F-L**, **Liu J-T**, **Liao VH-C**. The ameliorative and toxic effects of selenite on Caenorhabditis elegans. *Food Chem Toxicol* 49: 812–9, 2011.

Li W-H, **Shi Y-C**, **Chang C-H**, **Huang C-W**, **Hsiu-Chuan Liao V**. Selenite protects Caenorhabditis elegans from oxidative stress via DAF-16 and TRXR-1. *Mol Nutr Food Res* 58: 863–74, 2014b.

Liao Y, **Wang J**, **Jaehnig EJ**, **Shi Z**, **Zhang B**. WebGestalt 2019: gene set analysis toolkit with revamped UIs and APIs. *Nucleic Acids Res* 47: W199–W205, 2019.

Lin C-T, **He C-W**, **Huang T-T**, **Pan C-L**. Longevity control by the nervous system: Sensory perception, stress response and beyond. *Translational Medicine of Aging* 1: 41–51, 2017.

Liu T, **Cai D**. Counterbalance between BAG and URX neurons via guanylate cyclases controls lifespan homeostasis in C. elegans. *The EMBO Journal* 32: 1529–1542, 2013.

Mao S, **Qi Y**, **Zhu H**, **Huang X**, **Zou Y**, **Chi T**. A Tet/Q Hybrid System for Robust and Versatile Control of Transgene Expression in C. elegans. *iScience* 11: 224–237, 2018.

Mariani O, **Brennetot C**, **Coindre J-M**, **Gruel N**, **Ganem C**, **Delattre O**, **Stern M-H**, **Aurias A**. JUN oncogene amplification and overexpression block adipocytic differentiation in highly aggressive sarcomas. *Cancer Cell* 11: 361–374, 2007.

Martin GW, **Harney JW**, **Berry MJ**. Selenocysteine incorporation in eukaryotes: insights into mechanism and efficiency from sequence, structure, and spacing proximity studies of the type 1 deiodinase SECIS element. *RNA* 2: 171–182, 1996.

Mckay SJ, **Johnsen R**, **Khattra J**, **Asano J**, **Baillie DL**, **Chan S**, **Dube N**, **Fang L**, **Goszczynski B**, **Ha E**, **Halfnight E**, **Hollebakken R**, **Huang P**, **Hung K**, **Jensen V**, **Jones SJM**, **Kai H**, **Li D**, **Mah A**, **Marra M**, **Mcghee J**, **Newbury R**, **Pouzyrev A**, **Riddle DL**, **Sonnhammer E**, **Tian H**, **Tu D**, **Tyson JR**, **Vatcher G**, **Warner A**, **Wong K**, **Zhao Z**, **Moerman DG**. Gene Expression Profiling of Cells, Tissues, and Developmental Stages of the Nematode C. elegans. *Cold Spring Harbor Symposia on Quantitative Biology* 68: 159–170, 2003.

Millar KR. Distribution of Se75 in liver, kidney, and blood proteins of rats after intravenous injection of sodium selenite. *New Zealand Journal of Agricultural Research* 15: 547–564, 1972.

Miller DL, **Roth MB**. Hydrogen sulfide increases thermotolerance and lifespan in Caenorhabditis elegans. *Proc Natl Acad Sci U S A* 104: 20618–22, 2007.

Mix H, **Lobanov AV**, **Gladyshev VN**. SECIS elements in the coding regions of selenoprotein transcripts are functional in higher eukaryotes. *Nucleic Acids Res* 35: 414–423, 2007.

Monsalve GC, **Yamamoto KR**, **Ward JD**. A New Tool for Inducible Gene Expression in Caenorhabditis elegans. *Genetics* 211: 419–430, 2019.

Moreno-Arriola E, **El HM**, **Ortega-Cuéllar D**, **Carvajal K**. AMP-Activated Protein Kinase Regulates Oxidative Metabolism in Caenorhabditis elegans through the NHR-49 and MDT-15 Transcriptional Regulators. *PLoS One* 11, 2016.

Morgan KL, **Estevez AO**, **Mueller CL**, **Cacho-Valadez B**, **Miranda-Vizuete A**, **Szewczyk NJ**, **Estevez M**. The Glutaredoxin GLRX-21 Functions to Prevent Selenium-Induced Oxidative Stress in Caenorhabditis elegans. *Toxicol Sci* 118: 530–543, 2010.

Müller N, **Schwarz MJ**. Neuroimmune–endocrine crosstalk in schizophrenia and mood disorders. *Expert Review of Neurotherapeutics* 6: 1017–1038, 2006.

Müller N, **Weidinger E**, **Leitner B**, **Schwarz MJ**. The role of inflammation in schizophrenia. *Front Neurosci* 9, 2015.

Opella SJ, **DeSilva TM**, **Veglia G**. Structural biology of metal-binding sequences. *Current Opinion in Chemical Biology* 6: 217–223, 2002.

Orozco LD, **Rubbi L**, **Martin LJ**, **Fang F**, **Hormozdiari F**, **Che N**, **Smith AD**, **Lusis AJ**, **Pellegrini M**. Intergenerational genomic DNA methylation patterns in mouse hybrid strains. *Genome Biol* 15: R68, 2014.

Pallotta V, **D'Alessandro A**, **Rinalducci S**, **Zolla L**. Native Protein Complexes in the Cytoplasm of Red Blood Cells. *J Proteome Res* 12: 3529–3546, 2013.

Papp LV, **Lu J**, **Holmgren A**, **Khanna KK**. From Selenium to Selenoproteins: Synthesis, Identity, and Their Role in Human Health. *Antioxidants & Redox Signaling* 9: 775–806, 2007.

Patteson KG, **Trivedi N**, **Stadtman TC**. Methanococcus vannielii selenium-binding protein (SeBP): Chemical reactivity of recombinant SeBP produced in Escherichia coli. *PNAS* 102: 12029–12034, 2005.

Pohl NM, **Tong C**, **Fang W**, **Bi X**, **Li T**, **Yang W**. Transcriptional Regulation and Biological Functions of Selenium-Binding Protein 1 in Colorectal Cancer In Vitro and in Nude Mouse Xenografts. *PLOS ONE* 4: e7774, 2009.

Pol A, **Renkema GH**, **Tangerman A**, **Winkel EG**, **Engelke UF**, **Brouwer, Arjan P. M. de**, **Lloyd KC**, **Araiza RS**, **van den Heuvel L**, **Omran H**, **Olbrich H**, **Elberink MO**, **Gilissen C**, **Rodenburg RJ**, **Sass JO**, **Schwab KO**, **Schäfer H**, **Venselaar H**, **Sequeira JS**, **Camp, Huub J. M. Op den**, **Wevers RA**. Mutations in SELENBP1 , encoding a novel human methanethiol oxidase, cause extraoral halitosis. *Nature Genetics* 50: 120, 2018.

Prabakaran S, **Wengenroth M**, **Lockstone HE**, **Lilley K**, **Leweke FM**, **Bahn S**. 2-D DIGE Analysis of Liver and Red Blood Cells Provides Further Evidence for Oxidative Stress in Schizophrenia. *J Proteome Res* 6: 141–149, 2007.

Prahlad V, **Cornelius T**, **Morimoto RI**. Regulation of the Cellular Heat Shock Response in Caenorhabditis elegans by Thermosensory Neurons. *Science* 320: 811–814, 2008.

Pumford NR, **Martin BM**, **Hinson JA**. A metabolite of acetaminophen covalently binds to the 56 kDa selenium binding protein. *Biochem Biophys Res Commun* 182: 1348–55, 1992.

Qabazard B, **Li L**, **Gruber J**, **Peh MT**, **Ng LF**, **Kumar SD**, **Rose P**, **Tan C-H**, **Dymock BW**, **Wei F**, **Swain SC**, **Halliwell B**, **Stürzenbaum SR**, **Moore PK**. Hydrogen Sulfide Is an Endogenous Regulator of Aging in Caenorhabditis elegans. *Antioxidants & Redox Signaling* 20: 2621–2630, 2014.

Quan S, **Schneider I**, **Pan J**, **Hacht A**, **Bardwell JC**. The CXXC motif is more than a redox rheostat. *J Biol Chem* 282: 28823–33, 2007.

Raucci R, **Colonna G**, **Guerriero E**, **Capone F**, **Accardo M**, **Castello G**, **Costantini S**. Structural and functional studies of the human selenium binding protein-1 and its involvement in hepatocellular carcinoma. *Biochim Biophys Acta* 1814: 513–22, 2011.

Raymond F.Burk, **Paula E.Gregory**. Some characteristics of 75Se-P, a selenoprotein found in rat liver and plasma, and comparison of it with selenoglutathione peroxidase. *Archives of Biochemistry and Biophysics* 213: 73–80, 1982.

Reich HJ, **Hondal RJ**. Why Nature Chose Selenium. *ACS Chem Biol* 11: 821–841, 2016.

Reya T, **Clevers H**. Wnt signalling in stem cells and cancer. *Nature* 434: 843–850, 2005.

Rogers AN, **Chen D**, **McColl G**, **Czerwieniec G**, **Felkey K**, **Gibson BW**, **Hubbard A**, **Melov S**, **Lithgow GJ**, **Kapahi P**. Life Span Extension via eIF4G Inhibition Is Mediated by Posttranscriptional Remodeling of Stress Response Gene Expression in C. elegans. *Cell Metab* 14: 55–66, 2011.

Rohn I, **Anu Marschall T**, **Kroepfl N**, **Bendix Jensen K**, **Aschner M**, **Tuck S**, **Kuehnelt D**, **Schwerdtle T**, **Bornhorst J**. Selenium species-dependent toxicity, bioavailability and metabolic transformations in Caenorhabditis elegans. *Metallomics* 10: 818–827, 2018.

Rohn I, **Raschke S**, **Aschner M**, **Tuck S**, **Kuehnelt D**, **Kipp A**, **Schwerdtle T**, **Bornhorst J**. Treatment of Caenorhabditis elegans with Small Selenium Species Enhances Antioxidant Defense Systems. *Molecular Nutrition & Food Research* 63: 1801304, 2019.

Rost J, **Rapoport S**. Reduction-potential of Glutathione. *Nature* 201: 185–185, 1964.

Roux-Dalvai F, **Peredo AG de**, **Simó C**, **Guerrier L**, **Bouyssié D**, **Zanella A**, **Citterio A**, **Burlet-Schiltz O**, **Boschetti E**, **Righetti PG**, **Monsarrat B**. Extensive Analysis of the Cytoplasmic Proteome of Human Erythrocytes Using the Peptide Ligand Library Technology and Advanced Mass Spectrometry. *Molecular & Cellular Proteomics* 7: 2254–2269, 2008.

Sattar A, **Xie S**, **Hafeez MA**, **Wang X**, **Hussain HI**, **Iqbal Z**, **Pan Y**, **Iqbal M**, **Shabbir MA**, **Yuan Z**. Metabolism and toxicity of arsenicals in mammals. *Environmental Toxicology and Pharmacology* 48: 214–224, 2016.

Schrauzer GN. Selenomethionine: A Review of Its Nutritional Significance, Metabolism and Toxicity. *J Nutr* 130: 1653–1656, 2000.

Schultz LW, **Chivers PT**, **Raines RT**. The CXXC motif: crystal structure of an active-site variant of Escherichia coli thioredoxin. *Acta Crystallogr D Biol Crystallogr* 55: 1533–8, 1999.

Shaulian E. AP-1 — The Jun proteins: Oncogenes or tumor suppressors in disguise? *Cellular Signalling* 22: 894–899, 2010.

Singh S, **Padovani D**, **Leslie RA**, **Chiku T**, **Banerjee R**. Relative contributions of cystathionine beta-synthase and gamma-cystathionase to H2S biogenesis via alternative trans-sulfuration reactions. *J Biol Chem* 284: 22457–22466, 2009.

Smetana K, **Lacina L**, **Szabo P**, **Dvořánková B**, **Brož P**, **Šedo A**. Ageing as an Important Risk Factor for Cancer. *Anticancer Res* 36: 5009–5017, 2016.

Spuches AM, **Kruszyna HG**, **Rich AM**, **Wilcox DE**. Thermodynamics of the As(III)−Thiol Interaction: Arsenite and Monomethylarsenite Complexes with Glutathione, Dihydrolipoic Acid, and Other Thiol Ligands. *Inorg Chem* 44: 2964–2972, 2005.

Stasio MD, **Volpe MG**, **Colonna G**, **Nazzaro M**, **Polimeno M**, **Scala S**, **Castello G**, **Costantini S**. A possible predictive marker of progression for hepatocellular carcinoma. *Oncology Letters* 2: 1247–1251, 2011.

Steinbrenner H, **Micoogullari M**, **Hoang NA**, **Bergheim I**, **Klotz L-O**, **Sies H**. Selenium-binding protein 1 (SELENBP1) is a marker of mature adipocytes. *Redox Biology* 20: 489–495, 2019.

Steinbrenner H, **Speckmann B**, **Pinto A**, **Sies H**. High selenium intake and increased diabetes risk: experimental evidence for interplay between selenium and carbohydrate metabolism. *Journal of Clinical Biochemistry and Nutrition* 48: 40–45, 2010.

Steinmann D, **Nauser T**, **Koppenol WH**. Selenium and Sulfur in Exchange Reactions: A Comparative Study. *J Org Chem* 75: 6696–6699, 2010.

Stelzer G, **Rosen N**, **Plaschkes I**, **Zimmerman S**, **Twik M**, **Fishilevich S**, **Stein TI**, **Nudel R**, **Lieder I**, **Mazor Y**, **Kaplan S**, **Dahary D**, **Warshawsky D**, **Guan-Golan Y**, **Kohn A**, **Rappaport N**, **Safran M**, **Lancet D**. The GeneCards Suite: From Gene Data Mining to Disease Genome Sequence Analyses: The GeneCards Suite. In: *Current Protocols in Bioinformatics*, edited by Bateman A, Pearson WR, Stein LD, Stormo GD, Yates JR. John Wiley & Sons, Inc., p. 1.30.1-1.30.33.

Stróżyk A, **Osica Z**, **Przybylak JD**, **Kołodziej M**, **Zalewski BM**, **Mrozikiewicz-Rakowska B**, **Szajewska H**. Effectiveness and safety of selenium supplementation for type 2 diabetes mellitus in adults: a systematic review of randomised controlled trials. *Journal of Human Nutrition and Dietetics* 32: 635–645, 2019.

Studier FW, **Moffatt BA**. Use of bacteriophage T7 RNA polymerase to direct selective high-level expression of cloned genes. *J Mol Biol* 189: 113–30, 1986.

Sulston JE, **Schierenberg E**, **White JG**, **Thomson JN**. The embryonic cell lineage of the nematode Caenorhabditis elegans. *Developmental Biology* 100: 64–119, 1983.

Suzuki M, **Lee DY**, **Inyamah N**, **Stadtman TC**, **Tjandra N**. Solution NMR structure of selenium-binding protein from Methanococcus vannielii. *J Biol Chem* 283: 25936–43, 2008.

Szigeti B, **Gleeson P**, **Vella M**, **Khayrulin S**, **Palyanov A**, **Hokanson J**, **Currie M**, **Cantarelli M**, **Idili G**, **Larson S**. OpenWorm: an open-science approach to modeling Caenorhabditis elegans. *Front Comput Neurosci* 8, 2014.

Taffoni C, **Pujol N**. Mechanisms of innate immunity in C. elegans epidermis. *Tissue Barriers* 3: e1078432, 2015.

Tanase M, **Urbanska AM**, **Zolla V**, **Clement CC**, **Huang L**, **Morozova K**, **Follo C**, **Goldberg M**, **Roda B**, **Reschiglian P**, **Santambrogio L**. Role of Carbonyl Modifications on Aging-Associated Protein Aggregation. *Scientific Reports* 6: 19311, 2016.

Tatum MC, **Ooi FK**, **Chikka MR**, **Chauve L**, **Martinez-Velazquez LA**, **Steinbusch HWM**, **Morimoto RI**, **Prahlad V**. Neuronal Serotonin Release Triggers the Heat Shock Response in C. elegans in the Absence of Temperature Increase. *Current Biology* 25: 163–174, 2015.

Taubert S, **van Gilst MR**, **Hansen M**, **Yamamoto KR**. A Mediator subunit, MDT-15, integrates regulation of fatty acid metabolism by NHR-49-dependent and -independent pathways in C. elegans. *Genes Dev* 20: 1137–49, 2006.

Taubert S, **Hansen M**, **van Gilst MR**, **Cooper SB**, **Yamamoto KR**. The Mediator subunit MDT-15 confers metabolic adaptation to ingested material. *PLoS Genet* 4: 1000021, 2008.

Timmons L, **Court DL**, **Fire A**. Ingestion of bacterially expressed dsRNAs can produce specific and potent genetic interference in Caenorhabditis elegans. *Gene* 263: 103–112, 2001.

Udawela M, **Money TT**, **Neo J**, **Seo MS**, **Scarr E**, **Dean B**, **Everall IP**. SELENBP1 expression in the prefrontal cortex of subjects with schizophrenia. *Translational Psychiatry* 5: e615, 2015.

Uhlen M, **Fagerberg L**, **Hallstrom BM**, **Lindskog C**, **Oksvold P**, **Mardinoglu A**, **Sivertsson A**, **Kampf C**, **Sjostedt E**, **Asplund A**, **Olsson I**, **Edlund K**, **Lundberg E**, **Navani S**, **Szigyarto CA-K**, **Odeberg J**, **Djureinovic D**, **Takanen JO**, **Hober S**, **Alm T**, **Edqvist P-H**, **Berling H**, **Tegel H**, **Mulder J**, **Rockberg J**, **Nilsson P**, **Schwenk JM**, **Hamsten M**, **von Feilitzen K**, **Forsberg M**, **Persson L**, **Johansson F**, **Zwahlen M**, **von Heijne G**, **Nielsen J**, **Ponten F**. Tissue-based map of the human proteome. *Science* 347: 1260419–1260419, 2015.

Vihervaara A, **Sistonen L**. HSF1 at a glance. *J Cell Sci* 127: 261–266, 2014.

Vinceti M, **Filippini T**, **Giovane CD**, **Dennert G**, **Zwahlen M**, **Brinkman M**, **Zeegers MP**, **Horneber M**, **D'Amico R**, **Crespi CM**. Selenium for preventing cancer. *Cochrane Database of Systematic Reviews*, 2018a. doi:10.1002/14651858.CD005195.pub4.

Vinceti M, **Filippini T**, **Rothman KJ**. Selenium exposure and the risk of type 2 diabetes: a systematic review and meta-analysis. *Eur J Epidemiol* 33: 789–810, 2018b.

Vindry C, **Ohlmann T**, **Chavatte L**. Translation regulation of mammalian selenoproteins. *Biochimica et Biophysica Acta (BBA) - General Subjects* 1862: 2480–2492, 2018.

Voskoboinik I, **Strausak D**, **Greenough M**, **Brooks H**, **Petris M**, **Smith S**, **Mercer JF**, **Camakaris J**. Functional Analysis of the N-terminal CXXC Metal-binding Motifs in the Human Menkes Copper-transporting P-type ATPase Expressed in Cultured Mammalian Cells. *J Biol Chem* 274: 22008–22012, 1999.

Wang Y, **Fang W**, **Huang Y**, **Hu F**, **Ying Q**, **Yang W**, **Xiong B**. Reduction of selenium-binding protein 1 sensitizes cancer cells to selenite via elevating extracellular glutathione: a novel mechanism of cancer-specific cytotoxicity of selenite. *Free Radic Biol Med* 79: 186–96, 2015.

Wenzel D, **Palladino F**, **Jedrusik-Bode M**. Epigenetics in C. elegans: Facts and challenges. *genesis* 49: 647–661, 2011.

Weston CR, **Davis RJ**. The JNK signal transduction pathway. *Current Opinion in Cell Biology* 19: 142–149, 2007.

White PJ. The Genetics of Selenium Accumulation by Plants. In: *Selenium in plants: Molecular, Physiological, Ecological and Evolutionary Aspects*, edited by Pilon-Smits EAH, Winkel LHE, Lin Z-Q. Springer International Publishing, p. 143–163.

Wu Q, **Wu W**, **Fu B**, **Shi L**, **Wang X**, **Kuca K**. JNK signaling in cancer cell survival. *Medicinal Research Reviews* 0, 2019

Xu X, **Kim SK**. The GATA Transcription Factor egl-27 Delays Aging by Promoting Stress Resistance in Caenorhabditis elegans. *PLOS Genetics* 8: e1003108, 2012.

Yan L-J, **Forster MJ**. Chemical probes for analysis of carbonylated proteins: a review. *J Chromatogr B Analyt Technol Biomed Life Sci* 879: 1308–1315, 2011.

Yang J, **Minkler P**, **Grove D**, **Wang R**, **Willard B**, **Dweik R**, **Hine C**. Non-enzymatic hydrogen sulfide production from cysteine in blood is catalyzed by iron and vitamin B 6. *Commun Biol* 2: 1–14, 2019.

Yang W, **Diamond AM**. Selenium-binding protein 1 as a tumor suppressor and a prognostic indicator of clinical outcome. *Biomarker Research* 1: 15, 2013.

Yi SV. Birds do it, bees do it, worms and ciliates do it too: DNA methylation from unexpected corners of the tree of life. *Genome Biology* 13: 174, 2012.

Ying Q, **Ansong E**, **Diamond AM**, **Lu Z**, **Yang W**, **Bie X**. Quantitative Proteomic Analysis Reveals That Anti-Cancer Effects of Selenium-Binding Protein 1 In Vivo Are Associated with Metabolic Pathways. *PLOS ONE* 10: e0126285, 2015a.

Ying Q, **Ansong E**, **Diamond AM**, **Yang W**. A Critical Role for Cysteine 57 in the Biological Functions of Selenium Binding Protein-1. *Int J Mol Sci* 16: 27599–608, 2015b.

Zhang P, **Judy M**, **Lee S-J**, **Kenyon C**. Direct and Indirect Gene Regulation by a Life-Extending FOXO Protein in C. elegans: Roles for GATA Factors and Lipid Gene Regulators. *Cell Metabolism* 17: 85–100, 2013a.

Zhang S, **Li F**, **Younes M**, **Liu H**, **Chen C**, **Yao Q**. Reduced selenium-binding protein 1 in breast cancer correlates with poor survival and resistance to the anti-proliferative effects of selenium. *PLoS One* 8: 63702, 2013b.

Zhang Y, **Li W**, **Li L**, **Li Y**, **Fu R**, **Zhu Y**, **Li J**, **Zhou Y**, **Xiong S**, **Zhang H**. Structural Damage in the C. elegans Epidermis Causes Release of STA-2 and Induction of an Innate Immune Response. *Immunity* 42: 309–320, 2015.

Zhao C, **Zeng H**, **Wu RTY**, **Cheng W-H**. Loss of Selenium-Binding Protein 1 Decreases Sensitivity to Clastogens and Intracellular Selenium Content in HeLa Cells. *PLoS One* 11: 0158650, 2016.

Zhong L, **Arnér ES**, **Holmgren A**. Structure and mechanism of mammalian thioredoxin reductase: the active site is a redox-active selenolthiol/selenenylsulfide formed from the conserved cysteine-selenocysteine sequence. *Proc Natl Acad Sci USA* 97: 5854–5859, 2000.

Zugasti O, **Ewbank JJ**. Neuroimmune regulation of antimicrobial peptide expression by a noncanonical TGF-β signaling pathway in Caenorhabditis elegans epidermis. *Nat Immunol* 10: 249–256, 2009.

Appendix

Table 1 Strains: Caenorhabditis elegans

Name	Genotype	Description	Source
N2 (Bristol)	Wildtype Bristol N2	Wildtype	Caenorhabditis Genetics Center
PHX2066	*R11G10.2(syb2066)*	R11G10.2(phx2066); null	SunyBiotech
PHX2078	*Y37A1B.5(syb2078)*	Y37A1B.5(phx2078); null	SunyBiotech
LOK128	*pR11G10.2::R11G10.2::gfp + rol-6(su1006)*	Expression of R11G10.2 fused to GFP	Klotz lab
LOK158	*pY37A1B.5::Y37A1B.5::gfp + rol-6(su1006)*	Expression of Y37A1B.5 fused to GFP	Klotz lab
LOK182	*pklo-2::klo-2::gfp + rol-6(su1006)*	Expression of KLO-2 fused to GFP	Klotz lab
DA1290	*gcy-33::GFP + lin-15(+)*	GFP in BAG neurons	Caenorhabditis Genetics Center
PY1322	*gcy-8::GFP*	GFP in AFD neurons	Caenorhabditis Genetics Center

Table 2 Strains: Bacteria

Name	Description	Source
OP50	Wildtype	Caenorhabditis Genetics Center
L4440	HT115 (DE3) + L4440 vector	Ahringer RNAi feeding library
R11G10.2 RNAi	T7 inducible *R11G10.2* dsRNA	Source Bioscience
Y37A1B.5 RNAi	T7 inducible *Y37A1B.5* dsRNA	Ahringer RNAi feeding library
mdt-15 RNAi	T7 inducible *mdt-15* dsRNA	Ahringer RNAi feeding library
egl-27 RNAi	T7 inducible *egl-27* dsRNA	Ahringer RNAi feeding library

Table 3 Oligonucleotides for qPCR

Name	Accession #	Sequence (5' → 3')
R11G10.2	NM_073950.4	Fwd: TGCACATGAATACACTGACCAA
		Rev: GCATTTCATCACTTTGCCAAT
Y37A1B.5	NM_001268848.2	Fwd: TTTTAGAATTCATCCTGTTGAGGAG
		Rev: AAGAGCCCATCCACTTACTTTTT
tba-1	NM_001264283.2	Fwd: TCAACACTGCCATCGCCGCC
		Rev: TCCAAGCGAGACCAGGCTTCAG

Table 4 Oligonucleotides for strain validation

Name	Forward/ Reverse	Description	Sequence (5' → 3')
Primer1	Fwd	R11G10.2(syb2066) mRNA	CATCCTCCAAATATGCTCC
Primer2	Rev	R11G10.2(syb2066) mRNA	TACAGTCAGCATTGTGAAG
Primer3	Fwd	Y37A1B.5(syb2078) mRNA	CCCAAAAACCAAAATGTCC
Primer4	Rev	Y37A1B.5(syb2078) mRNA	CAGATTCTGGATCAATGTTG
Primer5	Fwd	R11G10.2(syb2066) gDNA	CGACACGTACTTCTTCATTT
Primer6	Rev	R11G10.2(syb2066) gDNA	CAGCATCATAACTCACTTTTAG
Primer7	Fwd	Y37A1B.5(syb2078) gDNA	CAAAAACCAAAATGTCCCC
Primer8	Rev	Y37A1B.5(syb2078) gDNA	ACCTCCTTCAATTTTTCCA
Primer9	Fwd	R11G10.2(syb2066) duplex	ACCTCGACATAATCTGATGAT
Primer10	Fwd	R11G10.2(syb2066) duplex	TTCATCCTCCAAATATGCTC
Primer11	Rev	R11G10.2(syb2066) duplex	CTTTTACTATCGTATGGCATTG
Primer12	Fwd	Y37A1B.5(syb2078) duplex	TCGTCCGCTTAATAATTCAT
Primer13	Fwd	Y37A1B.5(syb2078) duplex	TTTCTGAAGCTAAAAATGTTTG
Primer14	Rev	Y37A1B.5(syb2078) duplex	ATCTCGTGAGCCAAATAG

Table 5 Growth media and buffer for *C. elegans*

NGM agar		
17	g/l	Agar-Agar
3	g/l	NaCl
2.5	g/l	Tryptone/Peptone
		after sterilization:
1000	µl/l	$MgSO_4$ [1 M]
1000	µl/l	Cholesterol [5 mg/ml] in EtOH abs.
500	µl/l	$CaCl_2$ [1 M]
25	ml/l	Potassium phosphate buffer [1 M]
5	ml/l	Nystatin [1 g/100 ml]
NGM agar for RNAi		
		like NGM-Agar
		additionally, after sterilization:
1000	µl/l	Ampicillin
1000	µl/l	IPTG [1 M]
1000	µl/l	Tetracycline (lifespan starting day 10)

Nystatin [1 g/100 ml]		
50	ml/100 ml	Ammonium acetate [7,5 M]
46	ml/100 ml	EtOH
2	ml/100 ml	Isopropanol
2	ml/100 ml	H_20 (ultra-pure)
1	g/100 ml	Nystatin · 2 H_20
Potassium phosphate buffer [1 M], pH 6.0		
108.5	g/l	KH_2PO_4
35.28	g/l	K_2HPO_4 (anhydrate)
Magnesium phosphate ($MgSO_4$) [1 M]		
120.3	g/l	$MgSO_4$
Calcium chloride ($CaCl_2$) [1 M]		
110.9	g/l	$CaCl_2$
Cholesterol [5 mg/ml]		
0.5	g/100 ml	Cholesterol
		solve in EtOH abs.
S-Basal buffer		
5.85	g/l	NaCl
1	g/l	K_2HPO_4 (anhydrate)
6	g/l	KH_2PO_4
		pH 6.0 with NaOH/KOH
Freezing solution for *C. elegans*		
		S-Basal
30	ml/100 ml	Glycerol (30 %)
0.1	ml/100 ml	$MgSO_4$ (1 M)
Bleaching solution		
1660	µl	H_20 (ultra-pure)
500	µl	NaOH [10 M]
840	µl	NaOCl (12 %)
Ampicillin		
100	mg/ml	Ampicillin
Tetracycline		
12.5	mg/ml	Tetracycline
Isopropyl β-D-1-thiogalactopyranoside (IPTG)		
238.3	mg/ml	IPTG

Table 6 Growth media for bacteria

dYT medium		
16	g/l	Tryptone/Peptone
10	g/l	Bacto yeast extract
5	g/l	NaCl
Luria-Broth medium (LB-Lennox)		
16	g/l	LB Broth Base
Luria-Broth agar (LB-Lennox)		
16	g/l	LB Broth Base
8	g/l	Agar for bacteriology
Freezing solution for bacteria		
		LB Medium
40	ml/100 ml	Glycerol

Table 7 Buffer for RNA electrophoresis

50 x TAE buffer		
Tris/HCl		2 M
Acetic acid		5.71 % (v/v)
EDTA		50 mM
		Solved in dH_20
		pH 8.3
1 x TAE buffer		
50 x TAE buffer		20 ml in 1 L dH_2O
1 x Agarose for gel- electrophoresis		
Agarose (Invitrogen, #15510)	1%	0.5 g in 50 ml 1xTAE buffer
GelRed (GeneON, #S420)		1:50000

Table 8 cDNA mix for single-worm PCR

Component	End concentration in sample
Oligo (dT)-primer [ng/µl]	5
Random primer [ng/µl]	5
Reaction buffer [x]	1
dNTP [mM]	0.5
DNase [U/µl]	1
RNAse inhibitor [U/µL]	1
RevertAid reverse transcriptase [U/µl]	20

Table 9 PCR program, single worm

Step	Temperature	Time	Number of cycles
Initial denaturing	98°C	30 s	1
Denaturing	98°C	10 s	
Annealing	58–60°C	20 s	30
Extension	72°C	30 s/kb	
Finale Extension	72°C	2 min	1

Table 10 qRT-PCR program

Step	Temperature	Time	Number of cycles
Initial denaturing	95°C	3 min	1
Denaturing	95°C	10 sec	
Annealing	58 °C	15 sec	49
Extension	72°C	15 sec	
Final Extension	72°C	5 min	
Denaturing	95°C	10 sec	1
Annealing (Gradient)	58 °C	30 sec	
Melting curve	65°C to 95°C in 0,1°C steps	5 sec	each 1

Table 11 HPLC equipment and conditions for GSH measurement

Equipment (Jasco Labor- u. Datentechnik GmbH, Groß-Umstadt, Germany)			
Pump	PU-1580		
Degasser	DG-1580-53		
Ternary gradient unit:	LG-1580-02		
Autosampler:	AS-1555-10		
Fluorescence detector:	FP-920		
Software:	Chrom Nav 2.1		
Conditions			
Temperature:	6 °C (Autosampler), 25 °C (Column)		
Column:	Nucleodur C18 Pyramid, 4 x 250 mm 5 µ, #760202.40 (Macherey-Nagel)		
Flow:	0.6 mL/min		
Wavelength:	Ex. 340 nm / Em. 420 nm		
Eluent A	2 % Acetonitrile/98 % 50 mM Sodium acetate buffer, pH 7.0		
Eluent B	80 % Acetonitrile/20 % 50 mM Sodium acetate buffer, pH 7.0		
Gradient	Time/min	Eluent A/%	Eluent B/%
	0.1	100	0

15	50	50
17	50	50
18	0	100
19	0	100
20	100	0

Acknowledgements

Wow, diese dreieinhalb Jahre gingen nun doch vorbei wie im Flug! Am Anfang war ich mir tatsächlich nicht sicher ob ich diesen Weg bis zu Ende gehen könnte, aber nun ist es soweit und es war toll! Dies habe ich verschiedensten Menschen zu verdanken, denen ich nun in aller Kürze meinen Dank aussprechen möchte.

Zu aller erst möchte ich mich bei allen jetzigen und ehemaligen Mitgliedern der Arbeitsgruppe Nutrigenomik bedanken. Danke für die vielen Diskussionen, die Unterstützung und die netten Gespräche.

Ich möchte ich mich besonders bei Ihnen Prof. Klotz für das erstmalige Vertrauen bedanken. Danke, dass mir eine so spannende Masterarbeit anzuvertrauet haben und mich in meiner Entwicklung und meinem Können zu bestätigt haben, indem Sie mir noch vor Fertigstellung nicht nur eine Promotion bei Ihnen in Ihrer Arbeitsgruppe ermöglichten, sondern darüber hinaus mich auch als Mitglied für ProMoAge vorschlugen. Nicht nur mein Wissenschafts-verständnis auch mein Selbstvertrauen im Labor habe ich dem Austausch und der Betretung durch Sie zu verdanken.

Danke an dich Nadine, dass du mich in die Kunst der Würmer eingeführt hast und mich während meiner Masterarbeit und der Anfangsphase meiner Promotion betreut hast. Du hast mir viel Wissen an die Hand gegeben mit dem ich mich während Promotion weiterentwickeln konnte.

Vielen Dank auch an dich Pavel, für die geduldige Weise mir Vieles zu allen möglichen Themen rund um die Molekularbiologie näher zu bringen und natürlich für die Klonierung der GFP Konstrukte, welche ich schließlich nutzen konnte, um wertvolle Daten für diese Arbeit zu sammeln.

Danke auch an dich Katrin für deine direkte Art, deine Hilfsbereitschaft in allen Laborfragen, deine Hilfe bei der HPLC Analse und die vielen netten Stunden am Küchentisch.

Danke an dich Maria, für das Managen des Laboralltags in der TM44 und das nette Beisammensein um Büro.

Mein Dank gebührt auch dir Holger, für die vielen wertvollen Diskussionen, auch über Themen außerhalb der Wissenschaft. Dank für zahlreichen die Korrekturen verschiedenster

Poster, Abstracts, Paper und Vorträge und nicht zu Letzt der Verbesserungsvorschläge innerhalb dieser Arbeit.

Danke an Weiye, dass du als Masterstudent auf eine Weise selbstständig gearbeitet hast, die es mir ermöglicht hat meine Dissertation problemlos abzuschließen. Danke auch für die Mikroskopie Bilder des R11 knockdowns und für die engagierte Arbeit hier im Labor.

También te doy las gracias a ti, Antonio. Muchas gracias por la cooperación extremadamente fructífera y las muchas sugerencias. También agradezco a David su ayuda en la generación de nuestras cepas transgénicas.

Dear Martin, thank you for providing us with valuable information for identifying the neurons in our R11G10-GFP strain. Without your expertise, we might have been lost.

Mein Dank geht auch an PD. Dr. habil. Andreas Müller. Vielen Dank für Ihre Empfehlung an ProMoAge. Nicht nur mein damaliges Praktikum im Institut für Ernährungswissenschaften in Halle unter Ihrer Leitung, auch Ihre Vorlesungen haben mich damals überhaupt dazu motiviert den Weg eines Wissenschaftlers einzuschlagen.

Mein Dank gilt auch vielen Menschen am Fritz-Lipmann-Institut in Jena. Mein Dank geht an Christoph für deine Betreuung und die Integration ins FLI und deine Arbeitsgruppe. Außerdem möchte ich mich bei den Leitern der Core facilities "DNA Sequencing" und "Life science computing" Marco Groth und Karol Szafranski für die Durchführung und Beratung der RNA-Sequenzierung am FLI bedanken. Ein besonderer Dank geht an Philipp Koch, da du dich sehr engagiert mit meinen Fragen zur Analyse der RNA-Seq auseinandergesetzt hast.

Ein großer Dank gilt auch den Leitern und Organisatoren des Graduierten Kollegs ProMoAge, Andreas und Regine. Danke das Ihr dieses Kolleg ins Leben gerufen habt und uns PhDs und MDs ermöglicht habt uns zu vernetzen, uns auszutauschen und uns weiterzubilden. Vielen Dank auch an Anja und Nancy die viele ProMoAge Treffen organisierten haben. Ein besonderer Dank an dich Anja, ohne dich wäre ich vermutlich auf diesen Treffen verhungert ;).

Zu guter Letzt möchte ich den wichtigsten Menschen in meinem Leben Danken, ohne die ich heute nicht da wäre wo ich bin. Danke dir Papa, Maxi, Juli und Marie, dass ihr da seid und vor allem für den Zusammenhalt in der letzten Zeit. Danke dir Ela, Matthias, Emma und

Lilly für vielen schönen Stunden, die ich bei euch verbringen durfte. Ihr wart meine Oase in Zeiten, in denen vieles Düster war.

Danke Sophie für deine Freundschaft und die schöne Zeit die wir in den vielen Stunden in unserer WG verbracht haben. Danke für die politischen Diskussionen, für die Ratschläge, für dein Interesse, deine Empathie und fürs da sein, wenn mal alles so richtig Sch**** war.

Danke Markus, amk ;), dass du es bis jetzt mit mir als Freund ausgehalten hast. Danke für den Ansporn und die Competition beim Zocken und Bouldern. Danke auch fürs Zuhören, wenn ich mal was loswerden musste.

Danke Martin die Unterstützung in Zeiten wo ich Sie gebraucht habe. Danke an unsere unvergesslichen Fahrradtour. Danke für deine Freundschaft.

Vielen Dank meine Liebe Umida. Dein Witz, deine Fürsorge, dein Zuspruch und deine Liebe geben mir jeden Tag Kraft, alle Hürden zu meistern.

Liebe Mama, es bricht mir das Herz, dass du diesen Moment und alle weiteren schönen Momente nicht mehr miterleben kannst. Ohne deine Erziehung, deine Liebe und deine Führsorge, könnte ich diese Sätze heute nicht schreiben. Diese Arbeit ist dir gewidmet, da ohne dein Glaube an meine Fähigkeiten ich es nie von der Realschule aufs Gymnasium, nie von der Planlosigkeit ins Studium geschafft hätte und viele andere Hürden auch nicht gemeistert hätte. Danke dass du mir dieses Leben ermöglicht hast. Du wirst mir sehr fehlen.

Scientific contributions

Publications

Köhnlein K, Urban N, Guerrero-Gómez D, Steinbrenner H, Urbánek P, Priebs J, Koch P, Kaether C, Miranda-Vizuete A, Klotz LO. (2020) A Caenorhabditis elegans ortholog of human selenium-binding protein 1 is a pro-aging factor protecting against selenite toxicity. *Redox Biol*. 28:101323. doi: 10.1016/j.redox.2019.101323.

Liu H, Ding J, **Köhnlein K**, Urban N, Ori A, Villavicencio-Lorini P, Walentek P, Klotz LO, Hollemann T, Pfirrmann T. (2019) The GID ubiquitin ligase complex is a regulator of AMPK activity and organismal lifespan. *Autophagy*. 16:9 doi: 10.1080/15548627.2019.1695399.

Köhnlein K, Urban N, Steinbrenner H, Guerrero-Gómez D, Miranda-Vizuete A, Kaether C, Klotz LO. (2020) Selenite-induced Expression of a Caenorhabditis elegans Pro-aging Factor and Ortholog of Human Selenium-binding Protein 1. *Current Nutraceuticals*. 1:1. doi: 10.2174/2665978601666200212105825

Conferences

2016 European Worm Meeting, June 1 – 3, 2016, Max Delbrück Center (MDC), Berlin

Poster: Two putative selenium binding proteins as modulators of *C. elegans* tress response and life span

54. Wissenschaftlicher DGE-Kongress, March 1 – 3, 2017, Christian-Albrechts-Universität, Kiel

Poster: Depletion von Selenbindeprotein-1-Orthologen führt zur Verlängerung der Lebensspanne und Modulation des Energie- und Fettmetabolismus in *Caenorhabditis elegans*

Joint meeting of the OCC World Congress and Annual SFRR-E Conference, June 21 – 23, 2017, Radisson Blu, Berlin

Poster: Two putative selenium binding proteins as modulators of C. elegans stress response and life span

Modulating Ageing / Antiageing: from Molecular Biology to Clinical Perspectives, September 1 – 3, 2017, Martin Luther University, Halle (Saale)

Poster: Two putative selenium binding proteins as modulators of *C. elegans* stress response and life span

34th Annual Meeting of the German Society for Minerals and Trace Elements (GMS), June 07 – 09, 2018, Friedrich Schiller University, Jena

Poster: Two nematode homologues of human SELENBP1 protein modulate stress response and lifespan in C. elegans

EMBO Workshop: *C. elegans* development, cell biology and gene expression, June 13 – 17, 2018, World Trade Center, Barcelona

Poster: Two nematode homologues of human SELENBP1 modulate stress response and lifespan in C. elegans

11th Retreat: Fritz-Lippman Institute, September 17 – 19, 2018, Waldhotel Berghof, Luisental

Poster: Two homologues of SELENBP1 modulate stress response and lifespan in C. elegans

Mechanisms of Aging: From Bench to Translation, May 13 – 15, 2019, LEUCOREA, Lutherstadt Wittenberg

Presentation: Depletion of a SELENBP1 homologue increases stress resistance and lifespan in C. elegans - association with metabolic processes

Postgraduate Symposium of the Jena School of Medicine, June 21, 2019, Dornburg Castle, Dornburg

Presentation: Depletion of a SELENBP1 homologue increases stress resistance and lifespan in C. elegans - association with metabolic processes

Ehrenwörtliche Erklärung

Entsprechend der geltenden, mir bekannten Promotionsordnung der Fakultät für Biowissenschaften der Friedrich-Schiller-Universität Jena erkläre ich, dass ich die vorliegende Dissertation eigenständig angefertigt und alle von mir benutzten Hilfsmittel und Quellen angegeben habe. Personen, die an der Gewinnung der Daten, sowie der Auswertung und der Erstellung der Manuskripte hilfreich waren, wurden namentlich gekennzeichnet. Es wurde weder die Hilfe eines Promotionsberaters in Anspruch genommen, noch haben Dritte für Arbeiten, welche im Zusammenhang mit dem Inhalt der vorliegenden Dissertation stehen, geldwerte Leistungen erhalten. Die vorgelegte Dissertation wurde außerdem weder als Prüfungsarbeit für eine staatliche oder andere wissenschaftliche Prüfung noch als Dissertation an einer anderen Hochschule eingereicht.

Datum:_____ Unterschrift:_____